



HAL
open science

The role of paleogeography in Asian monsoon evolution: a review and new insights from climate modelling

Delphine Tardif, Anta-Clarisse Sarr, Frédéric Fluteau, Alexis Licht, M. Kaya,
Jean-baptiste Ladant, N. Meijer, Y. Donnadieu, G. Dupont-Nivet, C.T.
Bolton, et al.

► To cite this version:

Delphine Tardif, Anta-Clarisse Sarr, Frédéric Fluteau, Alexis Licht, M. Kaya, et al.. The role of paleogeography in Asian monsoon evolution: a review and new insights from climate modelling. *Earth-Science Reviews*, 2023, 243, pp.104464. 10.1016/j.earscirev.2023.104464 . hal-04301741

HAL Id: hal-04301741

<https://hal.science/hal-04301741v1>

Submitted on 12 Nov 2024

HAL is a multi-disciplinary open access archive for the deposit and dissemination of scientific research documents, whether they are published or not. The documents may come from teaching and research institutions in France or abroad, or from public or private research centers.

L'archive ouverte pluridisciplinaire **HAL**, est destinée au dépôt et à la diffusion de documents scientifiques de niveau recherche, publiés ou non, émanant des établissements d'enseignement et de recherche français ou étrangers, des laboratoires publics ou privés.

The role of paleogeography in Asian monsoon evolution: a review and new insights from climate modelling

D. Tardif^{1,2,3,4}, A-C. Sarr¹, F. Fluteau⁴, A. Licht¹, M. Kaya⁵, J-B. Ladant³, N. Meijer⁶, Y. Donnadieu¹, G. Dupont-Nivet^{7,8}, C.T. Bolton¹, G. Le Hir⁴, Q. Pillot¹, F. Poblete⁹, P. Sepulchre³, A. Toumoulin¹⁰, W. Banfield¹

¹Aix Marseille Univ, CNRS, IRD, INRAE, CEREGE, Aix-en-Provence, France

²IRD, DIADE, University of Montpellier, Montpellier, France

³Laboratoire des Sciences du Climat et de l'Environnement, LSCE/IPSL, CEA-CNRS-UVSQ, Université Paris-Saclay, 91191 Gif-sur-Yvette, France

⁴Université Paris Cité, Institut de physique du globe de Paris, CNRS, F-75005 Paris, France

⁵Department of Geological Engineering, Middle East Technical University, Ankara, Turkey

⁶Senckenberg Biodiversity and Climate Research Centre (SBiK-F), Senckenberganlage 25, D-60325

Frankfurt am Main, Germany

⁷Géosciences Rennes, UMR CNRS 6118, Univ Rennes, Rennes, France

⁸Institute of Geosciences, Potsdam University, Potsdam, Germany

⁹Departamento de Geología, Facultad de Ciencias Físicas y Matemáticas, Universidad de Chile, Chile

¹⁰Department of Botany and Zoology, Faculty of Science, Masaryk University, Brno, Czech Republic

Key Points:

- Modern Asian monsoonal characteristics appeared sequentially during the Cenozoic, driven by distinct paleogeographic and climatic forcing factors.
- Model results depict monsoon-like precipitation seasonality in parts of Southern and Eastern Asia since the Paleogene.
- Monsoon-like rainfall regime in Paleogene eastern Asia is triggered by the proto-Tibetan Plateau uplift.
- Increasing continentality, due to the retreat of the Paratethys Sea and the emergence of the Arabian Platform above sea level, are instrumental in the establishment of surface temperature gradients that promote moist air advection from the Indian Ocean towards Asia in summer.
- The Anatolian-Iranian and East African landforms contribute to reinforcing the Somali Jet that brings moisture to Southeastern Asia in summer.
- The uplift of the Mongolian Plateau drives the formation of the Siberian High in winter, which broadly reinforces the East Asian winter monsoon and induces aridification of the Gobi region.
- The uplift of the Tian Shan and Pamir mountain ranges blocks the westerly moisture flux, forces the northward migration of the Jet Stream in summer, and enhances inland Asian aridification. Their effect on the South Asian monsoon is likely dependent on the paleoelevation of neighboring landforms, especially the Anatolian-Iranian Plateau.
- Additional constraints on the respective timing of uplift and paleoelevation are key to improving our understanding of monsoon establishment.

Corresponding author: Delphine Tardif, delphine.tardif@lsce.ipsl.fr

Corresponding author: Anta-Clarisse Sarr, anta-clarisse.sarr@univ-grenoble-alpes.fr

Abstract

The Asian monsoons are triggered by complex interactions between the atmosphere, Asian and African orography, and the surrounding oceans, resulting in highly seasonal climate and specific regional features. It was thought that the Asian monsoon was established during the Neogene, but recent evidence for monsoon-like precipitation seasonality occurring as early as the Paleogene greenhouse period challenges this paradigm. The possible occurrence of monsoons in a climatic and paleogeographic context very different from the present-day questions our understanding of the drivers underpinning this atmospheric phenomenon, in particular with regard to its dependence on geography. In this study, we first take advantage of the wealth of new studies to tentatively draw an up-to-date picture of Asian tectonic and paleoenvironmental evolution throughout the Cenozoic. We then analyze a set of 20 paleoclimate simulations spanning the late Eocene to latest Miocene (~ 40 -8 Ma) in order to better understand the evolution of the distinct Asian monsoon subsystems. At odds with the traditional view of a monsoonal evolution driven mainly by Himalayan-Tibetan uplift, our work emphasizes the importance of peripheral mountain ranges in driving the evolution of Asian climate. In particular, the uplift of East African and Anatolian-Iranian mountain ranges, as well as the emergence of the Arabian Peninsula, contribute to shaping the modern South Asian summer monsoon. We also suggest that East Asian monsoon establishment and the aridification of inland Asia are driven by a combination of factors including increasing continentality, the orographic evolution of the Tibetan Plateau, Mongolia, Tian Shan and Pamir, and $p\text{CO}_2$ decrease during the Cenozoic.

1 Introduction

The South and East Asian monsoons (SAM and EAM) are highly seasonal climatic phenomena that today support the livelihoods of billions of people. During summer, the Arabian Platform and the Southern Asian continent overheat compared to adjacent Indian and Western Pacific Oceans. These continental masses become the locus of a wide low pressure belt, leading to a regional amplification of the Inter Tropical Convergence Zone (ITCZ) seasonal latitudinal migration, and to the formation of the Somali Jet along the East African coast (Fig. 1). This strong cross-equatorial flow steers low-level moist air from the Indian Ocean to the Asian continent and triggers nutrient-rich upwelling in the western Arabian Sea (Schott & McCreary, 2001; Lévy et al., 2007; Curry et al., 1992). Over the Bay of Bengal, this large scale circulation splits into two branches (SI Fig. 14 f). First, the Indo-Gangetic Low Level Jet (Acosta & Huber, 2017) bifurcates towards northern India and drives important orographic precipitation on the Himalayan foothills during the South Asian summer monsoon (SASM). The second branch continues towards eastern Asia (SI Fig. 14 f) and ascends over northwesterly air masses related to the Jet Stream in the subtropics (Kong et al., 2017; Molnar et al., 2010; Sampe & Xie, 2010), forming the Meiyu-Bayu front, a band of strong convective precipitation stretching from Myanmar to Japan, characterizing the East Asian summer monsoon (EASM) (Ninomiya & Shibagaki, 2007). The front progressively migrates northward during spring and summer, following the Jet Stream's seasonal displacement relative to the Tibetan Plateau (TP): it is located south of the TP in winter and moves to its northern edge in summer (Schiemann et al., 2009). In winter, the temperature and pressure gradients between the Asian continent and the neighboring oceans reverse, as a consequence of the lower troposphere strong radiative cooling over snow-covered Asia (Jeong et al., 2011; Cohen et al., 2001; Jhun & Lee, 2004). The Siberian High, a wide anticyclone, develops over the Mongolian Plateau (L. Wang & Chen, 2014) (SI Fig. 14 j), flanked by two oceanic low pressure centers, the Aleutian Low (over the Northwestern Pacific Ocean), and the Maritime Continent Low (over the equatorial Western Pacific Ocean). The East Asian winter monsoon (EAWM) results from these pressure patterns, which drive the advection of cold, dry and dust-laden air masses from inland Asia to Eastern and Southern Asia (Fig. 1).

91 The spectacular extent and intensity of the Asian monsoons, combined with the highly
92 dynamic tectonic context of the region, have triggered a lot of interest within the scientific
93 community, in order to understand potential links between orography, land-sea distribution
94 and Asian climate evolution. The Asian monsoons have long been viewed as an atmospheric
95 phenomenon intimately intertwined with the Himalayan-Tibetan Plateau uplift history (e.g.
96 Molnar et al., 1993; Zhisheng et al., 2001; Tada et al., 2016; X. Liu, Guo, et al., 2015).
97 Records of strong upwelling initiating in the Arabian Sea at ~ 8 Ma (Kroon et al., 1991)
98 and, later, evidence for important dust deposition on the Chinese Loess Plateau since ~ 22
99 Ma (Guo et al., 2002) have rooted the origin of the Asian monsoons in the Neogene. However,
100 a wealth of recent studies challenge this paradigm. Aeolian dust deposits in northeastern
101 Tibet, as well as paleobotanical and isotopic data indicating a seasonal climate in Myanmar
102 and China (Licht et al., 2014; Sorrel et al., 2017; Fang et al., 2021; Zheng et al., 2022;
103 Meng et al., 2018; Y. Xie et al., 2022) have been interpreted as evidence for an active
104 monsoon as early as the late Eocene (see Fig.2 for a summary of available paleoclimate
105 indicators). A potential Paleogene origin for the Asian monsoons questions the traditional
106 view of monsoon development in relation to the Himalayan-Tibetan Plateau uplift history.
107 First, because the Paleogene exhibited a generally warmer and ice-free climate compared to
108 the Neogene (Westerhold et al., 2020). And second, because most modern Asian mountain
109 ranges were in the early stages of their uplift history, and Asian continentality was lower
110 due to the presence of the Paratethys Sea to the west (Kaya et al., 2019) and higher global
111 sea level (see late Eocene paleogeography in Fig. 3 a).

112 Climate modeling provides a unique opportunity to individually test the effect of each
113 potential forcing factor on the resulting climate. For instance, model studies have overall
114 tended to highlight that paleogeography out-competes global $p\text{CO}_2$ variations or far-field
115 ice-sheet effects in driving the initiation and intensification of the SAM and EAM over
116 multi-million years time scales (e.g. Farnsworth et al., 2019; J.-Y. Lee et al., 2015; Zoura et
117 al., 2019; Roe et al., 2016; Thomson et al., 2021), independently of the model complexity,
118 resolution, or type of geography (derived from modern or more realistic paleogeography).
119 Sensitivity experiments of increasing complexity and resolution have helped disentangle the
120 effect of the Himalaya-Tibet (and its sub-units) uplift from that of peripheral landforms,
121 such as the Tian Shan ranges, the Anatolian-Iranian orogen, or the Eastern African and
122 Mongolian landforms (H. Tang et al., 2013; Acosta & Huber, 2020; R. Zhang, Jiang, &
123 Zhang, 2017), and from the effect of changes in land-sea distribution (Fluteau et al., 1999;
124 Z. Zhang et al., 2007). While modeling studies provide a mechanistic basis to test po-
125 tential drivers for monsoons and aridity, robust knowledge of the timing and evolution of
126 paleogeography and paleoclimate remains of paramount importance to understanding the
127 complex Cenozoic history of Asian monsoons. The past decade has been rich in both mod-
128 eling and field studies, with for example the extension of marine sediment cores back to the
129 Paleogene in the oceans surrounding Asia (see synthesis by Clift et al. (2022)), the increased
130 coverage of well-dated terrestrial paleoclimate indicators from the Asian continent, and new
131 constraints on Cenozoic tectonic and paleoclimate evolution in Asia.

132 In this contribution, we build upon previous work (Sarr et al., 2022; Tardif et al.,
133 2020; Barbolini et al., 2020) to provide a comprehensive spatial and temporal picture of
134 large-scale wind circulation, precipitation seasonality, and aridity in continental Asia from
135 the late Eocene to the late Miocene, using up-to-date paleoclimate simulations. In the
136 following sections, we first synthesize Asian monsoon history, as understood from proxy and
137 modeling perspectives, and highlight the remaining outstanding questions (section 2, Fig. 2).
138 Then, we compile a summary of the main paleogeographic events that affected continental
139 Asia and the regions surrounding the Indian Ocean during the Cenozoic (section 3). We
140 further introduce the late Eocene to late Miocene paleogeographic configurations used to
141 run the climate model (Fig.3), as well as the criteria used to track Asian monsoon evolution
142 throughout the different simulations (section 4). Our modeling results are analyzed and
143 discussed in light of current knowledge.

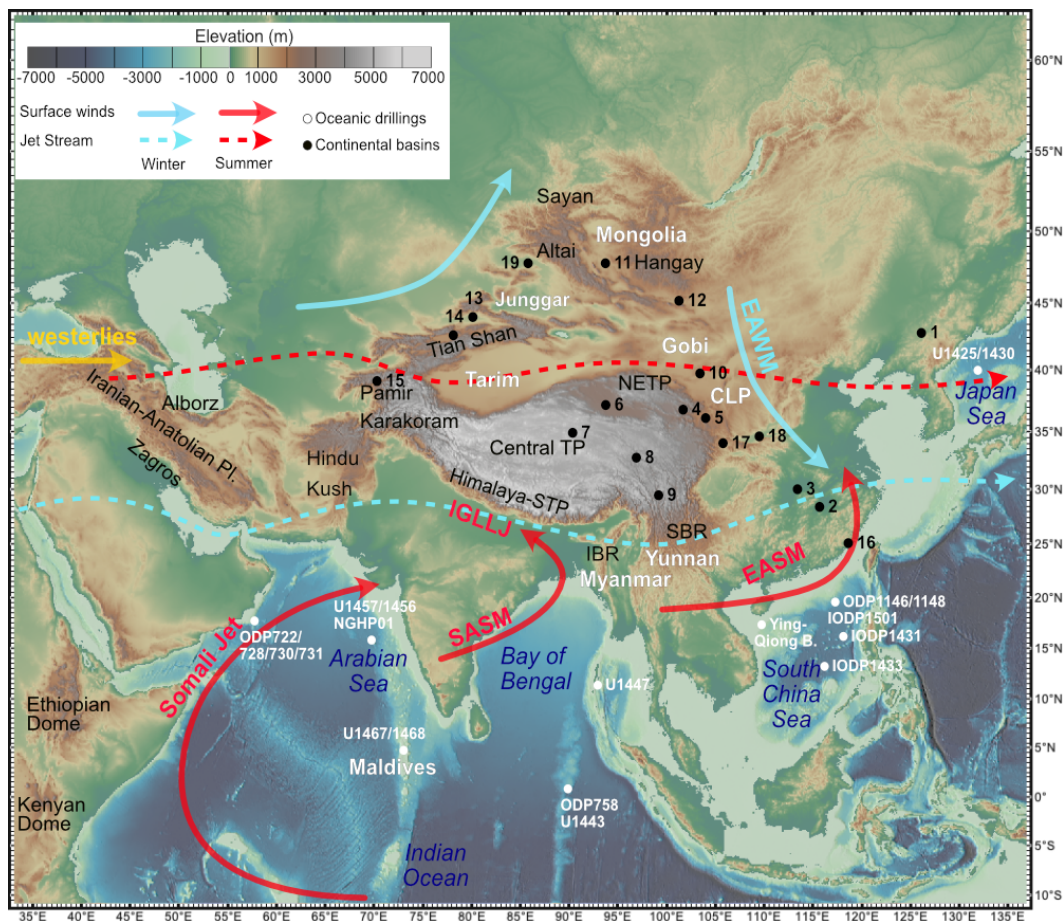


Figure 1. Asian orography (www.geomapapp.org), landforms (black labels), geographical regions (white labels), basins, oceanic drilling sites and seasonal winds, with the following abbreviations: EAWM - East Asian winter monsoon, SASM - South Asian summer monsoon, EASM - East Asian summer monsoon, IGLLJ - Indo-Gangetic Low Level Jet, STP - Southern Tibetan Plateau, NETP - Northeastern Tibetan Plateau, IBR - Indo-Burman Ranges, SBR - Sino-Burman Ranges, CLP - Chinese Loess Plateau. Numbered localities: (1) Huadian B., (2) Qingjiang B., (3) Jiangnan B., (4) Xining B., (5) Lanzhou B., (6) Qaidam B., (7) Hoh Xil B., (8) Nangqian B., (9) Markam B., (10) Bayanhot B., (11) Valley of Lakes, (12) Taatsin Gol, (13) Ili B., (14) Issyk Kul B., (15) Tajik B., (16) Zhangpu, (17) Tianshui B., (18) Weihe B., (19) Zaysan B.

144

2 Evidence for increasingly old Asian monsoons

145

146

147

148

149

150

151

152

153

154

155

The classical view of Asian paleoenvironmental evolution during the Cenozoic proposes a transition from a Paleogene "zonal climatic pattern" to a Neogene "monsoonal climatic pattern" (Guo et al., 2008; X. Sun & Wang, 2005; Jia et al., 2003; F. Wu et al., 2022). The zonal pattern is described as a widespread arid to semi-arid band stretching across China and bracketed in its southern and northern borders by two humid belts, whereas the monsoonal pattern consists of a core of pronounced aridity in the Asian interior, surrounded by monsoonal (seasonally wet) climate on its southern and eastern edges. This view is mostly based on paleoclimate proxy compilations (e.g. Boucot et al. (2013)) used to infer either humid (coal, indicators of forested environments, large mammals, etc.) or semi-arid to arid (evaporites, desert and shrub environments, etc.) conditions. Recent evidence for a highly seasonal climate in India, Myanmar and China as early as the Eocene, at least 20

156 Ma earlier than previously documented, nevertheless challenges this paradigm. This section
157 comprehensively reviews the broad paleoenvironmental changes inferred from paleoclimate
158 indicators in Asia from the late Eocene to the late Miocene, which are compiled in Figure 2
159 (upper part). Localities and basins mentioned throughout the text are detailed in Figure 1.

160 **2.1 Eocene to Oligocene paleoenvironmental evolution**

161 *2.1.1 A progressive increase in summer monsoon indicators*

162 The oldest evidence for strongly seasonal rainfall in Southern Asia comes from north-
163 western Indian early Eocene floras (Shukla et al., 2014; Bhatia, Khan, et al., 2021), as well as
164 from mid-late Eocene (~ 40 Ma) floras and isotopic measurements in freshwater gastropod
165 shells and mammal tooth enamel found in Myanmar (Licht et al., 2014; H. Huang et al.,
166 2021). Both regions were however located between $0-10^{\circ}\text{N}$ at this time (Shukla et al., 2014;
167 Westerweel et al., 2019), and such precipitation seasonality is therefore mainly interpreted
168 as a pronounced seasonal ITCZ migration rather than a monsoonal climate. Further east,
169 in the Yunnan region (Southwestern China), which is today subject to a mixture of SAM
170 and EAM influence, a shift from arid/semi-arid to humid environments is recorded during
171 the late Eocene and interpreted as the onset of the Asian monsoon (Sorrel et al., 2017; Fang
172 et al., 2021; Zheng et al., 2022). This climate transition is inferred by the presence of coal
173 layers, a transition from xerophytic to mixed forest pollen assemblage, a change in lithology
174 interpreted as lake and swamp expansions, as well as the occurrence of fossils of freshwater
175 fish and large mammals. A seasonally wet monsoonal climate is also inferred from isotopic
176 measurements in gastropods shells (Fang et al., 2021). The exact timing of this paleoen-
177 vironmental change is still debated between 41 and 35.5 Ma, but it nevertheless predates the
178 Eocene-Oligocene Transition (EOT, ~ 34 Ma). The proposed driving mechanisms of this re-
179 gional climate shift involve either a threshold response to Tibetan Plateau elevation (Zheng
180 et al., 2022), a side effect of the Paratethys Sea retreat in the west (that would have allowed
181 more moisture penetration from the ocean) (Fang et al., 2021), or the global climate cooling
182 initiated in the Middle Eocene and subsequent sea surface temperature changes (Sorrel et
183 al., 2017).

184 Evidence for the presence of an EASM during the Eocene is also debated. In east-
185 ern China, paleovegetation mostly points to warm, humid and weakly seasonal evergreen
186 forested environments close to the coast (Spicer et al., 2016; X. Ma et al., 2012; Pound
187 & Salzmann, 2017), except for late Eocene floras from Huadian (Meng et al., 2018) and
188 Qingjiang Basins (Y. Xie et al., 2022), situated in northeastern and eastern China respec-
189 tively, that already indicate highly seasonal rainfall. Further inland, towards the eastern
190 TP, a gradual transition from humid to subhumid and/or seasonally dry paleoenvironments
191 is suggested by botanical evidence (Han et al., 2022; Q. Li et al., 2022) and sedimentary
192 records from various basins displaying an alternation of mudstone and evaporite deposits
193 (D. Wang et al., 2013; Abels et al., 2011). High resolution deposits from the Jiangnan Basin
194 spanning the mid-Eocene to early Oligocene ($\sim 40-34$ Ma) (C. Huang & Hinnov, 2019) show
195 that the penetration of moisture into eastern China in the late Eocene was likely strongly
196 modulated by orbital forcing. These pieces of evidence suggest that the classical Paleo-
197 gene wet/dry zonal climatic pattern (Guo et al., 2008; X. Sun & Wang, 2005) was already
198 periodically disturbed in the late Eocene, preceding the more widespread appearance of
199 monsoon-like precipitation seasonality in the Oligocene.

200 Evidence for increased rainfall seasonality during the Oligocene to early Miocene be-
201 comes more common in floras from both China (X. Ma et al., 2012; Herman et al., 2017;
202 Vornlocher et al., 2021; J. Ren et al., 2021; Miao et al., 2013; Ling et al., 2021; S. Li et al.,
203 2018; C. Huang & Hinnov, 2019; H. Tang et al., 2020) and India (Bhatia, Khan, et al., 2021;
204 Spicer et al., 2017; Srivastava et al., 2012). Additionally, paleoceanographic records from
205 the adjacent Bay of Bengal and South China Sea have been used to track the SAM and
206 EAM evolution from the middle Oligocene onwards. Records from the Ying-Qiong Basin

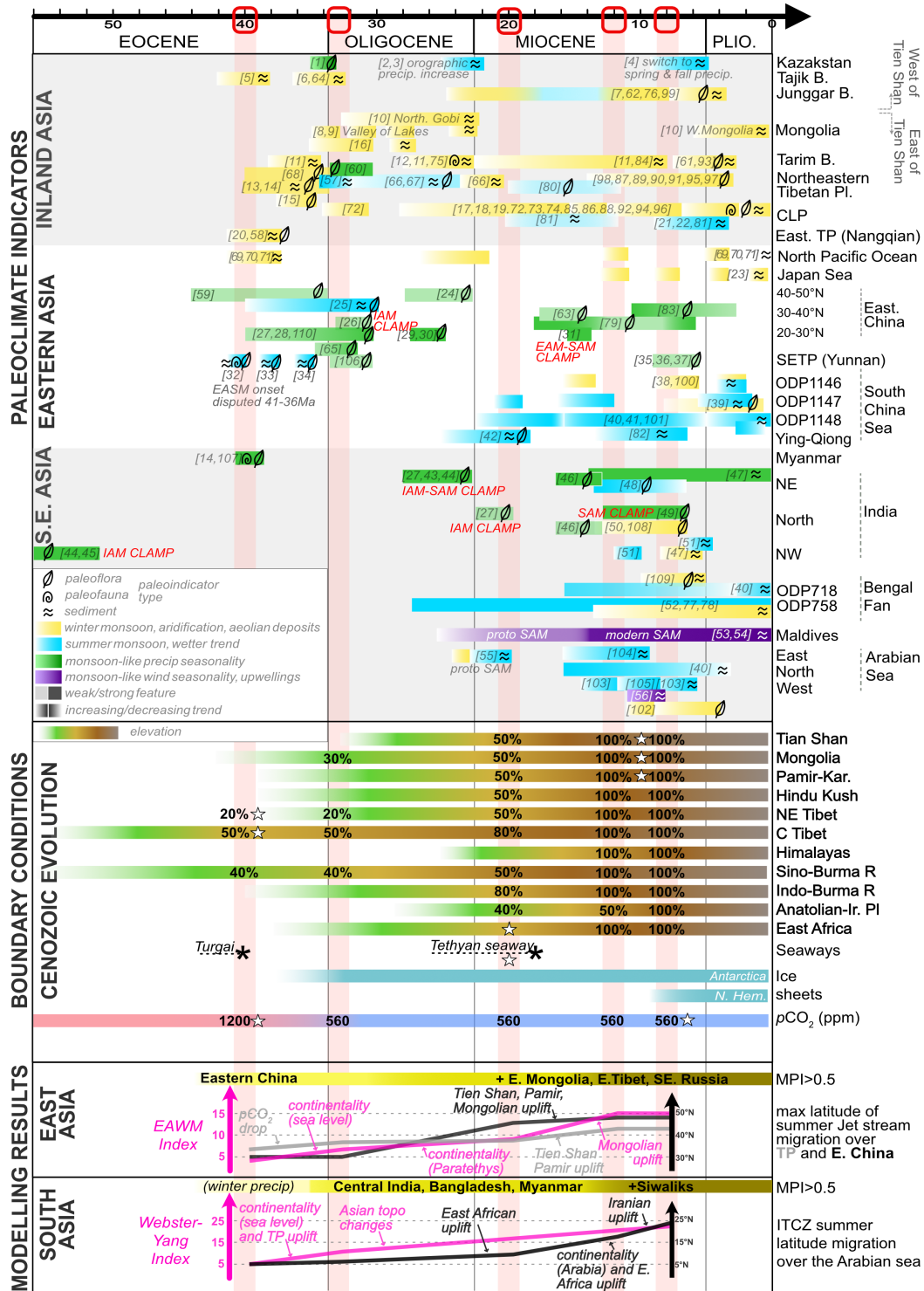


Figure 2. upper Paleoclimate trends recorded in Asia. Bibliographic references in brackets are listed in SI Table 3 ; center Evolution of main landforms, seaways, ice sheets and pCO₂ during the Cenozoic overlain with values used in our reference simulations (elevations expressed in % of modern). White stars indicate parameters that were tested in the sensitivity experiments discussed in the text; bottom Overview of the main monsoon indicator evolution computed from simulations presented in this study. We use the following abbreviations: NETP (SETP) - Northeastern (Southeastern) Tibetan Plateau, CLP - Chinese Loess Plateau.

(South China Sea) show an increase in terrigenous organic matter influx together with a higher proportion of tropical-subtropical angiosperm pollen at ~ 25 Ma, interpreted as a sign of increasing EASM intensity (W. Ding et al., 2021). In the Bay of Bengal (ODP Site 758), the radiogenic isotopic composition of clays indicates relatively constant weathering patterns over the last 27 Ma, and by inference stable SASM activity since at least the late Oligocene (S. Ali et al., 2021).

2.1.2 *Late Eocene aridification in response to the Paratethys Sea retreat and global climate cooling*

Markers of subhumid to arid climate are widespread in inland Asia in the Eocene, with many basins (e.g. Xining, Hoh Xil, Qaidam and Tarim) recording pollen assemblages characteristic of a steppe-desert environment (Q. Yuan et al., 2020; Miao, Wu, et al., 2016; X. Ma et al., 2012). During the mid-late Eocene (~ 40 -34 Ma), inland Asia evolves towards even drier conditions, as suggested by increased proportions of xerophytic plants such as *Nitraria* and *Ephedra* in eastern and northeastern Tibet and in the Tarim Basin (Q. Yuan et al., 2020; Barbolini et al., 2020; Hoorn et al., 2012; Miao, Wu, et al., 2016), $\delta^{18}\text{O}$ measurements on oyster shells in the Tarim Basin (Bougeois et al., 2018), decreasing saline lakes in the Xining Basin (Abels et al., 2011), reduced chemical weathering observed in the Qaidam and Xining Basins (Fang et al., 2019), $\delta^2\text{H}$ isotope analyses on sedimentary leaf waxes *n-alkanes* in the Qaidam Basin (M. Wu et al., 2021) and lipid biomarkers and carbon isotopic compositions from bulk sediments in the Nangqian Basin (J. Wei et al., 2022). The presence of detrital material identified as Asian dust in sediments from the central North Pacific (GPC3 and ODP Site 1215) since ~ 40 Ma also likely indicates the presence of dry conditions on land (Pettke et al., 2002; D. Rea et al., 1985; Ziegler et al., 2007).

This late Eocene aridification episode could result from a reduced westerly moisture input following two successive Paratethys Sea regression phases from the Tarim and the Tajik Basins between ~ 41 -37 Ma (Carrapa et al., 2015; J. Sun et al., 2020, 2022; Bougeois et al., 2018; Bosboom et al., 2014b; Kaya et al., 2019). High resolution sedimentary records, such as those of the Xining Basin (northeastern Tibet), exhibiting good correlation between wetter saline lake deposits during Paratethys Sea transgressions (Meijer et al., 2019; Bosboom et al., 2014a), confirm the key role played by the westerlies and the Paratethys Sea as a major moisture source for inland Asia in the Eocene. Additionally, the strong obliquity cyclicity imprinted on Xining evaporite/mudflat alternations in the late Eocene (40-34 Ma), coeval with the appearance of loess-like dusts in the alluvial mudflats (Meijer et al., 2021; Licht et al., 2014), hint at a marked influence of high latitude dynamics (incipient polar ice-sheets, variations in the Siberian High intensity) on winter inland Asian climate at that time (Abels et al., 2011; Xiao et al., 2010; Meijer et al., 2021).

2.1.3 *Oligocene climate evolution and inception of modern Asian deserts*

In the early Oligocene, a few sites situated within the westerly moisture area display increased humidity, recorded by $\delta^{18}\text{O}$ isotopic measurements in pedogenic carbonates in the Tarim and western Qaidam Basins (Kent-Corson et al., 2009), together with $\delta^2\text{H}$ measurements in leaf waxes (M. Wu et al., 2021). Leaf fossil CLAMP analysis (Climate Leaf Analysis Multivariate Program (Feng & Poulsen, 2016; Wolfe, 1993; Jacques, Su, et al., 2011)), further suggest a rather wet (but not monsoonal) rainfall regime in western Qaidam (Song et al., 2020). On the other hand, evidence for a drier climate is reported within the EAM domain by $\delta^{18}\text{O}$ isotopic measurements in pedogenic carbonates from eastern Qaidam (Y. Sun et al., 2020; Kent-Corson et al., 2009) and in Lanzhou Basin in the Chinese Loess plateau area (B. Li et al., 2016). CLAMP analysis on fossil leaves in the Lanzhou (Miao et al., 2013) and southeastern Tibetan Markam Basin (T. Su, Spicer, et al., 2019) advocate for an increased (and monsoon-like) precipitation seasonality due to the TP uplift. Interpretations for this climatic trend in eastern China suggest that it may indicate either decreased EASM rainfall due to global cooling after the EOT (M. Wu et al., 2021) or increased winter

258 aridity due to the Paratethys Sea retreat and/or to global sea level fall after the EOT (B. Li
259 et al., 2016).

260 In Inner Mongolia (Taatsin Gol region), $\delta^{18}\text{O}$ and $\delta^{13}\text{C}$ isotopic measurements in
261 pedogenic carbonates indicate aridification since the early Oligocene (Caves Rugenstein et
262 al., 2014) and possible loess occurrence as early as ~ 34 Ma (J. Sun & Windley, 2015).
263 Proposed mechanisms for this drying involve increased continentality due to Paratethys
264 Sea retreat at 34 Ma (J. Sun & Windley, 2015) and an early Hangay Dome uplift that
265 would have acted as a barrier to moisture advection from Siberia to Mongolia as early as
266 the Oligocene (Caves Rugenstein et al., 2014). However, high resolution records reveal
267 several pulses of aridification at ~ 34 -33, ~ 31 , ~ 28 and ~ 23 Ma, coeval with periods of
268 ice-sheet expansion, suggesting that these cooling phases were likely the main drivers of
269 Mongolian hydrological dynamics (Baldermann et al., 2021). Further south, in the Gobi
270 region (Bayanhot Basin), two bursts of aridification inferred from environmental magnetic,
271 mineralogical and geochemical data at ~ 31 and ~ 28 Ma further hint at an influence of high
272 latitude ice-sheet fluctuations on Mongolian Oligocene climate (Wasiljeff et al., 2022).

273 In the mid to late Oligocene, eolian dust deposits are documented in three major
274 sites (see Meijer et al. (2021) for a review), namely the Chinese Loess Plateau, from ~ 29
275 Ma onwards (Garzzone et al., 2005; Qiang et al., 2011), the Tarim Basin at ~ 27 -22 Ma
276 (Zheng et al., 2015), and the Junggar Basin at ~ 24 Ma (J. Sun et al., 2010). Aridification
277 is also inferred from $\delta^{18}\text{O}$ isotopic measurements in oysters and pedogenic carbonates from
278 the Tarim Basin at ~ 25 Ma (Bougeois et al., 2018; Kent-Corson et al., 2009) and from
279 isotopic records in stromatolites from the Junggar Basin, loosely dated to the early Miocene
280 (W. Yang et al., 2019). This second step of aridification is coeval with $\delta^{18}\text{O}$ and $\delta^{13}\text{C}$ isotopic
281 measurements from pedogenic carbonates suggesting increased orographic precipitation in
282 the Issyk Kul and Ili Basins, both situated on the western side of the Tian Shan ranges
283 (Hellwig et al., 2018; Macaulay et al., 2016). Collectively, these observations are interpreted
284 as an indication of an uplift episode of the Tian Shan-Pamir ranges, which would have
285 started shielding the Tarim and Junggar Basins from westerly moisture input and favored
286 their aridification (Bougeois et al., 2018; W. Yang et al., 2019). This late Oligocene to
287 early Miocene aridification of the Asian interior is also depicted in several oceanic records,
288 where an increase in dust mass accumulation rate is recorded in the Pacific at ~ 25 Ma (Site
289 GPC3) (D. K. Rea, 1994; Pettke et al., 2002) and at ~ 22 Ma (ODP Site 1215) (Ziegler et
290 al., 2007). A reduction in $\Delta\delta^{13}\text{C}$ coeval to an increase in bulk sediment Mn/Fe and Mn/Ti
291 and foraminiferal Mn/Ca in the eastern Arabian Sea at ~ 23 Ma (NGHP01 Site), reflecting
292 an increase in water column mixing and ventilation, are considered as further evidence for
293 the existence of a proto winter monsoon wind system (Beasley et al., 2021).

294 **2.2 Evolution of seasonal and regional monsoons in the Neogene**

295 The better coverage in both continental and marine records in the Neogene allows
296 drawing a more precise picture of monsoon evolution during the Late Cenozoic. This section
297 reviews the many pieces of evidence which now tend to support a scenario of diachronous
298 evolution of regional monsoons, with a decoupling between summer and winter seasons as
299 well as between monsoon-like precipitation seasonality and monsoon-like wind circulation
300 establishment.

301 **2.2.1 Neogene South Asian monsoon variations**

302 The occurrence of monsoon-like rainfall seasonality in the eastern SAM domain is at-
303 tested to by relatively constant isotopic composition of clays derived from silicate weathering
304 since ~ 27 Ma in the central Bay of Bengal (ODP Site 758) (S. Ali et al., 2021). Middle
305 Miocene (~ 13 Ma) plant macrofossils from northeasternmost India (Arunachal Pradesh)
306 also attest to modern-like rainfall seasonality at that time (Khan et al., 2014). In Yunnan,
307 the disappearance from the fossil record of *Metasequoia*, a plant whose modern descendant

308 is intolerant to dry winters, may further attest to a SAM rainfall seasonality intensification
309 after the middle Miocene (L. Wang et al., 2019). On the other hand, plant macrofossils
310 and pollen from the northwestern SAM domain (Nepal, northwestern India and Pakistan)
311 show a progressive vegetation shift from evergreen to deciduous forests from the middle to
312 the latest Miocene, and finally to C4 grasslands (Hoorn et al., 2000; Bhatia et al., 2022;
313 Bhatia, Srivastava, et al., 2021; Srivastava et al., 2018; Tauxe & Feakins, 2020; Vögeli et al.,
314 2017; Sanyal et al., 2004). This vegetation change is also recorded in bulk sediments, leaf
315 waxes, pollen and macrofossils in the Arabian Sea at \sim 8-7 Ma (ODP Site 722 and IODP
316 Site U1457, (Feakins et al., 2020; Y. Huang et al., 2007; Clift et al., 2022)), and in the
317 Bengal fan at \sim 7-6 Ma (ODP Sites 717/718, (Polissar et al., 2021)).

318 Chemical weathering and sediment accumulation rates from both the Indus Fan and
319 the Bay of Bengal suggest that SASM precipitation reached a maximum in the middle
320 Miocene (\sim 16-10 Ma) before declining between \sim 8-3 Ma (Clift et al., 2008, 2019; Zhou
321 et al., 2021). This has been suggested to reflect an intensification of the SASM (S. Ali
322 et al., 2021), possibly concomitant with a weakening of the SASM (J. Lee et al., 2020). Wind
323 proxies also point to the presence of a seasonal wind reversal, and corroborate the existence
324 of a winter monsoon since the middle Miocene. In the Arabian Sea, an increased relative
325 abundance of the foraminifera *Globigerina Bulloides* in the sediments was initially used to
326 infer an intensification (or an onset) of the SASM wind circulation at \sim 8 Ma (Kroon et
327 al., 1991), based on the assumption that stronger monsoonal winds would translate into
328 stronger upwelling activity. Those records have since been extended back in time (Bialik
329 et al., 2020; Zhuang et al., 2017; Gupta et al., 2015) and combined with the analysis of
330 current-controlled drift sediments and geochemical tracers from the Maldives archipelago
331 (Betzler et al., 2016). These new studies now point to the establishment of a proto SAM
332 wind circulation in the late Oligocene (\sim 25 Ma), and of its reinforcement in the middle
333 Miocene (\sim 13-10 Ma) (Betzler et al., 2016; Zhuang et al., 2017; Bialik et al., 2020). Strong
334 SAM wind circulation since at least 10 Ma is also supported by export productivity and
335 sediment accumulation patterns from records in the southern Bay of Bengal (IODP Site
336 U1443) (Bolton et al., 2022), together with clay mineralogy in the Andaman Sea (IODP
337 Site 1447) (J. Lee et al., 2020) and isotopic and chemical analyses on sediments in the
338 eastern Arabian Sea (IODP Site 1456) (Tripathi et al., 2017)). An intensification of the
339 SAM in the late Miocene (\sim 8-7 Ma) has also been inferred based on an increase in percent
340 in *G. Bulloides* and Total Organic Carbon content in sediments from Oman margin (Gupta
341 et al., 2015) but remains debated, as it is not observed in all paleoceanographic records from
342 the Arabian Sea and the Bay of Bengal (Bolton et al., 2022; Tripathi et al., 2017; Betzler
343 et al., 2016; Y. Huang et al., 2007).

344 **2.2.2 East Asian Summer Monsoon evolution in the Neogene**

345 Summer precipitation typical of the EASM likely occurred throughout the Neogene,
346 as shown by records from the South China Sea such as weathering indices (Clift et al., 2008,
347 2014), $\delta^{13}\text{C}$ measurements in black carbon (Jia et al., 2003), pollen, biomarkers, kerogen
348 maceral composition and clay mineralogy (W. Ding et al., 2021). On land, $\delta^{18}\text{O}$ values from
349 paleosol carbonates in the Chinese Loess Plateau (Suarez et al., 2011) and most Chinese
350 paleobotanical and palynological data suggest summer precipitation amounts comparable to
351 modern (Q. Wang et al., 2021; Yao et al., 2011; Xing et al., 2012; Hui et al., 2021; B. Wang
352 et al., 2021; Q.-g. Sun et al., 2002). Many localities nevertheless point to wetter winters
353 due to weaker winter monsoons until the late Miocene (Q. Wang et al., 2021; Liang et al.,
354 2022), except for the mid-Miocene Zhangpu biota flora (southeastern China), whose CLAMP
355 signature shows affinities with EAM and SAM floras, thus suggesting adaption to modern-
356 like rainfall seasonality (B. Wang et al., 2021). A warm and wet period has been identified
357 during the Middle Miocene Climatic Optimum (\sim 17-14 Ma) in both continental as well as
358 oceanic records and was likely less seasonal than during the rest of the Miocene (Clift et al.,
359 2022). The penetration of EASM moisture would have reached as far as the Qaidam Basin,
360 as suggested by lotus fossils (Luo et al., 2022), increased abundance of *Fupingopollenites*, an

361 extinct palynomorph highly dependent on summer moisture (Miao, Song, et al., 2016), and
 362 characterization of iron oxides from the Chinese Loess Plateau (H. Zhao et al., 2020). This
 363 warm and wet mid-Miocene climate peak is also inferred from chemical weathering proxies
 364 and indicators of stronger physical erosion and fluvial input measured in sediments from the
 365 South China Sea at 15-12 Ma (Clift et al., 2014), and from $\delta^{13}\text{C}$ in black carbon at 15 Ma
 366 (Jia et al., 2003).

367 The variations in EASM intensity during the late Miocene and Pliocene remain con-
 368 troversial in both continental and marine records, with variations in the suggested timing of
 369 changes (Clift et al., 2022). A decline in EASM intensity induced by decreasing $p\text{CO}_2$ after
 370 the Mid-Miocene Climate Optimum is suggested by weathering, paleoceanographic indices
 371 and pollen from the South China Sea (ODP Site 1146) (Clift et al., 2014; Holbourn et al.,
 372 2021, 2018; Miao et al., 2017; G. Wei et al., 2006), as well as pollen records from the Liupan
 373 Mountains (North China) (Jiang & Ding, 2008). On the other hand, in the South China
 374 Sea, late Miocene EASM intensification is inferred from $\delta^{18}\text{O}$ and Mg/Ca derived records
 375 of surface and sub-surface water characteristics (IODP Site U1501) (C. Yang et al., 2021)
 376 and by black carbon $\delta^{13}\text{C}$ (Jia et al., 2003). In China, wetter conditions during the lat-
 377 est Miocene are suggested by mineralogical, chemical and magnetic analysis of sedimentary
 378 deposits in the Chinese Loess Plateau (Ao et al., 2016, 2021; H. Zhao et al., 2020), pollen
 379 records from the Tianshui (Hui et al., 2021) and the Weihe Basins (L. Zhao et al., 2020),
 380 and by fossil wood, mammals and fish in the Qaidam Basin (Cheng & Yang, 2016; X. Wang
 381 et al., 2007). EASM intensification at this time is usually attributed to global warming (Ao
 382 et al., 2021; H. Wang et al., 2019) and/or to Neogene TP uplift phases (Hui et al., 2021;
 383 X. Ren et al., 2020; H. Zhao et al., 2020).

384 ***2.2.3 Miocene-Pliocene aridification pulses in response to regional uplift***

385 Throughout the Miocene, dust deposition continued in the Chinese Loess Plateau
 386 (Guo et al., 2002; Meijer et al., 2021), Tarim-Taklimakan (Kent-Corson et al., 2009; Zheng
 387 et al., 2015; Heermance et al., 2018) and Junggar Basins (J. Sun et al., 2010). After a
 388 phase of relatively wetter conditions during the Mid-Miocene Climate Optimum (see section
 389 2.2.2), a pronounced step-wise aridification was then recorded in most of inland Asia until
 390 the Miocene-Pliocene boundary (Lu et al., 2010; Lu & Guo, 2014; Z.-H. Tang & Ding,
 391 2013). The timing of aridification pulses varies depending on the region and is attributed
 392 to either northeastern TP uplift (Miao et al., 2012), Altai and Tian Shan mountain uplift
 393 (Caves Rugenstein et al., 2014, 2017) and/or to late Miocene cooling (Lu et al., 2010; Lu
 394 & Guo, 2014; Peng et al., 2016). In the eastern part of inland Asia, encompassing the
 395 Chinese Loess Plateau, central China and northeastern TP, data provide strong evidence
 396 for aridification, including pollen and biomarkers documenting a step-wise transition from
 397 a sub-humid to an arid environment starting at ~ 15 Ma (J. Liu et al., 2016; Miao et al.,
 398 2011; Jiang & Ding, 2008; Peng et al., 2016), massive grassland expansions at $\sim 11-7$ Ma
 399 (Suarez et al., 2011; Barbolini et al., 2020; Y. Ma et al., 2005; L. Zhao et al., 2020; H. Wang
 400 et al., 2019), widespread eolian dust deposition at $\sim 8-7$ Ma (X. Ma & Jiang, 2015; Guo
 401 et al., 2002; Qiang et al., 2011; B. Li et al., 2016; Jiang et al., 2017), increased $\delta^{18}\text{O}$ of
 402 pedogenic carbonates and terrestrial mammal tooth enamel at $\sim 14-13$ and $\sim 7-5$ Ma (B. Li
 403 et al., 2016; Kent-Corson et al., 2009; M. Wu et al., 2021; W. Liu et al., 2014; Y. Sun et
 404 al., 2020; Kaakinen et al., 2006; Y. Wang & Deng, 2005), n -alkane analysis from Qaidam
 405 sediments since 13 Ma (Z. Liu et al., 2014) and the dominance of cold-aridiphilous mollusks
 406 in the Chinese Loess Plateau from 7-5 Ma (F. Li et al., 2008). The Tarim and Junggar
 407 Basins also provide multiple evidence for mid to late Miocene aridification, such as increased
 408 proportions of xerophytic plants and grass pollen at $\sim 7-5$ Ma (J. Sun et al., 2010; J. Sun
 409 & Zhang, 2008; J. Sun et al., 2008; Z. Zhang & Sun, 2011; Barbolini et al., 2020), massive
 410 aeolian deposition in the western Tarim Basin at $\sim 12-7$ Ma (Heermance et al., 2018) and the
 411 permanent drying of lakes in the eastern Tarim Basin at ~ 5 Ma (W. Liu et al., 2014). The
 412 pedogenic carbonate $\delta^{18}\text{O}$ records of these regions nevertheless offer diverging patterns of
 413 evolution, that have tentatively been explained by their locations with respect to the Tian

414 Shan and Altai mountains (Caves Rugenstein et al., 2017). Records from regions today lying
 415 upwind of the Tian Shan and Altai mountains, such as the Issyk Kul (Macaulay et al., 2016),
 416 Junggar (Charreau et al., 2012) and Zaysan Basins (Caves Rugenstein et al., 2017) exhibit
 417 a decline in $\delta^{18}\text{O}$ between 10-5 Ma, which has been interpreted as a shift to spring/fall
 418 precipitation following the uplift of the Altai and Tian Shan mountains (Caves Rugenstein
 419 et al., 2017). Perennial lake formation in the windward Ili Basin (Kazakhstan) at ~ 10 Ma
 420 may further attest that the Tian Shan ranges acted as an orographic barrier for westerlies
 421 moisture input (Frisch et al., 2019). On the other hand, records from the Tarim Basin,
 422 situated downwind of the Tian Shan ranges, display $\delta^{18}\text{O}$ trends similar to those of the
 423 Qaidam Basin (Kent-Corson et al., 2009) with increased values since ~ 15 Ma peaking at
 424 ~ 7 -5 Ma and which are interpreted as indicating aridification at that time.

425 EAWM intensification is also recorded in the South China Sea at ~ 15 -12, ~ 8 -5 and
 426 ~ 3 Ma, based on increased black carbon accumulation (whose transportation to the sea
 427 would be favored by stronger winter winds) (Jia et al., 2003), planktic and benthic $\delta^{18}\text{O}$
 428 records and mixed layer temperatures (Holbourn et al., 2021, 2018), and clay mineralogy
 429 and grain size analysis (Wan et al., 2007). In the Sea of Japan, clay mineral assemblages
 430 and isotopic analyses of the silicate fraction covering the last 15 Ma suggest a step-wise
 431 drying of Central Asia at 12, 8 and 3.5 Ma (Shen et al., 2017). A sea surface temperature
 432 drop of ~ 8 °C recorded between 8-6.6 Ma (IODP Site U1425) is further interpreted as a
 433 sign for a marked EAWM intensification (Matsuzaki et al., 2020). At approximately the
 434 same time (8-4 Ma), an analysis of aluminosilicate end-member contributions shows a shift
 435 from a Taklimakan source to a Gobi-Chinese Loess Plateau source in dust exported to the
 436 Sea of Japan (Site U1430), suggesting changes in winter wind circulation patterns, or in the
 437 extent of these deserts (Anderson et al., 2020). Further east, in the North Pacific, a relative
 438 increase in Asian dust is also recorded at ~ 10 and ~ 4 Ma (D. Rea et al., 1985; Pettke et
 439 al., 2002).

440 2.3 Assessing monsoon forcing factors through climate models

441 The major drivers of long-term monsoonal variability are topography, land-sea distri-
 442 bution and global climate variations. Attributing a specific change to one or several of these
 443 factors is nevertheless complicated because they may co-vary, produce non-linear responses
 444 with potentially opposite effects, and are sometimes poorly dated or quantified. Modeling
 445 experiments, initially utilizing present-day geographies and boundary conditions, have en-
 446 abled a better understanding of the role played by these different forcing factors in shaping
 447 the regional monsoons.

448 2.3.1 Topographic influences on the South and East Asian monsoon with 449 present-day geography

450 The TP has long been considered instrumental in driving the Asian monsoonal cir-
 451 culation and precipitation, due to its elevated heated surface in summer acting as a "heat
 452 pump" driving the convergence of the surrounding air masses, in particular the ITCZ con-
 453 veying moisture from the Indian Ocean (Kutzbach et al., 1993; Zoura et al., 2019; Molnar
 454 et al., 1993; G. Wu et al., 2012). While the presence of the TP would indeed play a key role
 455 in the EASM establishment, with the heating of the Plateau inducing a cyclonic circulation
 456 anomaly promoting the advection of moist air masses towards Eastern Asia (Z. Zhang et
 457 al., 2007; H. Tang et al., 2013; R. Zhang, Jiang, & Zhang, 2017; G. Wu et al., 2012), several
 458 studies suggest that the orographic thermal forcing of the Plateau is not as important as
 459 previously thought for the SAM establishment. Instead, the physical barrier created by the
 460 topography would insulate the high moist static energy air (warm wet air masses) from the
 461 tropics from the low moist static energy air (cold dry air) brought by the westerlies and
 462 induces abundant orographic precipitations in northern India, through steering and forced
 463 ascension of moist air masses (Boos & Kuang, 2010, 2013; Acosta & Huber, 2020). Al-
 464 though the debate between a thermal versus mechanical role for TP on atmospheric flow

465 is still ongoing, a consensus emerged for the need of having an energetic-based framework
 466 to study monsoon mechanisms at all timescales (Biasutti et al., 2018), and integrate them
 467 within the planetary scale circulation dynamics (Rodwell & Hoskins, 1996). The condensa-
 468 tion of moisture in these ascending air masses leads to important latent heat release in the
 469 high troposphere over northern India, which acts as a positive feedback sustaining summer
 470 convection and precipitation in South Asia (He, 2017). On the other hand, the large-scale
 471 advection of the ITCZ over Asia in late spring and early summer is essentially driven by
 472 surface ocean-continent temperature gradients and resulting pressure patterns (Acosta &
 473 Huber, 2020; Merlis et al., 2013). Additionally, numerical simulations show that such en-
 474 hanced migration of the summer ITCZ is scaled to Asian continental extent, and was likely
 475 weaker in the past, when conditions of higher sea level and the presence of the Paratethys Sea
 476 prevailed and translated into surface temperature gradients different from today (Z. Zhang
 477 et al., 2007).

478 Smaller orographic features have also been shown to play a critical role in shaping and
 479 strengthening both the SAM and EAM. The East African highlands, positioned in the path
 480 of the ITCZ flow, impact both African and South Asian climate (Bannon, 1979; Rodwell
 481 & Hoskins, 1995; Sepulchre et al., 2006). Recent studies have specifically demonstrated
 482 that the East African highlands contribute greatly to the strengthening and concentration
 483 of the Somali Jet, but that their absence would result, somewhat counter-intuitively, in
 484 higher summer precipitation over the SAM region due to increased advection directly from
 485 the ocean to the continent (H.-H. Wei & Bordoni, 2016; Chakraborty et al., 2009). This
 486 last aspect hints that strong upwelling in the Arabian Sea, related to a strong Somali
 487 Jet, may not always be positively correlated with heavy rainfall on land. The Anatolian-
 488 Iranian landforms, by channeling the Somali Jet and insulating it from the subtropical
 489 dry westerly flow, greatly contribute to enhancing moisture transport towards India and
 490 eastern Asia (Acosta & Huber, 2020; He, 2017; H. Tang et al., 2013). Additionally, the
 491 orographic precipitation observed over smaller Asian landforms, for example the Indian
 492 Ghats or the Indo-Burman ranges, have been shown to promote moisture advection and
 493 enhanced precipitation in adjacent regions located windward, especially over the Arabian
 494 Sea, Bay of Bengal and South China Sea (S.-P. Xie et al., 2006).

495 The effect of the Pamir, Tian Shan and northeastern TP uplifts on the SAM remains
 496 unclear. When these landforms are uplifted together with the Mongolian Plateau, a decrease
 497 in precipitation is simulated over India (H. Tang et al., 2013). On the other hand, increased
 498 rainfall is simulated in India while testing Pamir, Tian Shan and northeastern TP uplift but
 499 maintaining a low Mongolian Plateau (R. Zhang, Jiang, & Zhang, 2017; R. Zhang, Jiang,
 500 Zhang, Cheng, & Zhang, 2017), highlighting potential counter effects of those mountains
 501 on the Asian climate. The Pamir, Tian Shan and Mongolian landforms are also perfectly
 502 situated in the mid-latitudes to interfere both dynamically and thermally with planetary-
 503 scale atmospheric circulation. Numerical simulations show that their uplift enhances aridity
 504 in inland Asia (modern Gobi and Taklimakan deserts) and reinforces the EAWM circulation
 505 patterns (X. Liu & Yin, 2002; X. Liu, Sun, et al., 2015; Baldwin & Vecchi, 2016; Sato, 2009;
 506 R. Zhang, Jiang, Zhang, Cheng, & Zhang, 2017). By creating a cold pool and deviating
 507 the westerlies towards northern Siberia, the Mongolian orography has been proposed to be
 508 responsible for the northward migration of the subtropical Jet Stream in summer (White et
 509 al., 2017; Shi et al., 2015; Sha et al., 2020), and for most of the Siberian High location and
 510 intensity in winter (Sha et al., 2015; R. Zhang, Jiang, Zhang, Cheng, & Zhang, 2017).

511 ***2.3.2 Modeling experiments using paleogeographic reconstructions***

512 Modeling studies based on present-day geographies are limited in the extent to which
 513 they allow us to understand past changes, especially for periods when very different ge-
 514 ographies prevailed. Paleoclimate simulations using presumed "realistic" paleo-boundary
 515 conditions are however rarer, because they usually entail high computational cost and re-
 516 quire important background knowledge of past boundary conditions (paleogeography, CO₂,

517 solar constant, ice-sheet volume). Such modeling experiments confirm that increasing Asian
518 continentality during the Oligocene and the Miocene, either due to the Paratethys Sea re-
519 treat and/or global eustatic sea level fall, is a key driver of increased moisture advection
520 towards Asia in summer (Fluteau et al., 1999; Ramstein et al., 1997; Z. Zhang et al., 2014;
521 Sarr et al., 2022). Under Oligocene conditions, the uplift of the peripheral Tian Shan, Pamir
522 and northeastern portions of the TP has also been shown to promote inland Asian aridity,
523 in contrast to the sole uplift of the central TP (R. Zhang, Jiang, & Zhang, 2017). Under late
524 Eocene conditions, the latitude at which the proto TP uplifts significantly and non-linearly
525 impacts East Asian climate; an uplift in the tropics ($\sim 11^\circ\text{N}$) induces precipitation on the TP
526 foothills but aridification in most of China, whereas an uplift at its modern latitude ($\sim 26^\circ\text{N}$)
527 increases moisture advection to eastern China and aridification in inland Asia (R. Zhang et
528 al., 2018).

529 Paleoclimate modeling offers a contrasted view regarding Eocene climate, with some
530 studies that simulate the presence of monsoonal climates at that time (Huber & Goldner,
531 2012; Licht et al., 2014; Z. Zhang et al., 2022), and others that do not (Tardif et al.,
532 2020; Z. Zhang et al., 2012; R. Zhang et al., 2018). Discrepancy among simulations can be
533 attributed to many differences in model structure, resolution, parametrization and setting
534 of boundary conditions, among which the choice of paleogeographic reconstruction is a key
535 aspect. Indeed, many features of Eocene paleogeography remain highly controversial, such as
536 the height of the incipient Tibetan topography, the shape of the Indo-Asian collision zone,
537 the height of peripheral landforms, or the land-sea distribution. Paleoclimate modeling
538 has nevertheless emphasized the importance of geography, rather than $p\text{CO}_2$ variations
539 or far-field ice-sheets effects, as the main driver of both SAM and EAM establishment and
540 intensification on long time scales (Farnsworth et al., 2019; Thomson et al., 2021). Accurate
541 paleogeographic constraints as well as a higher number of sensitivity experiments in a paleo
542 framework are therefore needed, and this is what we intend to contribute with this study.

543 **2.4 Summary: a diachronous establishment of SAM and EAM seasonal** 544 **features, the influences of geography and topography and remaining** 545 **uncertainties**

546 The past decade has welcomed a large amount of new data based on fossil material
547 and sedimentary archives, both onshore and offshore. The onset of the SAM, EASM and
548 EAWM and their evolution are now clearly shown to be diachronous and is tightly linked to
549 the evolution of land-sea distribution, topography and global climate over long time scales.
550 Some questions, nevertheless, remain to be answered. First, it is unclear whether Paleogene
551 records of highly seasonal precipitation at low latitudes ($< 20^\circ\text{N}$) describe a monsoon in
552 the strict sense, given that no wind proxies currently exist for this period and that Eocene
553 paleoclimate modeling studies propose widely diverging scenarios. CLAMP paleobotani-
554 cal analyses provide interesting insights on this point. They generally show that, although
555 strong precipitation seasonality is likely present since the Paleogene in broad parts of South-
556 eastern Asia (Bhatia, Khan, et al., 2021; Spicer et al., 2017; Herman et al., 2017), leaves did
557 not develop the morphological features characteristic of plants growing in present-day SAM
558 or EAM regions until the middle Miocene (~ 13 Ma) (Spicer et al., 2017; Bhatia, Srivas-
559 tava, et al., 2021). Instead, Paleogene Asian floras display a signature typical of the regions
560 dominated by the ITCZ seasonal migration, also referred to as the Indonesian-Australian
561 monsoon. The reorganization from an ITCZ-dominated to a monsoonal wind circulation
562 pattern may have initiated in the Oligocene (~ 28 - 23 Ma, Fig. 2), according to fossils from
563 northeastern India exhibiting a mixture of SAM and ITCZ leaf signatures (Spicer et al.,
564 2017). These typical monsoonal signatures in floras were likely driven by a combination
565 of both biotic and abiotic factors, although the CLAMP method is unable to disentangle
566 the forcing factors responsible for these specific signatures. They do, however, add to the
567 body of evidence suggesting that precipitation seasonality may have been established prior
568 to typical monsoonal wind circulation.

569 Second, although modeling studies have started to explore the effects of localized
 570 mountain ranges on Asian climate in a paleo context, there is plenty of room for improve-
 571 ment. For example, the climatic impact of these landforms have often been investigated
 572 simultaneously in a single climate simulation (e.g. the uplift of the Tian Shan and Mongo-
 573 lian orogens), though the main uplift episodes of these landforms may not be coeval (see
 574 section 3.1.2). Various hypotheses remain to be tested, such as identifying the drivers of the
 575 Siberian High development, and its impact on inland Asian aridity. Indeed, the presence of
 576 loess-like deposits since the Eocene in the Xining Basin were tentatively explained by the
 577 presence of an active Siberian High at that time (Meijer et al., 2021; Licht et al., 2014).
 578 This questions whether the Tian Shan and/or Mongolian orogens are as important for this
 579 wide anticyclone as predicted by modeling experiments, since these landforms are thought
 580 to have uplifted later, in the Oligocene to late Miocene (see section 3.1.2). In addition, the
 581 notion of elevation thresholds is a key point to tackle, as strongly non-linear responses of
 582 atmospheric circulation with respect to this parameter are expected. These considerations
 583 highlight the need for an accurate representation of Asian paleogeographic evolution in order
 584 to better understand monsoon history over long time-scales.

585 **3 Cenozoic paleogeographic evolution**

586 Although presenting a full literature review of paleogeographic evolution throughout
 587 the Cenozoic for the whole region of interest is outside the scope of this study, this section
 588 aims at providing an overview of the main features and persistent uncertainties regarding
 589 the paleogeographic evolution during the Cenozoic in our region of interest. This allows
 590 us to justify which sensitivity tests were performed on specific geographic units (Fig. 3),
 591 further introduced in section 4.2.1.

592 **3.1 Indo-Asia collision and Asian topography evolution**

593 The initiation of the Indo-Asian collision, marking the closure of the Neotethys Ocean,
 594 is dated around ~ 58 Ma based on sedimentological and paleomagnetic evidence (van Hins-
 595 bergen et al., 2019; Ingalls et al., 2016). The morphology of the *Greater India* portion (i.e.
 596 northern India) before the collision remains unclear. Depending on the collision scenario
 597 considered (see Kapp and DeCelles (2019); Poblete et al. (2021); J. R. Ali and Aitchison
 598 (2005) for reviews), it is represented as fully emerged (Ingalls et al., 2016; C. Wang et al.,
 599 2014), partially flooded or divided into two blocks separated by an oceanic basin until the
 600 middle-late Eocene (van Hinsbergen et al., 2012, 2019; W. Huang et al., 2015). From the
 601 Eocene onwards, the progressive migration of India to the north, its indentation into the
 602 Asian continent, and its counterclockwise rotation (Molnar et al., 2010) trigger widespread
 603 orographic changes in Asia, which are summarized below. The most important of these
 604 events is the TP and Himalayas uplift, and the growth of peripheral mountain ranges such
 605 as the Pamir, Tian Shan and the Mongolian Plateau.

606 **3.1.1 Himalayas-Tibetan Plateau uplift history**

607 The early uplift history of the Tibetan Plateau is highly debated. Oxygen isotope paleo-
 608 oaltimetry studies suggest that the Gangdese (Southern TP, Lhasa terrane) and Qiangtang
 609 mountains (Central TP) were already as high as ~ 4000 - 5000 m during the early Eocene
 610 (Rowley & Currie, 2006; L. Ding et al., 2014; Xu et al., 2013; Xiong et al., 2020; C. Wang et
 611 al., 2014). The robustness of this method is however questioned by isotope-enabled climate
 612 models, which demonstrate that factors other than elevation affect the $\delta^{18}\text{O}$ precipitation
 613 signature, including air mass provenance, climate, or water recycling (Poulsen & Jeffery,
 614 2011; Botsyun et al., 2016). A revised TP paleo-elevation of most likely lower than ~ 3000
 615 m in the Oligocene has therefore been suggested (Botsyun et al., 2019). The presence of
 616 frost-intolerant fossil flora assemblages in the central TP in the middle Eocene (T. Su et al.,
 617 2020) and late Oligocene (T. Su, Farnsworth, et al., 2019), as well as clumped isotope mea-

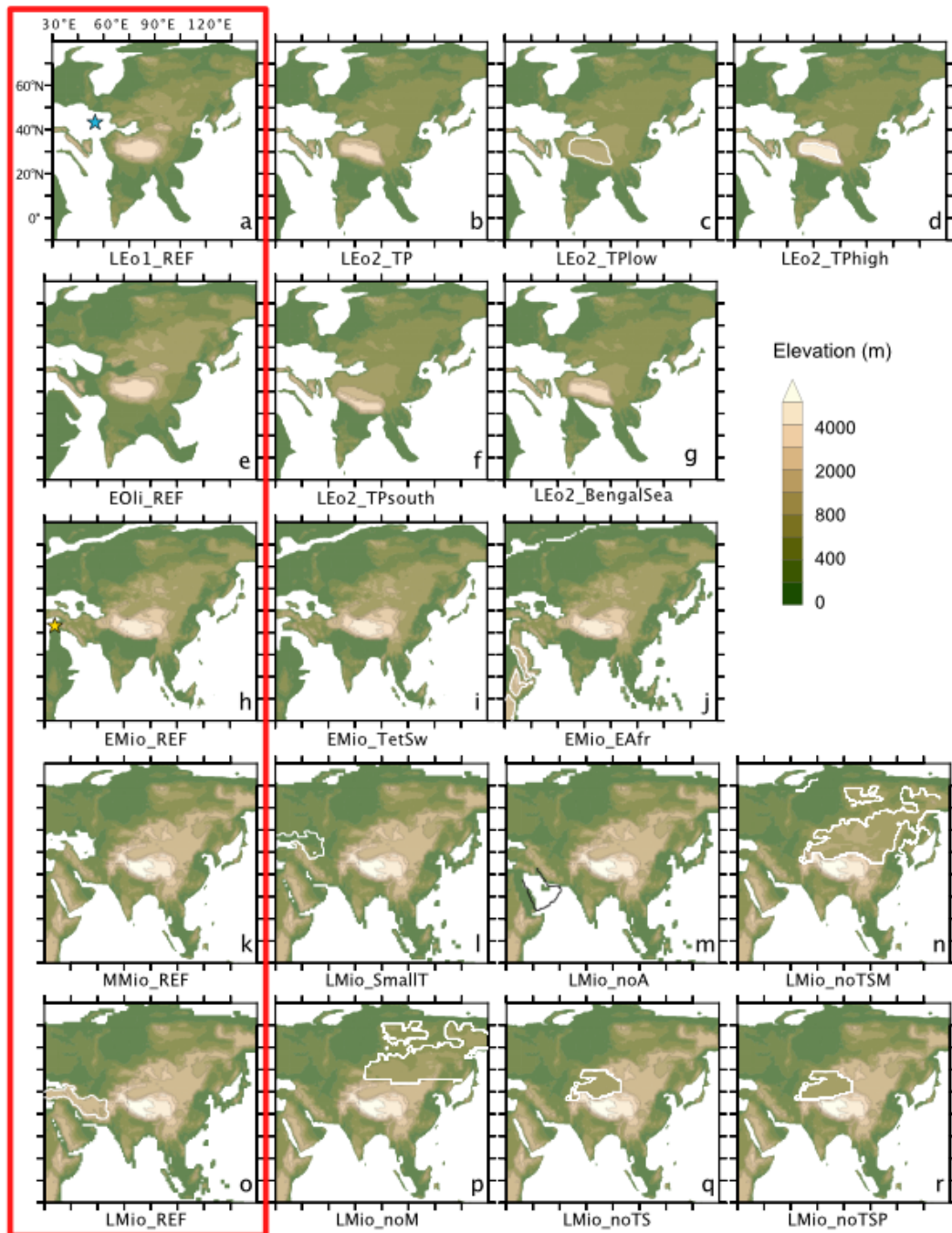


Figure 3. Paleogeographic configurations used in this study for the reference experiments (red box) and alternative configurations used for sensitivity tests. Blue star in (a) highlights the Paratethys Sea location, yellow star in (h) highlights the location of the Tethyan Seaway.

618 surements (Xiong et al., 2022) advocating for a subtropical climate in this region, also seem
619 incompatible with a TP exceeding 4000 m. Therefore, a more complex morphology for this
620 proto TP has been proposed, suggesting the presence of a low-elevation (~ 1500 m) valley
621 dividing the almost fully uplifted (~ 3000 - 4000 m) Lhasa and Qiangtang terranes until the
622 late Oligocene (T. Su, Farnsworth, et al., 2019; Xiong et al., 2020; Spicer et al., 2020; Xiong
623 et al., 2022). In the periphery of the proto TP, data collected from different basins offer
624 contradictory interpretations. In southeastern Tibet, at the extremity of the Qiangtang ter-
625 rane, paleo-elevation calculated using the CLAMP method suggests that the Markam Basin
626 was already high in the late Eocene (~ 3000 m) and could have reached its modern elevation
627 (~ 3900 m) by the earliest Oligocene (T. Su, Spicer, et al., 2019). Alternately, paleo-elevation
628 based on oxygen isotopic measurements of the nearby Jianchuan Basin (part of the same
629 terrane) could not have exceeded ~ 1200 m in the late Eocene (Gourbet et al., 2017). The
630 northern TP is proposed to have remained relatively low (< 2000 m) in the Eocene, before
631 uplifting in the Oligocene or the early Miocene, based on isotopic paleoaltimetry from the
632 Hoh Xil Basin (C. Wang et al., 2014). An early uplift of the northeastern TP has been
633 proposed as early as the late Eocene by increased coniferous pollen proportion in the Xining
634 Basin (Hoorn et al., 2012), although global cooling and the Paratethys Sea retreat may also
635 have promoted coniferous trees expansion in this region, without uplift (Barbolini et al.,
636 2020).

637 The history of the TP build-up from the Miocene onwards is less controversial. The
638 Central TP is thought to have reached modern elevation by the early Miocene, while the
639 northern TP uplift was completed by the late Miocene (C. Wang et al., 2014). Stratigraphy
640 and detrital zircon analyses indicate that the western TP (Pamir-Karakoram-Hindu Kush)
641 may have undergone several phases of uplift between the mid-Eocene to latest Miocene
642 (Bershaw et al., 2012; L. Li et al., 2021; Blayney et al., 2016; Carrapa et al., 2015; D. Liu et
643 al., 2017). Finally, the Himalayas start uplifting in the early Miocene (~ 20 Ma) and reach
644 their modern elevation by the mid-late Miocene (~ 15 Ma) (Gébelin et al., 2013; L. Ding et
645 al., 2017; Xu et al., 2018; C. Wang et al., 2014; Webb et al., 2017).

646 *3.1.2 Inland Asia and Myanmar mountain building*

647 Asian terranes located in the vicinity of the Himalaya-TP complex are impacted by the
648 Indo-Asian collision. In Myanmar, the Indo-Burman ranges built up in a three-step process,
649 in the late Eocene, at the Oligo-Miocene boundary and Pliocene respectively (Najman et
650 al., 2020; Morley, 2018; Maurin & Rangin, 2009; Westerweel et al., 2020; Licht et al., 2018),
651 as a result of the progressive indentation of the Burma block into the eastern Himalayan
652 collision zone. The Sino-Burman Ranges, which inherit old landforms from previous colli-
653 sions between Indochina and Sibumasu terranes (Metcalf, 2013), experienced major uplift
654 in the mid-late Miocene (~ 13 - 9 Ma) (Cook & Royden, 2008; Clark et al., 2005), as a result
655 of the eastward expansion of the Tibetan Plateau by crustal flow.

656 North of the TP, the collision propagates through reactivated pre-existing tectonic
657 structures and triggers the uplift of the inland Asian orogenic belt: the Tian Shan and the
658 Mongolian (Altai, Hangay and Sayan) landforms (Jolivet et al., 2010). The southwestern
659 and Central Tian Shan uplift initiation is very loosely constrained, either in the middle to
660 late Miocene (~ 15 Ma, (Käbner et al., 2016)) or during the late Oligocene to early Miocene
661 (~ 25 Ma) (Bande et al., 2017; Macaulay et al., 2016, 2014; D. Liu et al., 2017). The
662 northeastern Tian Shan, together with the Sayan and Altai regions (in western Mongolia),
663 likely remained quiescent until the late Miocene (Bullen et al., 2003; Caves Rügenstein et al.,
664 2017). After a pulse of uplift in the latest Miocene (~ 8 Ma) for the whole Tian Shan, Sayan
665 and Altai mountains (W. Yuan et al., 2006; Caves Rügenstein et al., 2017; Charreau et al.,
666 2005), regional landforms probably reached their modern elevation after a final Pliocene
667 uplift phase (~ 5 - 3 Ma, (Bullen et al., 2003; Caves Rügenstein et al., 2014; De Grave et al.,
668 2007, 2009; Jolivet et al., 2007; Vassallo et al., 2007)). The Hangay Dome uplift (in central
669 Mongolia) began in the mid-Oligocene (Caves Rügenstein et al., 2014; Cunningham, 2001),

670 but the date of completion of the uplift remains debated, either in the mid-Miocene (~ 13
671 Ma, (Smith et al., 2016)), or the Pliocene (~ 3 Ma, (Yarmolyuk et al., 2008)).

672 **3.2 Evolution of the Peri-Tethys and Middle East region under the inter-** 673 **play of tectonics and global sea level changes**

674 Throughout the Cenozoic, sea level fluctuations in a context of tectonic convergence
675 have led to a profound paleogeographic reorganization and a general increase in continen-
676 tality of the regions encompassing the Mediterranean Sea, Middle East and inland Asia.

677 **3.2.1 Retreat of the Paratethys Sea and closure of the Neotethys Ocean**

678 During the Paleocene-Eocene, Eurasia was largely flooded by the proto Paratethys, an
679 epicontinental sea connected to the Arctic Ocean via the Turgai Strait and to the Neotethys
680 Ocean (Meulenkamp & Sissingh, 2003; Golonka, 2009). Paleoenvironmental analyses suggest
681 a maximal extension of the proto Paratethys Sea reaching the Tajik and Tarim Basins in
682 inland Asia at the Paleocene-Eocene transition (~ 56 Ma), followed by a long-term westward
683 retreat punctuated by marine transgressions of decreasing magnitude (Kaya et al., 2019;
684 Bosboom et al., 2014b, 2017; Carrapa et al., 2015). In Central Asia, the shrinkage of
685 the proto Paratethys Sea during the Eocene is attributed to far-field effects of the Indo-
686 Asia collision and to the early indentation of the Pamir and TP, leading to the progressive
687 infilling of the basins with sediments (Kaya et al., 2019; Carrapa et al., 2015; D. Liu et
688 al., 2017). The onset of the Antarctic ice-sheet at the EOT (~ 33.5 Ma) resulted in a
689 sea-level drop of ~ 70 m (Miller et al., 2020)), which drastically reduced the extent of the
690 Paratethys and favored its isolation (Kaya et al., 2019; Bosboom et al., 2014b, 2017). Water
691 exchanges between the Paratethys and neighboring oceans were progressively restricted, as
692 indicated by the increasing divergence between the $\delta^{18}\text{O}$ and $\delta^{13}\text{C}$ signatures of Paratethys
693 foraminifera shells and the other oceanic signals at that time (Ozsvárt et al., 2016). The
694 Tethyan Seaway, connecting the Indian and Atlantic Oceans, remained fully open before the
695 Miocene (Straume et al., 2020). ϵNd isotope data from foraminifers suggest that it became
696 strongly restricted around ~ 22 Ma (Bialik et al., 2019), with intermittent periods of closure,
697 as indicated by evidence of mammal exchanges between Eurasia and Africa across a land
698 bridge (Rögl, 1999; Harzhauser & Piller, 2007). The Tethyan Seaway permanently closed at
699 ~ 14 Ma, due to the combined effect of Arabian-Eurasian plate collision and glacio-eustatic
700 sea level fall associated with cooling following the Mid-Miocene Climatic Optimum (Bialik
701 et al., 2019). Until the late Miocene, the Paratethys Sea experienced phases of transgression,
702 extending as far as $\sim 60^\circ$ E, and regression that may have reduced its surface by up to 70%
703 (Palcu et al., 2021), thus highly modulating Eurasian continentality.

704 **3.2.2 Middle-East: Anatolian-Iranian Plateau, Zagros and Alborz Moun-** 705 **tains uplift**

706 During the Cenozoic, the Middle-East experienced multiple changes in land-sea distri-
707 bution and topography, forced by the collision of the Arabian plate with Eurasia that drove
708 the uplift of the Zagros Mountains and of the Iranian Plateau. The exact timing of the
709 Arabia-Eurasia collision in eastern Anatolia remains highly debated, with estimated dates
710 ranging from the Eocene-Oligocene (Karaođlan et al., 2016; Darin et al., 2018; McQuarrie
711 & Hinsbergen, 2013; Pirouz et al., 2017), the early Miocene (Okay et al., 2010; Gülyüz et
712 al., 2020), to the late Miocene (H. Su & Zhou, 2020; Z. Zhang et al., 2017). Most stud-
713 ies however propose an early Miocene age (~ 20 Ma) for the hard collision related to the
714 arrival of thick Arabian crust along the Bitilis suture zone (Okay et al., 2010; Cavazza et
715 al., 2018; Gülyüz et al., 2020) and a Miocene age for the uplift of most landforms (Zagros
716 and Alborz mountains, Anatolian-Iranian Plateau). After the collision, the Zagros oro-
717 gen builds up during three successive pulses occurring within the last ~ 20 Ma (Agard et
718 al., 2011; Mouthereau, 2011). Field geology, stable isotopes and thermochronology suggest

719 that the Alborz mountains uplift (north of the Zagros) occurred during the middle Miocene
 720 (~ 17.5 -13 Ma) (Ballato et al., 2010, 2015) and may have continued until the latest Miocene
 721 (Mouthereau et al., 2012). A Miocene age for the initiation of the eastern Anatolian-Iranian
 722 Plateau growth is also suggested, based on its youngest marine unit (~ 17 Ma) (Gülyüz
 723 et al., 2020) and apatite fission-track data (18-13 Ma) (Okay et al., 2010; Karaođlan et
 724 al., 2016). Stratigraphic evidence suggests an uplift phase of the eastern Anatolian-Iranian
 725 Plateau between 15 and 12 Ma due to crustal shortening and thickening (Mouthereau et al.,
 726 2012). In contrast, numerical simulations suggest that the final buildup of the Plateau is
 727 only reached during the late Miocene (~ 7 -10 Ma), likely sustained by slab break-off, mantle
 728 flow disruption and associated changes in dynamic topography, and followed by isostatic
 729 adjustment (François et al., 2014).

730 **3.3 East Africa and Arabian Peninsula evolution**

731 While much attention has been paid to the Eastern African topography evolution in the
 732 Neogene due to its implication for early hominins development, its history fits into a broader
 733 paleogeographic context rooted in the Paleogene (see Couvreur et al. (2021); Guillocheau et
 734 al. (2018) for a synthesis). Landforms in East Africa (Kenyan and Ethiopian plateaus) de-
 735 veloped during the late Cenozoic, triggered by a combination of tectonics, basaltic flooding,
 736 and large wave-length deformation related to the African superswell activity (Moucha &
 737 Forte, 2011; Faccenna et al., 2019; Roberts et al., 2012). Uplift in the Ethiopian region be-
 738 gan during the Eocene, with a doming event sustained by dynamic topography (Roberts et
 739 al., 2012; Faccenna et al., 2019) that then propagated to Kenya during the middle Miocene.
 740 In the early Oligocene, basaltic flooding in Ethiopia is thought to have contributed to the
 741 formation of these large-scale elevated features (Sembroni et al., 2016). Rifting initiated
 742 during the middle Miocene with the main uplift of rift shoulders (Wichura et al., 2015).
 743 Overall, past elevations during the Cenozoic are poorly constrained in East Africa, but
 744 modern elevations were most likely reached by the late Miocene to early Pliocene (Couvreur
 745 et al., 2021).

746 The Arabian Peninsula records successive marine and freshwater environments from
 747 the early Oligocene to the late Miocene, as indicated by paleo-ichthyofaunas (Otero & Gayet,
 748 2001). Before the Neogene, the Arabian plate is assumed to have been flat and at low
 749 elevation (Daradich et al., 2003) and thus particularly sensitive to sea-level changes. It was
 750 therefore largely submerged during the Eocene, and its southwestern part became partially
 751 emerged after the sea-level fall at the EOT (Barrier et al., 2018). During the Miocene, the
 752 Arabian plate was tilted when transiting over the East-Africa mantle plume (Vicente de
 753 Gouveia et al., 2018), leading to the uplift of the Red Sea margin, and the flooding of its
 754 northeastern corner, due to mantle convective drawdown (Daradich et al., 2003; Moucha
 755 & Forte, 2011). This mechanism promoted temporary transgression phases in the subdued
 756 northeastern region in early Miocene times (Barrier et al., 2018), until its full emergence
 757 in the late Miocene, possibly favored by global sea-level fall after the mid-Miocene Climate
 758 Transition (Golonka, 2009; Harzhauser & Piller, 2007; Miller et al., 2020).

759 **4 Materials and Methods**

760 **4.1 IPSL-CM5A2 model**

761 We perform simulations with the IPSL-CM5A2 Earth System Model (Sepulchre et
 762 al., 2020), an updated version of the IPSL-CM5A model (Dufresne et al., 2013) designed
 763 for deep-time paleoclimate simulations. It is composed of the atmospheric model LMDz5A
 764 (Hourdin et al., 2013), the land surface and vegetation model ORCHIDEE (Krinner et al.,
 765 2005) and the oceanic model NEMO (v3.6) (Madec, 2016) that also includes the LIM2 sea-
 766 ice model (Fichefet & Maqueda, 1997). The OASIS coupler ensures synchronization between
 767 the different model components (Valcke et al., 2006). The atmospheric model has a nominal
 768 horizontal resolution of 96x95 grid points (3.75° in longitude by 1.9° in latitude) with 39

769 irregularly distributed vertical levels from the surface to 40 km high. The ORCHIDEE model
 770 is coupled with LMDZ5a and redirects runoff water towards the ocean. The vegetation
 771 cover is represented through 11 Plant Functional Types, including one describing bare soil.
 772 NEMO solves ocean dynamics and thermodynamics equations on a tripolar grid, with two
 773 poles located below continental masses in the Northern Hemisphere, thereby avoiding North
 774 Pole singularity in the ocean (Madec & Imbard, 1996). It has a nominal resolution of 2° by
 775 2° refined up to 0.5° in the equatorial region, with 31 vertical levels, the thickness of which
 776 ranges from 10 meters near the surface to 500 meters in the deep ocean. Full description of
 777 IPSL-CM5A2 can be found in Sepulchre et al. (2020); Dufresne et al. (2013). IPSL-CM5A2
 778 has been previously used for paleoclimatic simulations of the Miocene (Burls et al., 2021;
 779 Sarr et al., 2022; Pillot et al., 2022) and the Eocene (Tardif et al., 2020, 2021; Toumoulin
 780 et al., 2022, 2020; Barbolini et al., 2020). The ability of the model to simulate the modern
 781 Asian climate has previously been described (Sepulchre et al., 2020; Tardif et al., 2020)
 782 and compared to observations (SI Fig. 14). While general atmospheric circulation patterns
 783 are well reproduced, IPSL-CM5A2 overall underestimates precipitation amounts and delays
 784 inland monsoonal precipitation onset by about a month, which are characteristics shared
 785 with the earlier IPSL-CM5A version of the model (Sepulchre et al., 2020).

786 4.2 Numerical simulations design

787 Simulations presented in this study are performed with paleogeographic configurations
 788 used in previous work, presented in Figure 3 and Table 1 and detailed below. The reference
 789 experiments have been run for 3000 years and the deep ocean has reached quasi-equilibrium
 790 after ~ 2000 years of integration. Sensitivity experiments are restarted from their reference
 791 experiment and run for 300 to 500 years until upper ocean equilibrium. Model outputs are
 792 averaged over the last 50 years of each simulation.

793 4.2.1 Paleogeographic reconstructions and sensitivity tests

794 Our late Eocene reference paleogeography (**LEo1_REF**, ~ 40 Ma, Fig. 3 a), previously
 795 introduced in Tardif et al. (2020), displays a fully emerged *Greater India* and a ~ 3000 m
 796 elevation TP. The proto Paratethys Sea fills the Tarim Basin, the Turgai Strait is closed and
 797 East African topography is low. Considering the ongoing debate surrounding the extension
 798 of India and TP morphology at that time, other configurations are tested: **LEo2_TP** (Fig. 3
 799 b) is an alternative late Eocene paleogeography, with a slightly different TP shape obtained
 800 with the "double collision model" (Poblete et al., 2021), from which sensitivity tests with
 801 a lower (~ 800 m, **LEo2_TP_{low}**, Fig. 3 c) and a higher TP (~ 4500 m, **LEo2_TP_{high}**,
 802 Fig. 3 d) are derived. Two additional tests are performed. The first exhibits a TP located
 803 more to the South (**LEo2_TP_{south}**, Fig. 3 f) and is obtained with the collision model
 804 from Jagoutz et al. (2015). The second features the presence of a remaining inlet between
 805 India and continental Asia (**LEo2_BengalSea**, Fig. 3 g), according to van Hinsbergen et al.
 806 (2012, 2019). The early Oligocene simulation (**Eoli_REF**, ~ 33 Ma, previously introduced
 807 in Barbolini et al. (2020)) is designed to represent the Asian paleogeography right after the
 808 Eocene-Oligocene Transition (Fig. 3 e). The late Eocene paleogeography of LEo1_REF is
 809 used as a base, on which the sea level is eustatically lowered by 70 m (Miller et al., 2020),
 810 to account for a modern-sized ice sheet over Antarctica, as an end-member scenario. This
 811 leads to the emergence of continental portions in Arabia and North Africa and the drying
 812 of the Tarim Basin and lowlands north of the Turgai Strait, which all act to significantly
 813 increase Asian continentality. The former shallow connection between the Paratethys and
 814 the Tethys ceases in the Pamir-Zagros region at that time.

815 The early Miocene paleogeography (**EMio_REF**, ~ 20 Ma, Fig. 3 h), is from Poblete
 816 et al. (2021) and was previously introduced in Sarr et al. (2022) and Burls et al. (2021).
 817 It displays an Indian subcontinent translated 5° further north compared to the Eocene
 818 and an uplifted Central TP close to its modern elevation (~ 5000 m), whereas western and
 819 northeastern TP portions are lower (2000-3000 m). The Tethyan Seaway that previously

Table 1. List of reference simulations (bold) and sensitivity experiments used in this study. Abbreviations stand for East Antarctic Ice Sheet (EAIS), Antarctic Ice Sheet (AIS) and Greenland + Antarctic Ice Sheet (G+AIS). The last column details the paleogeographic configurations, highlighting the pairs of simulations that can be compared. For example, the effect of $p\text{CO}_2$ halving in the Eocene is obtained with the "LEo1_REF - LEo1_2X" anomaly.

Simulation	$p\text{CO}_2$	Ice sheets	Paleogeography
LEo1_REF	1120	-	from (Tardif et al., 2020)
LEo2_TP	1120	-	from (Poblete et al., 2021)
LEo2_TPlow	1120	-	from LEo2_TP, TP lowered to 800 m
LEo2_TPhigh	1120	-	from LEo2_TP, TP raised to 4500 m
LEo2_TPsouth	1120	-	from LEo2_TP, TP shifted to the South (Poblete et al., 2021)
LEo2_BengalSea	1120	-	from LEo2_TP, with a Bengal Sea (Poblete et al., 2021)
LEo1_2X	560	-	from LEo1_REF, $p\text{CO}_2$ halved to 560 ppm
Eoli_REF	560	AIS	from LEo1_REF, 70 m sea level drop (Barbolini et al., 2020)
EMio_REF	560	EAIS	from (Poblete et al., 2021)
EMio_TetSw	560	EAIS	from EMio_REF, open Tethyan Seaway (120 m depth)
EMio_EAfr	560	EAIS	from EMio_REF, modern East African landforms
MMio_REF	560	AIS	from (Sarr et al., 2022)
LMio_smallT	560	AIS	from MMio_REF, reduced Paratethys
LMio_noAr	560	AIS	from LMio_smallT, immersed Arabia
LMio_noM	560	AIS	from LMio_smallT, Mongolia lowered to 800 m
LMio_noTS	560	AIS	from LMio_smallT, Tian Shan lowered to 800 m
LMio_noTSM	560	AIS	from LMio_smallT, Tian Shan+Mongolia lowered to 800 m
LMio_noTSP	560	AIS	from LMio_smallT, Tian Shan+Pamir lowered to 800 m
LMio_REF	560	G+AIS	from (Sarr et al., 2022)
LMio_1.5X	420	G+AIS	from LMio_REF, $p\text{CO}_2$ lowered to 420 ppm

820 connected the Mediterranean Sea and the Indian Ocean is closed, but a shallow sea persists
 821 at the location of the Arabian Peninsula. The alternative configuration **EMio_TetSw**, with
 822 a 120 m deep Tethyan seaway, is tested (Fig. 3 i). Considering the large uncertainties related
 823 to East African elevation, we also test the impact of a full uplift of this region as early as
 824 the early Miocene with the **EMio_EAfr** experiment (Fig. 3 j).

825 The mid and late Miocene paleogeographies are based on the PRISM4 reconstruction
 826 (Dowsett et al., 2016) used in PlioMIP2 (Haywood et al., 2020) with manual modifica-
 827 tions including the Australian continent shifted southward compared to present day and an
 828 emerged Sunda Shelf (Torsvik et al., 2008; Hall et al., 2012) (see Sarr et al. (2022) for details).
 829 In the middle (**MMio_REF**, ~12 Ma, Fig. 3 k) and late Miocene (**LMio_REF**, ~8 Ma, Fig.
 830 3 o) reference paleogeographic configurations, the Himalayas, Tibetan Plateau, Myanmar,
 831 inland Asia and East African landforms have reached their present-day configuration (Fig.
 832 3). In the mid-Miocene, the elevation of the Anatolian-Iranian orogen is half (~1000 m) that
 833 of present-day and the Paratethys Sea extends up to 60°E (**MMio_REF**), while by the late
 834 Miocene (**LMio_REF**), the Paratethys is strongly reduced and the Anatolian-Iranian land-
 835 forms have reached their modern elevation. An intermediate mid-late Miocene reconstruc-
 836 tion is tested, in which the impact of a Paratethys retreat is investigated (**LMio_smallT**,
 837 Fig. 3 l). Sensitivity tests are also performed on inland Asian landforms, by lowering to
 838 ~800 m the Mongolian Plateau (**LMio_noM**, Fig. 3 p), Tian Shan (**LMio_noTS**, Fig. 3
 839 q), Mongolia and Tian Shan (**LMio_noTSM**, Fig. 3 n), and finally, Tian Shan and Pamir
 840 (**LMio_noTSP**, Fig. 3 r). Additionally, **LMio_noAr** (Fig. 3 m), displaying an almost
 841 fully flooded Arabian Peninsula, is designed to account for the high sensitivity of this region
 842 to sea level fluctuations during that period. Note that **LMio_smallT** is the paleogeography
 843 to which all other late and middle Miocene simulations can be compared to.

844 4.2.2 *pCO₂, ice-sheets, solar constant and vegetation*

845 CO₂ concentrations vary from 1120 ppm in the late Eocene to 560 ppm in the late
 846 Miocene (Table 1) (Foster et al., 2017; Rae et al., 2021) and other greenhouse gases are
 847 maintained at pre-industrial values. Acknowledging uncertainties regarding precise *pCO₂*
 848 concentrations during the Cenozoic, we perform two additional sensitivity tests on this
 849 parameter by prescribing 560 ppm in a late Eocene simulation (**LEo1.2X**) and 420 ppm
 850 in a late Miocene simulation (**LMio.1.5X**). Late Eocene experiments are considered ice-
 851 free, as *pCO₂* is above the threshold for permanent Antarctic glaciation (Ladant et al.,
 852 2014; DeConto & Pollard, 2003). Unipolar glaciation over the Antarctic continent is used
 853 for the Oligocene, early and mid-Miocene, and both Greenland and Antarctic ice-sheets
 854 are present in late Miocene configurations (Bierman et al., 2016). The solar constant is
 855 adjusted (Gough, 1981) and set to 1360.19 W.m⁻² for late Eocene and early Oligocene
 856 simulations, 1362.92 W.m⁻² for early Miocene simulations and 1364.30 W.m⁻² for late and
 857 middle Miocene simulations. Although orbital variations are known to impact monsoonal
 858 circulation (Zhisheng et al., 2015; P. Wang et al., 2005; Tardif et al., 2021), we prescribe
 859 a modern-like orbital configuration in all simulations because this study focuses on the
 860 impact of paleogeography. In the absence of congruent global vegetation reconstructions over
 861 the Cenozoic, all the experiments are forced with prescribed latitudinal bands of idealized
 862 vegetation cover based on modern distribution, as done in previous studies (Tardif et al.,
 863 2020; Laugié et al., 2020).

864 4.3 Monsoon metrics

The evolution of Asian monsoons over time is assessed through specific markers that
 are characteristic of the present-day SAM and EAM, such as precipitation amounts, season-
 ality, and wind direction and strength. The evolution of precipitation seasonality using the
 Monsoon Precipitation Index (MPI) (B. Wang & Ding, 2008) is expressed as follows:

$$\text{MPI} = \frac{\text{Seasonal range of precipitation}}{\text{Mean annual precipitation}}$$

865 where the seasonal range of precipitation is the difference between May to September minus
 866 November to March precipitations. Monsoon-like seasonality is considered to occur if the
 867 seasonal range is superior to 300 mm and more than half of the precipitation falls during the
 868 extended summer season ($MPI > 0.5$). This metric has the benefit of proposing a discrete
 869 metric for seasonality amplitude (from 0 to 1, instead of "with or without" monsoon). It also
 870 imposes that the wet season occur in summer, unlike other existing precipitation metrics
 871 (such as the ratio of the 3 wettest month over the 3 driest month precipitation, commonly
 872 used in paleobotany studies).

873 The wind patterns, described via their shape and strength, are the second fundamental
 874 characteristic that we focus on. First, we track the latitudinal migration of the Somali Jet
 875 over the Arabian Sea (Fluteau et al., 1999) as a proxy for SASM intensity. Second, we use the
 876 Webster-Yang Index (Webster et al., 1998), calculated as the difference between the zonal
 877 component of 850 and 200 hPa winds ($U_{850} - U_{200}$) in the region $0^{\circ}:20^{\circ}N$ to $40^{\circ}E:110^{\circ}E$, to
 878 evaluate the wind shear between the low and high troposphere over India, which describes the
 879 vigor of the SASM zonal circulation. Third, we use the positive thermal anomaly observed
 880 at 300 hPa over northern India in summer as a marker of the deep convection characterizing
 881 the modern SASM (Boos & Kuang, 2010; Acosta & Huber, 2020). This anomaly is due to
 882 the important latent heat release in the high troposphere provoked by the condensation of
 883 moisture in convecting air masses ascending the southern flank of the Himalayas (see Fig.
 884 14 d).

In addition to the precipitation seasonality, we explore the EASM evolution through
 the latitudinal displacement of the Jet Stream with respect to Tibetan and inland Asian
 landforms and with surface wind patterns. The EAWM is tracked principally with the
 evolution of temperature and pressure gradients, leading to the Siberian High formation
 in winter, and of its associated wind patterns. We also use the EAWM index (L. Wang
 & Chen, 2014), that accounts for both the North-South (Siberia-Maritime continent) and
 West-East (Siberia-North Pacific) pressure gradients and is expressed as follows:

$$I_{EAWM} = (2 \times SLP_S - SLP_{NP} - SLP_{MC}) / 2$$

885 where SLP_S , SLP_{NP} and SLP_{MC} is the area-averaged Sea Level Pressure (SLP) over Siberia
 886 ($40^{\circ}:60^{\circ}N$, $70^{\circ}:120^{\circ}E$), North Pacific ($30^{\circ}:50^{\circ}N$, $140^{\circ}E:170^{\circ}W$) and the Maritime continent
 887 ($20^{\circ}S:10^{\circ}N$, $110^{\circ}:160^{\circ}E$), respectively.

888 5 Results

889 For each regional monsoon, we first present the results obtained for the five reference
 890 numerical simulations (red box in Fig. 3). The underlying forcing factors are then explored,
 891 taking advantage of the sensitivity tests summarized in Table 1. The main outcomes in
 892 terms of seasonal winds and precipitations are qualitatively summed up in Table 2.

893 5.1 The South Asian monsoon, controlled by the orography surrounding 894 the Indian Ocean

895 5.1.1 Evolution of spatial and seasonal precipitation patterns

896 In the late Eocene, a wide arid region (< 500 mm/year) spreads from northern In-
 897 dia to north of proto Tibet (Fig. 4 a). The extent of this simulated arid region is most
 898 likely overestimated, which is further discussed in section 6.1. High mean annual precip-
 899 itation amounts (> 3000 mm/yr) are simulated over equatorial regions in southern India
 900 and southeastern Asia. There is no monsoon-like seasonality according to the MPI index in
 901 India, because the rainy season in this region occurs in winter (as previously described in
 902 Tardif et al. (2020)). The precipitation pattern evolves from the early Oligocene onwards,
 903 as the arid region progressively shifts to Arabia and northern Africa (Fig. 4 e, i, m, q).
 904 This allows the penetration of rainfall in summer into southeastern Asia and the onset of a

Table 2. Overview of each tested forcing factor on seasonal precipitation and wind circulation simulated in each region. Abbreviations stand for Transition Area (TA), cardinal directions (E, W, S, N), basins mentioned in Figure 1 (e.g. Tajik Basin, Tjk)

	SAM				EAM				Inland Asia			
	Precipitation		Winds		Precipitation		Winds		Precipitation		Summer	
	Winter	Summer	Seasonality	Summer	Winter	Summer	Seasonality	Summer	Winter	Summer		
No TP (LEo)	~	++			+	--	-	~	+	(W)	~	~
High TP uplift (LEo)	~	+	~		++	+	-				-	~
TP South (LEo)	-	+			~	+	+				~	~
Bengal Sea (LEo)	+	++	-		+	+	~				+	+
CO2 decrease (EOT)	--	++	+(TA)	+	+	~	~	~	+		+	+
CO2 and sea level fall (EOT)	---	+++	+(TA, North. India)	++	--	++	+	+(E)	++(W/NW)		--	+
East Africa uplift (EMio)	+	++	-(India) + (TA, Himalaya)	+++ (Somali Jet)	+	+	-	+(SW)			+	-
Paratethys retreat (LMio)	~	++	+	++	+	+	~	+(SW)			--	~
Arabian peninsula emergence (LMio)	+	+	~	+(Somali Jet)	-	+	+	~	+(NW)		-	-
Iranian uplift (LMio)	--	++	+++	+++ (Somali Jet)	-	+	+				+	++
Mongolia uplift (LMio)	~	~	+		---	~	+++				+(orog.)	++(orog.) -- (Gobi, Takl., TS, Tjk)
TienShan uplift (LMio)	+	~	-		-	~	+	+(S)			+(orog.)	+(orog.)
TienShan+Mongolia a uplift (LMio)	+	~	+		---	~	+++				+(orog.)	+(orog.) -(Takl. Tjk.)
TienShan+Pamir uplift (LMio)	+	+	--	+(Somali Jet)	~	~	~	+(SW)			+(orog.)	++(orog.) -(Tjk)

monsoon-like seasonality in this region, as well as a reinforcement of monsoon-like seasonality in Eastern Asia. Over the course of the Miocene, as India drifts northwards, its southern tip receives less precipitation (~ 1500 mm/yr in the late Miocene, Fig. 4 q) and the intensity and extent of highly seasonal precipitation increases greatly over southern and eastern Asia (red dotted regions in Fig. 4 e, i, m, q). Orographic precipitation over the southern flank of the Himalayas initiates in the mid-Miocene simulation (~ 900 mm/yr, Fig. 4 m) and further increases in the late Miocene simulation (~ 1200 - 1500 mm/yr, Fig. 4 q). These changes in precipitation patterns in both space and time are triggered by a profound reorganization of surface pressure patterns and winds throughout the set of Cenozoic simulations.

5.1.2 Summer pressure and wind pattern reorganization

The summer (June to August, JJA) sea level pressure patterns in Eurasia in the late Eocene experiment (Fig. 4 b) contrast strongly with the modern ones (SI Fig. 14 f). A low-pressure center forms, driven by extreme summer temperature over southeastern Asia (up to 50 °C over *Greater India*, Fig. 4 d) whereas the Paratethys Sea and Neotethys Ocean are the locus of a wide high pressure cell (Fig. 4 b). This pressure pattern induces low tropospheric anticyclonic winds that counteract potential moisture advection from the Indian Ocean towards South Asian regions. From the early Oligocene onwards, the shrinkage of the Paratethys Sea and Neotethys Ocean increases Eurasian continentality and the surface of emerged land, such as Anatolia and Arabia. They become the locus of high summer temperatures (35 - 45 °C, Fig. 4 l, p, t), leading to the progressive widening of the South Asian low-pressure belt, while the Neotethyan anticyclone gradually regresses westward (Fig. 4 f, j, n, r). This low pressure cell reaches its modern-like extent in the mid-Miocene simulation (Fig. 4 n) but a modern-like magnitude (~ 14 hPa over Arabia and northern India) occurs only in the late Miocene simulation (Fig. 4 r, SI Fig. 14).

Mirroring this progressive strengthening and widening of the summer low-pressure belt over south Asia and Arabia, an increasing amount of moisture-loaded air masses are gradually advected from the Indian Ocean towards the continent over the Cenozoic. A weak cross equatorial flow (< 4 m/s, Fig. 4, against ~ 25 m/s today, SI Fig. 14), confined to low latitudes ($< 10^\circ$ N, Fig. 5 a, simulations LEo1_REF and EOli_REF), is simulated over the Arabian Sea in the late Eocene and early Oligocene experiments (Fig. 4 b, f). A mostly zonal proto-Somali Jet, also confined to low latitudes ($< 11^\circ$ N), is simulated in the early Miocene simulation (Fig. 5 b, simulation EMio_REF). From the mid-Miocene onwards, and following the reinforcement of the Asian low-pressure belt, the now fully-formed Somali Jet increases in strength and migrates further north over the Arabian Sea (~ 18 - 24° N) (Fig. 4 n, r, Fig. 5 b, simulations MMio_REF and LMio_REF). The simulated tropospheric circulation above southern Asia is drastically rearranged from the late Eocene to the Miocene simulation, as indicated by the Webster-Yang Index. This index doubles between the late Eocene and the early Oligocene (from ~ 5 to 11 m/s, Fig. 5 c, reference simulations LEo1_REF and EOli_REF) and keeps increasing in the Miocene (from ~ 16 to 21 m/s, Fig. 5 d, simulations EMio_REF, MMio_REF and LMio_REF). Finally, while a heating of the high troposphere (~ 300 hPa) due to deep convection is observed in most experiments (Fig. 4 d, h, l, p, t), this heat anomaly relocates over northern India only in the mid-Miocene experiment, following the increase in summer convective precipitation in this region driven by orographic uplift.

5.1.3 Limited effect of $p\text{CO}_2$ decrease and alternative Eocene Tibetan Plateau configurations on South Asian summer monsoon evolution

The non-linearity in the response of the Somali Jet through time calls for an individual analysis of the different forcing factors between each of these simulations. Our sensitivity experiments reveal the weak sensitivity of the SASM to $p\text{CO}_2$ changes in comparison to paleogeographic forcing. This is true for the late Eocene experiments, in which a change from 1120 ppm to 560 ppm (difference between experiments LEo1_2X and LEo1_REF) only induces minimal variations in the Webster-Yang Index, summer northward ITCZ migration

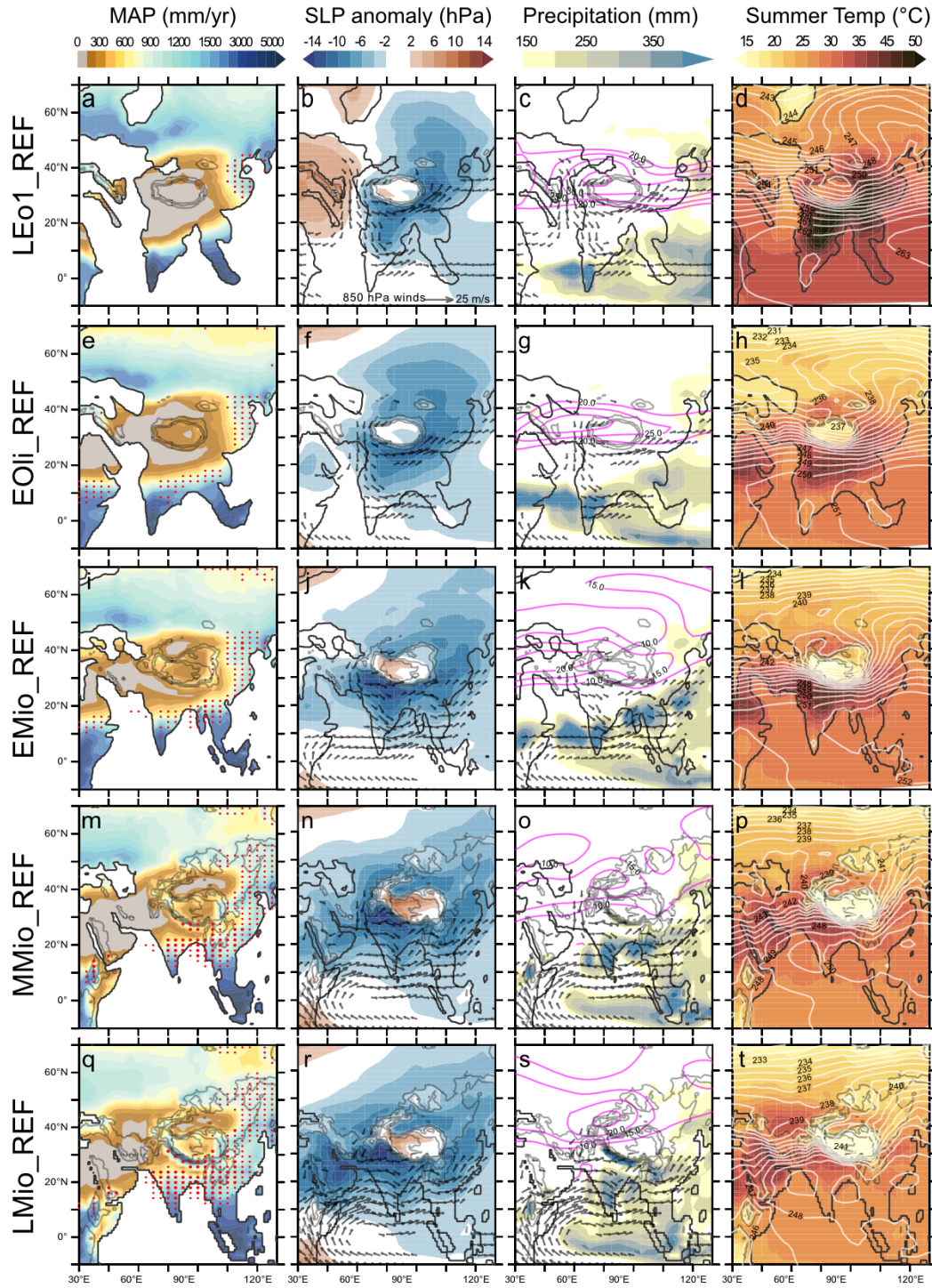


Figure 4. Evolution of summer monsoon diagnostics since the Eocene. **First column:** Mean Annual Precipitation (shading, mm/yr) overlain with regions where the Monsoon Precipitation Index is over 0.5 (thin red dots) and 0.75 (thick red dots); **Second column:** June-August (JJA) normalized Sea Level Pressure (SLP) anomaly defined as the difference between summer SLP and mean annual SLP (shading, hPa) and 850 hPa winds over 4 m/s (vectors); **Third column:** August Jet Stream speed (magenta contour, maximal zonal wind velocity in the mid to high troposphere, in m/s), August monthly precipitation amounts (shading, mm/month) and 850 hPa winds over 4 m/s (vectors); **Fourth column:** JJA mean temperature at 2 m (shading, Celsius) and 300 hPa atmospheric temperature (white contour, Kelvin). On all figure panels, topography is overlain as grey contours, at 1000 m intervals.

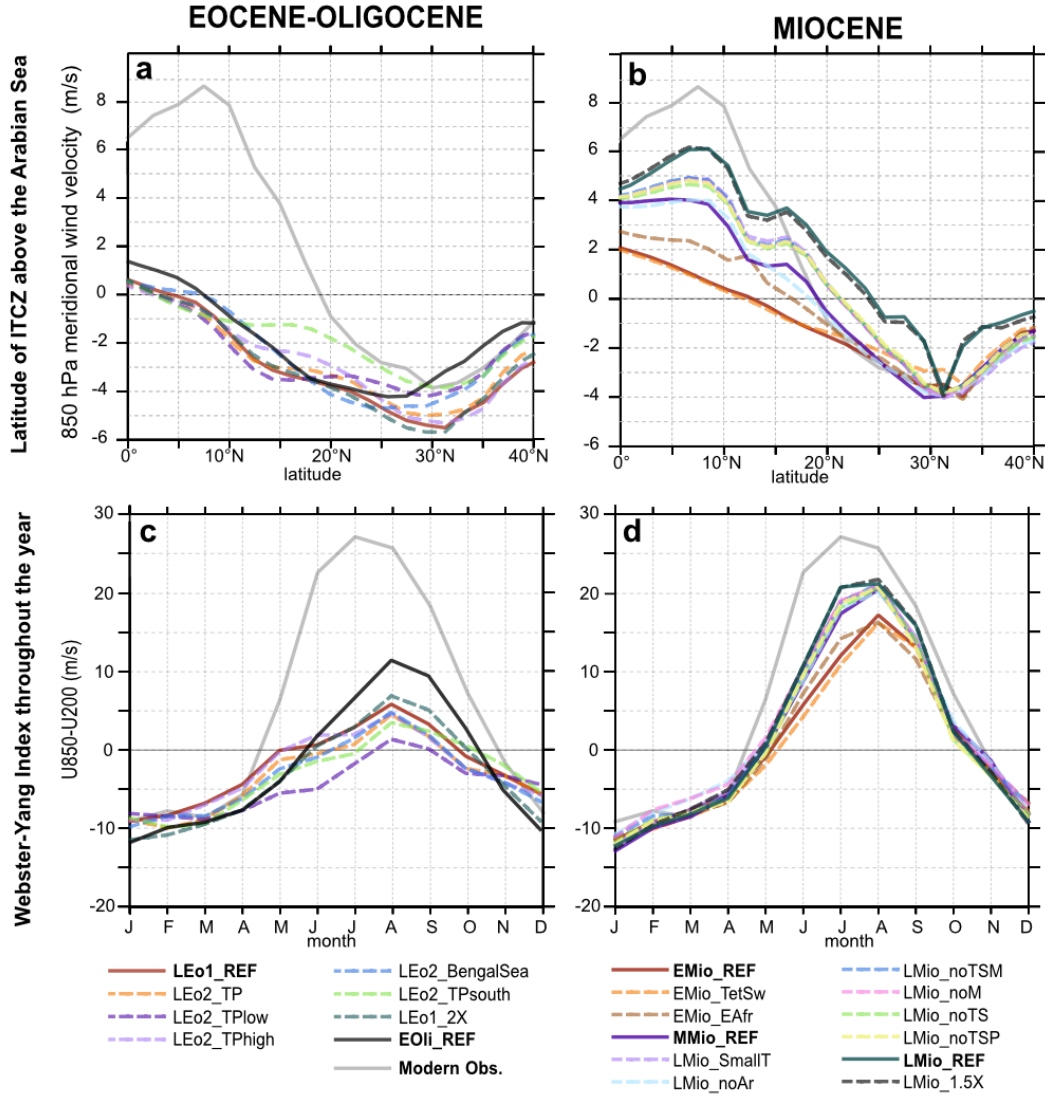


Figure 5. Estimation of the evolution of South Asian monsoon strength in all the simulations via: (a, b) the calculation of the summer (JJA) cross-equatorial flow latitude over the Arabian Sea, after Fluteau et al. (1999) and (c, d) the calculation of the Webster-Yang Index (WYI, 850 hPa minus 200 hPa zonal wind velocity, in the region 0°:20°N ; 40°:110°E, after Webster and Yang (1992)). For better readability, the experiments are split into Eocene-Oligocene (a, c) and Miocene (b, d) simulations. Reference simulations are highlighted in bold characters and continuous lines, while sensitivity tests are in dotted lines.

(Fig. 5 a, c), or monsoon-like seasonality extension (Fig. 7 f). This is also the case for the late Miocene experiments when the $p\text{CO}_2$ is changed from 560 ppm to 420 ppm (difference between experiments LMio_1.5X and LMio_REF in Fig. 5 b, d). The paleogeography of *Greater India* and Tibetan regions have been repeatedly proposed as a driver of monsoon onset or intensification (R. Zhang et al., 2012; Yu et al., 2018; Molnar et al., 1993). While alternative TP configurations lead to slightly different results, their impact on the simulated SASM large-scale wind circulation remains limited (Fig. 5 a, c, Fig. 6). In the late Eocene, increasing TP elevation strengthens the zonal wind shear over India (3000 m, Webster-Yang Index = ~ 6 m/s, for experiment LEO2_TP, Fig. 5 c) with respect to the Eocene experiment with low TP topography elevation (Webster-Yang Index = 1 m/s, LEO2_TPlow). Additionally, the magnitude of the Webster-Yang Index gradually increases with TP latitude, with values of 3 m/s for a southern edge at $\sim 20^\circ\text{N}$ (LEO2_TPsouth), 4 m/s at $\sim 25^\circ\text{N}$ (LEO2_TP), and 6 m/s at $\sim 30^\circ\text{N}$ (LEO1_REF). The presence of a sea inlet flooding *Greater India* in the late Eocene configuration limits the northward migration of the ITCZ in summer (from ~ 7 to 3°N between experiments LEO2_BengalSea and LEO2_TP, Fig. 5 c). It also produces a decrease in year-round precipitation, especially in south and inland Asia (Fig. 6 m, n, o).

5.1.4 *Continentality increase and East African and Iranian uplifts as major drivers of the South Asian monsoon*

The changes induced by the TP uplift or by its latitudinal location on South Asian climate are by far out-competed by the effects of land-sea distribution changes, or by the uplift of peripheral mountain ranges (Fig. 5). Indeed, the increase in continentality driven by the Eocene-Oligocene sea level fall induces colder and drier winters (Fig. 7 g), as well as warmer and wetter summers (Fig. 7 h). This results in a monsoon-like seasonality signal expanding over southeastern Asia (Fig. 7 i). It also translates into a doubling of the Webster-Yang Index (from 6 to 11 m/s between experiments EOLI_REF and LEO1_REF, Fig. 5 c) and an important reorganization of the summer Jet Stream behavior (see section 5.2.2). Likewise, increasing continentality during the Miocene appears to be key for inducing a more pronounced migration of the ITCZ over the Arabian Sea (from 18 to 21°N in the more continental case, Fig. 5 b), as well as a slight increase of the Webster-Yang Index (Fig. 5 d). This is achieved either with the emergence of the Arabian Platform (Fig. 8 h), or with the shrinkage of the Paratethys Sea (Fig. 8 e). In both cases, the amplification of the summer low pressure belt increases moisture advection from the Arabian Sea, leading to enhanced summer rainfall in the SAM domain. The increase in precipitation seasonality in the SAM domain is, however, more widespread with a Paratethys Sea retreat than with an emerged Arabian platform (Fig. 8 f, i), due to the contrasted effect of these paleogeographic changes on winter precipitation (Fig. 8 d, g). Both events are also shown to strongly impact central Asian aridity and the climate of the EAM domain.

Additionally, the buildup of both East African (difference between experiments EMio_EAfr-EMio_REF) and Anatolian-Iranian landforms (difference between experiments LMio_REF-LMio_smallT) is critical for the amplification of the ITCZ migration and strengthening of the SAM. Each uplift triggers a $\sim 4\text{-}5^\circ$ northward migration of the ITCZ over the Arabian Sea in summer, as well as a slight increase in the Webster-Yang Index in July (Fig. 5 b, d and SI Fig. 16). The uplift of East African landforms under Early Miocene conditions reinforces the Somali Jet and brings moisture to Iran and the SAM domain in summer (Fig. 9 e), which results in an intensification of monsoon-like seasonality in the Himalayan foothills and in southeastern Asia (mainly Myanmar, Fig. 9 f). Anatolian-Iranian landforms' final uplift under late Miocene conditions promotes winter aridity and summer precipitation in the SAM domain through a large strengthening of the Somali Jet, resulting in reinforced monsoon-like seasonality (Fig. 9 j, k, l). By preventing the advection of drier westerly mid-latitudes winds to lower latitudes, the Anatolian-Iranian Plateau channels humidity towards inland Asia in summer, reducing the aridity of the region. On the other hand, the sole effect of the Tethyan Seaway closure, without strong modification of land extension in the Arabian Peninsula region, remains limited in our experiments (+1 m/s for the Webster-Yang Index

1009 between experiments EMio_REF and EMio_TetSw in Fig. 5 d), in contrast to the hypoth-
 1010 esis that the closure of the Tethyan Seaway may contribute to altering the intensity of the
 1011 monsoon during the Miocene (Bialik et al., 2019, 2020; Rögl, 1997; J. Sun et al., 2021),

1012 **5.2 The East Asian monsoon under the combined influence of Asian orog-** 1013 **raphy, continentality and $p\text{CO}_2$**

1014 ***5.2.1 East Asian summer monsoon: precipitation patterns and summer*** 1015 ***Jet Stream position evolution***

1016 As opposed to the South Asian region, monsoon-like precipitation seasonality is sim-
 1017 ulated in eastern Asia in all reference experiments, although it remains initially confined
 1018 to northeastern China in the Eocene (Fig. 4 a). As this region of monsoon-like precipi-
 1019 tation expands to southeastern and inland China throughout the Cenozoic and reaches a
 1020 modern-like extent in the mid-Miocene experiment, the Paleogene broad zonal arid band
 1021 retreats from China (Fig. 4 m). Today, precipitation in eastern China is triggered by the
 1022 penetration of the Meiyu-Bayu front as it follows the migration of the Jet Stream north of
 1023 the TP during summer (Kong et al., 2017). In our simulations, the summer Jet Stream (ap-
 1024 proximated by the location of maximum zonal wind velocity in the troposphere in August)
 1025 circulates above the proto TP and eastern China in a strong zonal flux in the Eocene and
 1026 Oligocene experiments (up to 30-35 m/s centered at $\sim 30^\circ\text{N}$ Fig. 4 c, g). It then weakens
 1027 (10-20 m/s) and progressively migrates north of the TP in the Miocene experiments (Fig. 4
 1028 k, o, s). The Jet configuration evolves from purely zonal (east-west) to more SW-NE. This
 1029 relocation of the Jet Stream is accompanied by increased precipitation in eastern China,
 1030 southeastern Siberia and Japan, reaching 200-300 mm in August (Fig. 4 k, o, s), which
 1031 locally accounts for up to 25% of the annual precipitation. These results suggest that the
 1032 evolution of the Jet Stream seasonal displacement indeed amplifies the EASM rainy season,
 1033 although seasonal precipitation is simulated prior to the Jet acquiring its modern position
 1034 in summer.

1035 ***5.2.2 Summer Jet Stream migration driven by $p\text{CO}_2$ decrease at the EOT*** 1036 ***and Tian Shan uplift in the Miocene***

1037 Our sensitivity experiments allow us to identify the drivers responsible for the estab-
 1038 lishment of modern-like Jet Stream seasonal migrations over Asia. All 1120 ppm Eocene
 1039 simulations display a behavior of the Jet opposite to its modern counterpart, with a north-
 1040 ward migration in winter and a southward migration in summer independent of the TP
 1041 configuration (Fig. 10 a, Fig. 6 e, h, k, n). Halving $p\text{CO}_2$ at the EOT reverses this ten-
 1042 dency (LEo1.2X and Eoli_REF, compared to LEo1_REF), inducing a migration north of
 1043 the TP in late summer to early fall (Fig. 10 a, Fig. 7 e, h) and an important decrease in
 1044 winter zonal velocity (~ 50 m/s against ~ 70 m/s in other Eocene simulations, Fig. 10 a).
 1045 This northward migration is however restricted to the TP region and the Jet Stream remains
 1046 at low latitude over eastern Asia ($\sim 35^\circ\text{N}$, Fig. 10 b, SI Fig. 18), with low summer rainfall
 1047 amounts (100-150 mm/month). All subsequent Miocene simulations display an important
 1048 latitudinal migration of the Jet over the year, both in the TP region (Fig. 10 c, e) and over
 1049 eastern Asia (Fig. 10 d, f). The northward migration of the Jet is comparable between
 1050 early Oligocene and early Miocene experiments (up to $\sim 38-40^\circ\text{N}$ in September), despite a
 1051 higher (from 3000 to 4000 m) and wider TP, due to the incipient uplift of northeastern
 1052 and northwestern TP portions in the early Miocene simulation (the Tian Shan is ~ 1000 m
 1053 and the NE Tibet ~ 2000 m high). We therefore suggest that the Jet Stream latitudinal
 1054 migration is primarily driven by $p\text{CO}_2$ decrease and resulting changes in tropospheric tem-
 1055 perature gradients, and that a significant threshold in the behavior of the Jet Stream may
 1056 be crossed at the greenhouse-icehouse transition (EOT, ~ 34 Ma). In contrast, variations in
 1057 the Jet Stream latitudinal migration during the Miocene appear to be driven by topographic
 1058 changes. Indeed, sensitivity experiments show that the Tian Shan, and to a lesser extent
 1059 Mongolian and Pamir topographies, are critical to deviate the Jet northward in summer,

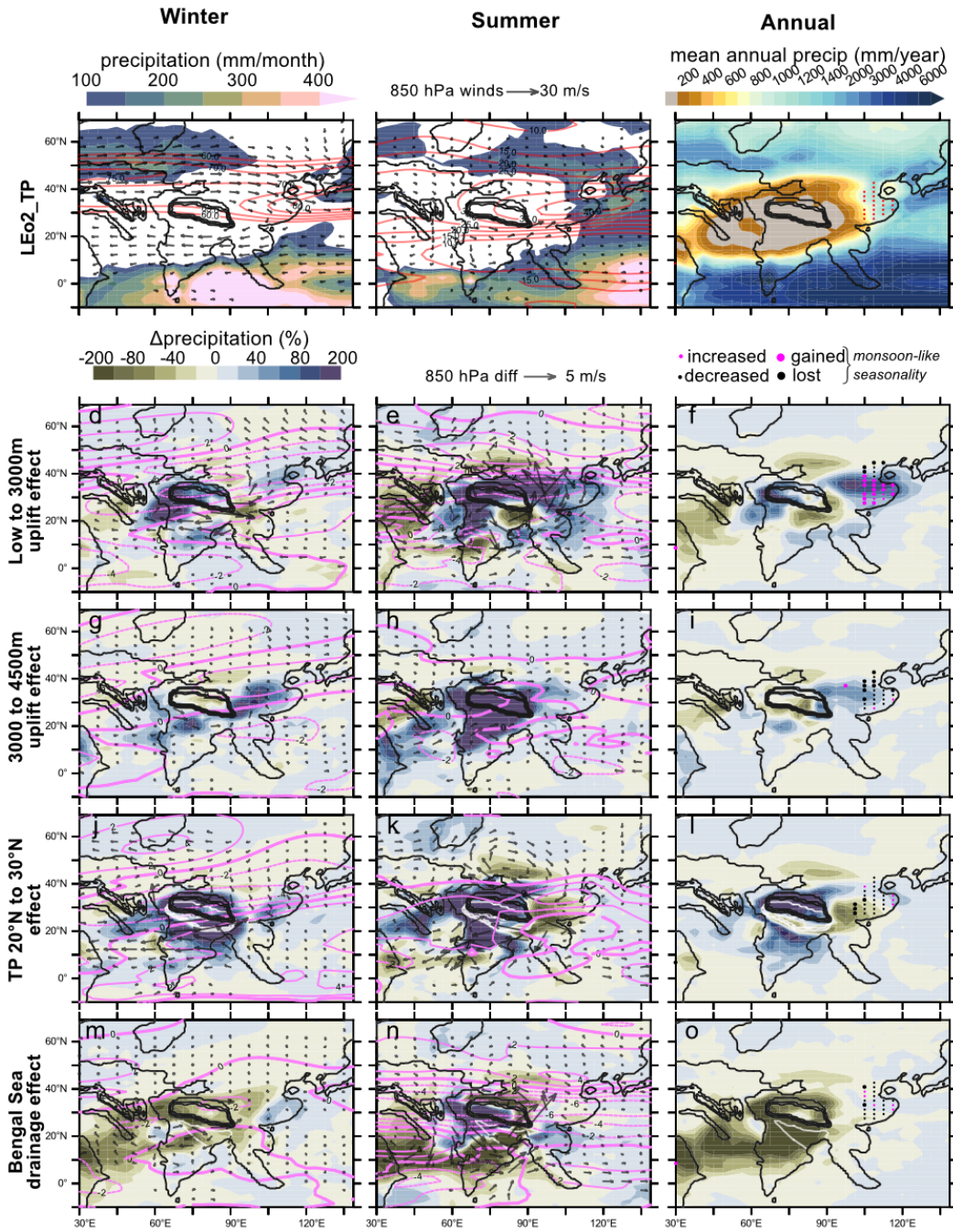


Figure 6. Sensitivity to the Tibetan configurations on Eocene climate: (a, d, g, j, m) winter precipitation (shading), 850 hPa winds (vectors), jet stream speed (contour) ; (b, e, h, k, n) on summer precipitation (shading), 850 hPa winds (vectors), jet stream speed (contour); (c, f, i, l, o) mean annual precipitation (shading) and monsoon-like seasonality according to the MPI index (red dots). Sensitivity tests are compared to the LEO2_TP simulation (a, b, c) and anomalies (d to o) are expressed as "test - LEO2_TP", except for the "lowered TP effect" which is "LEO2_TP - LEO2_TPflat"). Precipitation anomalies (shading) are expressed in % and normalized by the averaged precipitation of both simulations (therefore, a change from or to zero mm/year accounts for +/- 200%). In (f, i, l, o): four types of seasonality change induced by uplift are displayed (e.g., regions showing a decrease of monsoon-like seasonality after lowering the TP are in small black dots) ; white and black topographic contours indicate the LEO2_TP and tested topography.

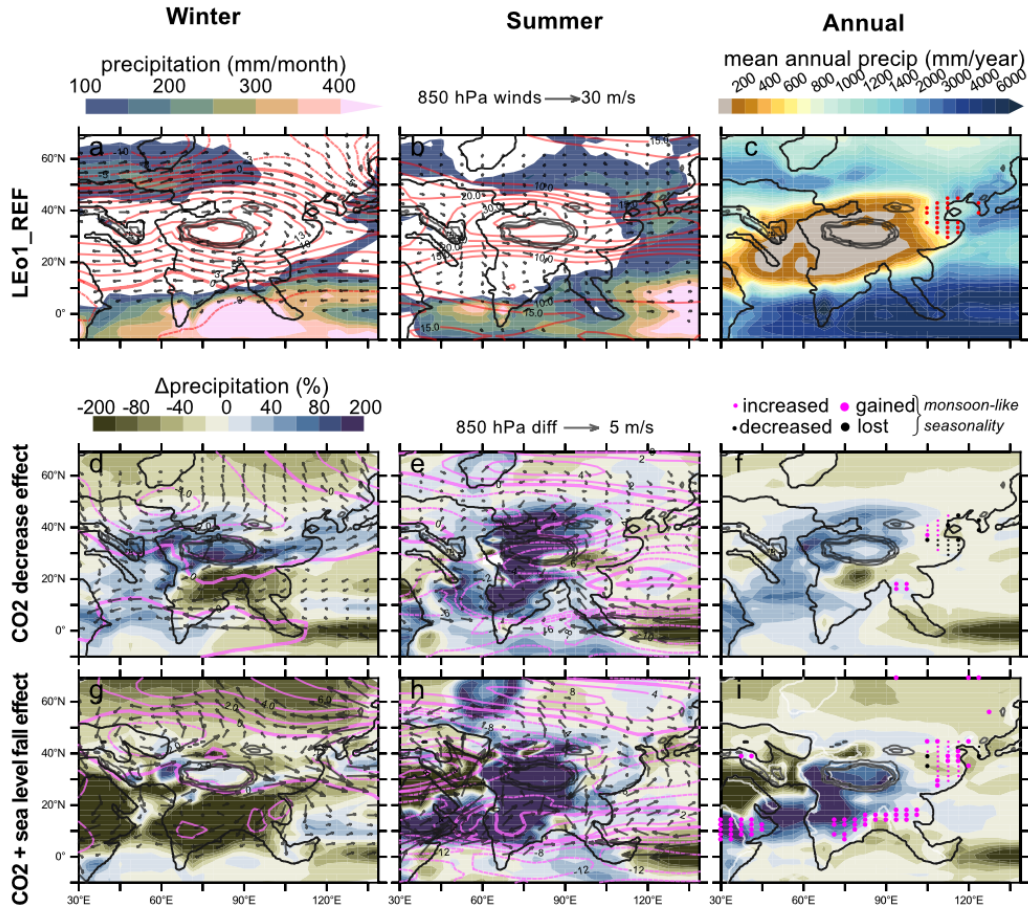


Figure 7. Influence of $p\text{CO}_2$ decrease and sea level fall at the EOT on: (a, d, g) winter precipitation (shading), 850 hPa winds (vectors), Sea Level Pressure (contour) ; (b, e, h) on summer precipitation (shading), 850 hPa wind (vectors), jet stream speed (contour); (c, f, i) mean annual precipitation (shading) and monsoon-like seasonality according to the MPI index (red dots). Sensitivity tests are compared to the LEO1_REF simulation (a, b, c) and anomalies (d to i) are expressed in order to highlight the impact of the test (i.e. test-LEO1_REF). We refer the reader to Figure 6 for an extended description of the panels.

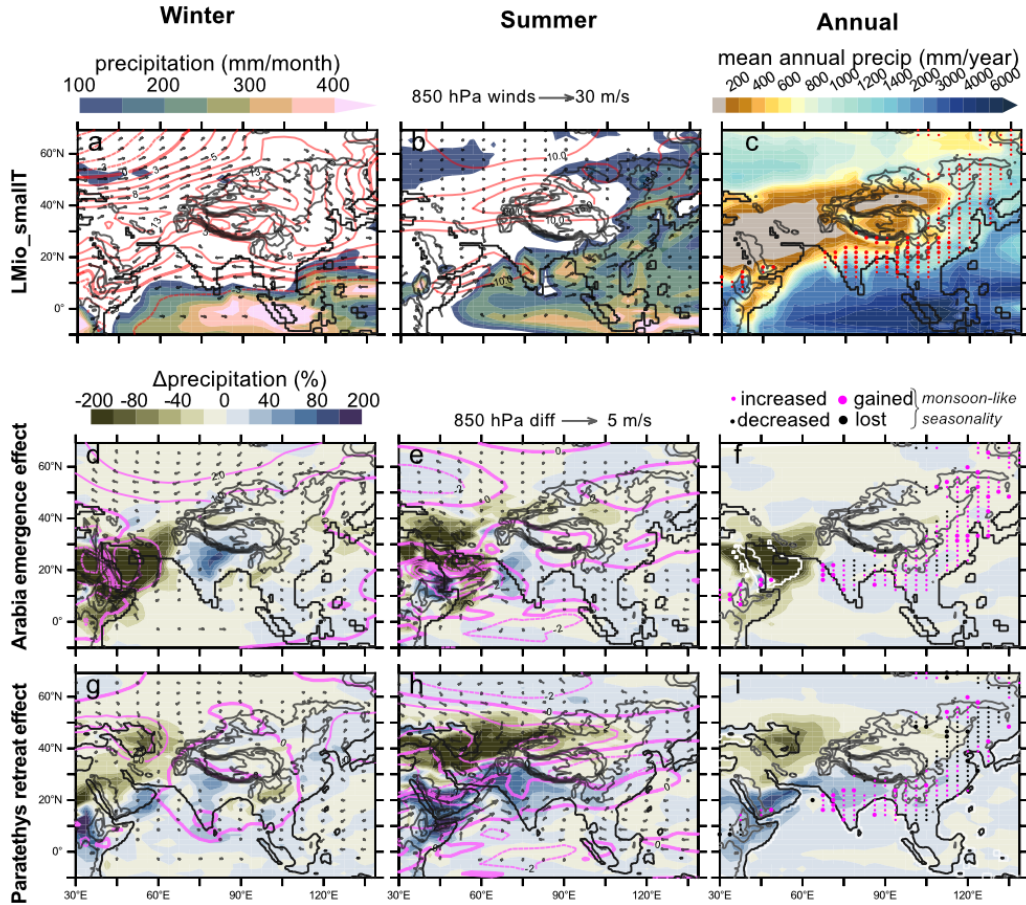


Figure 8. Influence of continentality increase in a mid-late Miocene context on: (a, d, g) winter precipitation (shading), 850 hPa winds (vectors), Sea Level Pressure (contour) ; (b, e, h) on summer precipitation (shading), 850 hPa winds (vectors), jet stream speed (contour); (c, f, i) and on mean annual precipitation (shading) and monsoon-like seasonality according to the MPI index (red dots). Sensitivity tests are compared to the LMio_smallT simulation (a, b, c) and anomalies (d to i) are expressed in order to highlight the impact of the continentality increase (i.e. LMio_smallT-test). We refer the reader to Fig. 6 for an extended description of the panels.

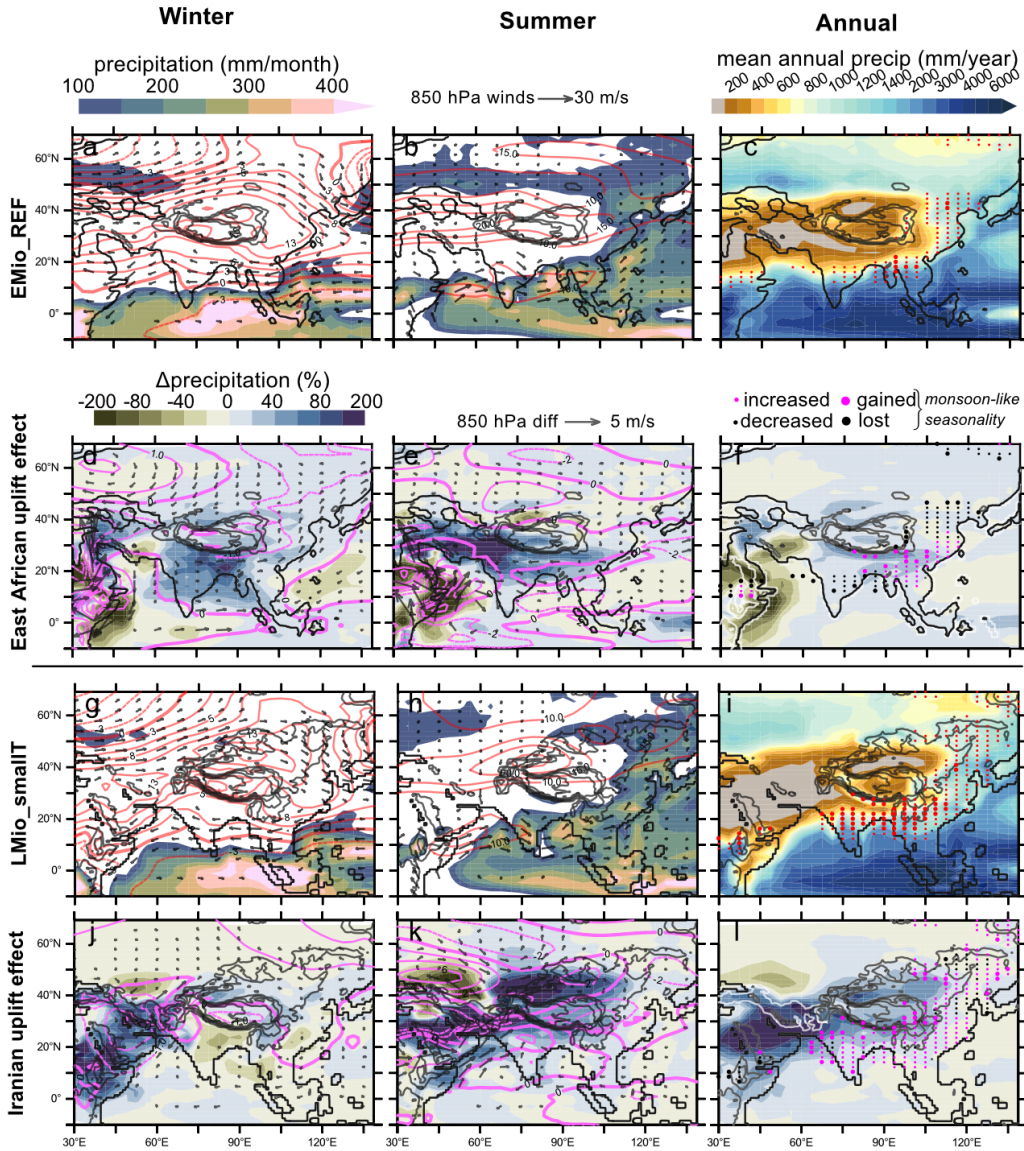


Figure 9. Influence of East African uplift in the early Miocene (a to f) and of Anatolian-Iranian uplift in the late Miocene (g to l) on: (a, d, g, j) winter precipitation (shading), 850 hPa winds (vectors), Sea Level Pressure (contour) ; (b, e, h, k) on summer precipitation (shading), 850 hPa winds (vectors), jet stream speed (contour); (c, f, i, l) and mean annual precipitation (shading) and monsoon-like seasonality according to the MPI index (red dots). East African (Anatolian-Iranian) uplift is compared to the EMio_REF simulation (LMio.SmallT) (a, b, c and g, h, i) and anomalies (d, e, f and j, k, l) are expressed in order to highlight the impact of uplift (i.e. EMio_EAfr-EMio_REF and LMio_REF-LMio_smallT respectively). We refer the reader to Figure 6 for an extended description of the panels.

1060 both in the TP region and in eastern Asia (from 39-41°N in LMio_noTS, LMio_noTSP,
 1061 LMio_noTSM and LMio_noM to 43°N in MMio_REF and LMio_REF, Fig. 10 e, Fig. 11 h,
 1062 k, n). Northward migration of the Jet Stream in summer induces orographic precipitation
 1063 on the uplifted landforms, aridification in the windward regions (-20 to -60% of summer pre-
 1064 cipitation in eastern Kazakhstan and Uzbekistan) and increased summer rainfall in eastern
 1065 Asia (Fig. 11 e, h, k, n). Monsoon-like seasonality in eastern Asia (magenta dots in Fig. 11
 1066 f, i, l, o) also greatly increases, due to the important effect of uplift of these mountains on
 1067 wintertime climate as well (see section 5.2.4). On the other hand, changes in the configura-
 1068 tion of the Tethyan Seaway in the early Miocene (comparing EMio_REF and EMio_TetSw),
 1069 the Anatolian-Iranian Plateau uplift (comparing LMio_SmallT and LMio_REF), or a $p\text{CO}_2$
 1070 decrease (comparing LMio_REF and LMio_1.5X) in the late Miocene, do not yield important
 1071 variations in the Jet Stream migration (Fig. 10 c to f).

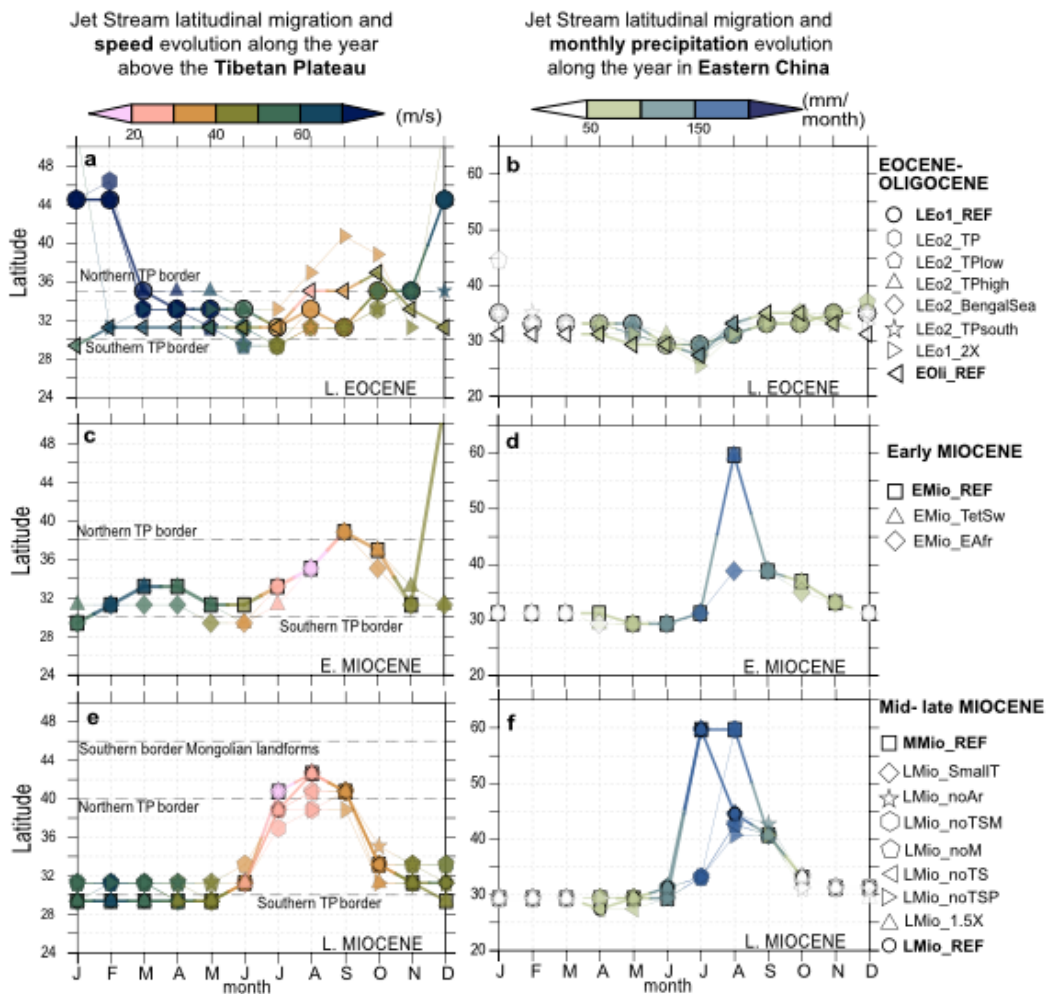


Figure 10. Jet Stream behavior throughout the year over the Tibetan Plateau and eastern China for all sensitivity experiments, divided into (**up**) late Eocene, (**mid**) early Miocene and (**bottom**) mid to late Miocene. (**left**) Jet Stream latitudinal migration and speed (shading) evolution along the year in the Tibetan region (averaged over 80:90°E). Mean latitudes of the northern and southern bounds of the Himalaya-Tibet and Mongolian landforms are indicated. (**right**) Jet Stream latitudinal position and precipitation amounts (shading) throughout the year in east Asia (averaged over 100:120°E).

1072

5.2.3 *East Asian winter monsoon: the Siberian High genesis*

1073

1074

1075

1076

1077

1078

1079

1080

1081

1082

1083

1084

1085

1086

1087

1088

1089

1090

1091

1092

1093

1094

1095

1096

1097

1098

1099

Our results suggest that pressure and wind patterns characterizing the modern EAWM established progressively, following an important reorganization of surface temperature gradients (Fig. 12, Fig. 13). In our Eocene experiment, a high-pressure band centered around 30°N is simulated but remains mainly zonal, following the large-scale winter descending branch of the Hadley cell driven by latitudinal surface temperature gradients (Fig. 12 b). The temperature difference between the Tibetan region (~ 10 °C, located below the high pressure cell) and neighboring North Pacific Ocean (~ 30 °C) remains relatively low (~ 20 °C, Fig. 12 a) compared to modern winter temperature difference (~ 40 °C, Fig. 14 h). As a result, no significant pressure difference is simulated between the Asian continent and the North Pacific in the Eocene and the calculated EAWM index is low (< 5 , Fig. 13), reflecting only the North-South pressure gradient between Asia and the Maritime Continent. The extent of the Asian high pressure zone increases gradually in the early Oligocene and early Miocene experiments (Fig. 12 d, f), but a modern-like Siberian High is only simulated in the mid and late Miocene experiments, when the anticyclone relocates over Siberia (~ 40 - 60 °N, Fig. 12 h, j). Additionally, the (North Pacific) Aleutian low relocates 10° to the south from the early Oligocene onwards and steadily weakens until the late Miocene (from over ~ 14 to 10 hPa anomaly). These changes concur to progressively increase both North-South and East-West pressure gradients, and therefore the EAWM index, which reaches maximal values in the mid and late Miocene experiments (~ 15 , Fig. 13). Following this simulated pressure pattern reorganization, low tropospheric winds circulating over China display a progressive change in orientation: while remaining primarily zonal in the Paleogene and early Miocene experiments (Fig. 12 b, d), they increasingly tilt in the meridional direction under the development of the Siberian High in the mid and late Miocene experiments (Fig. 12 h, j). This profound reorganization of atmospheric circulation is driven by temperature gradient changes and mainly due to the progressive cooling of the Tibetan, Mongolian and Siberian regions, as illustrated by the $\sim 22^\circ$ southward shift of the 0 °C isotherm between the late Eocene and the late Miocene simulations (Fig. 12 a, i).

1100

1101

5.2.4 *Siberian High inception driven mainly by Mongolian uplift in the Miocene and its impact on precipitation seasonality*

1102

1103

1104

1105

1106

1107

1108

1109

1110

1111

1112

1113

1114

1115

1116

1117

1118

1119

1120

1121

1122

1123

Our sensitivity experiments reveal the very strong impact of the Mongolian landform uplift (alone or together with the Tian Shan) in the mid-late Miocene on Asian winter pressure patterns. Indeed, their growth induces a strengthening of both the Siberian High (up to ~ 6 hPa, Fig. 11 d, g) and the Aleutian Low, resulting in a reinforcement of the East-West and North-South pressure gradients and ultimately of the EAWM index (from ~ 8 to ~ 15 , Fig. 13). Mongolian (and/or Tian Shan and/or Pamir) uplift also results in localized precipitation intercepted by the landforms (Fig. 11 d to o), despite the overall dryness of the inland Asian region (SI Fig. 15). As Mongolian uplift deviates the winter westerlies flux northward, Eastern China is swept by colder and drier winds coming from Siberia, which translates into a marked decrease in winter precipitation (up to 80% decrease, Fig. 11 d). These changes in the wintertime climate lead to an important expansion of regions displaying monsoon-like precipitation seasonality in eastern Asia (Fig. 11 f, i). The uplift of Tian Shan landforms, alone or together with the Pamir, has a lower impact on the winter pressure patterns compared to Mongolia uplift (Fig. 13) but nonetheless generates an almost complete drying on their eastern flanks (modern Gobi and Taklimakan deserts) because they act as an orographic barrier to westerly moisture flux (Fig. 11 g, j, m). Considering other sensitivity experiments, Asian winter climate exhibits only a weak response to changing Tibetan orography or $p\text{CO}_2$ values for Eocene conditions (SI Fig. 17 a to g, Fig. 13). Likewise, the Miocene winter pressure patterns in Asia are only mildly impacted by the Anatolian-Iranian landform uplift, the closure of the Tethyan Seaway, the Paratethys extent, or a $p\text{CO}_2$ drop from 560 to 420 ppm, when compared to the effect triggered by the Mongolian Plateau uplift (Fig. 13, SI Fig. 17 i to n and s, t).

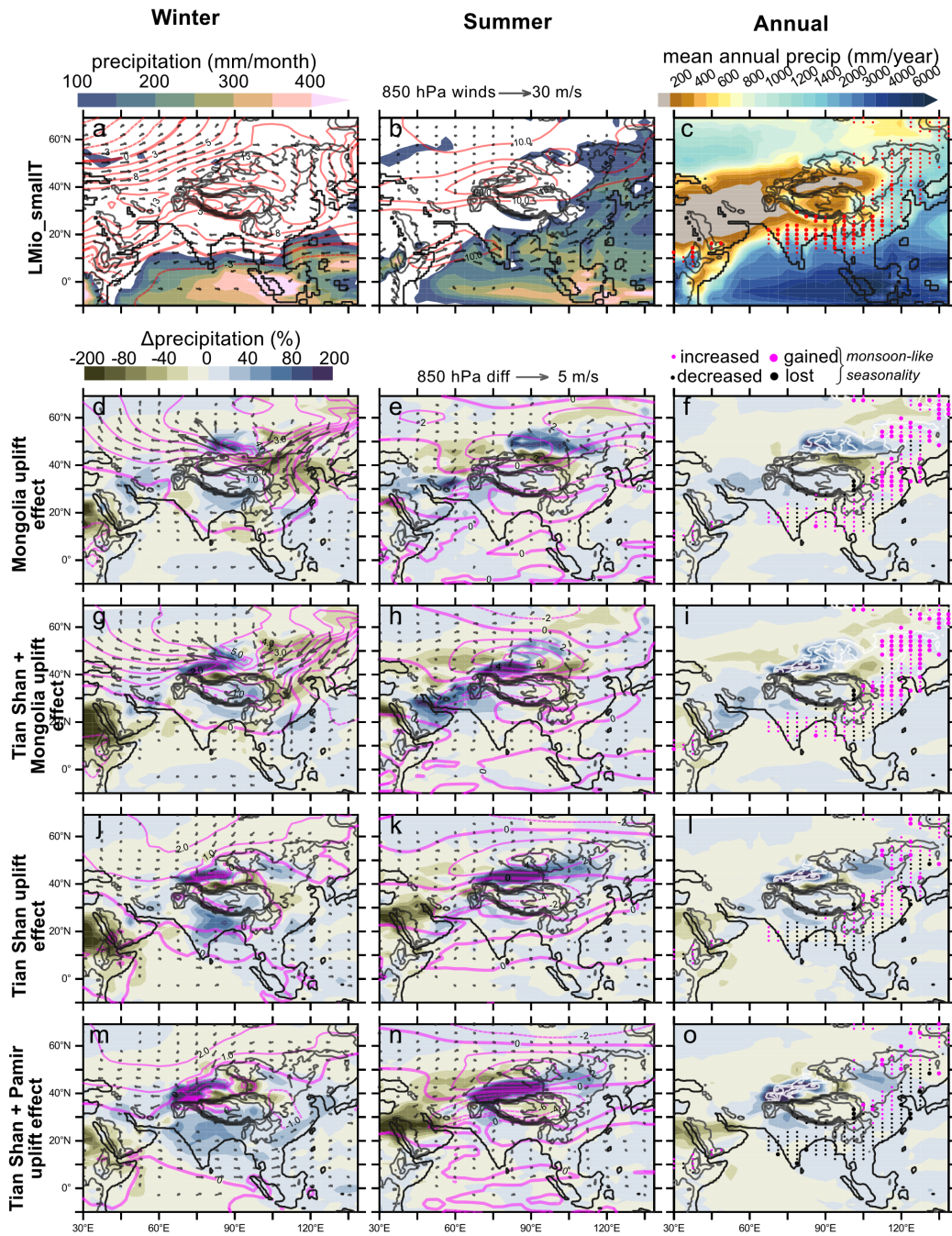


Figure 11. Influence of Mongolia, Tian Shan and Pamir regional uplifts on **(left column)** winter precipitation (shading), 850 hPa winds (vectors), Sea Level Pressure (contour) ; **(middle column)** on summer precipitation (shading), 850 hPa wind (vectors), jet stream speed (contour); **(right column)** mean annual precipitation (shading) and monsoon-like seasonality according to the MPI index (red dots). Sensitivity tests are compared to the LMio_smallT simulation (**a, b, c**) and anomalies (**d to o**) are expressed in order to highlight the impact of the uplift (i.e. LMio_smallT-test). We refer the reader to Figure 6 for an extended description of the panels.

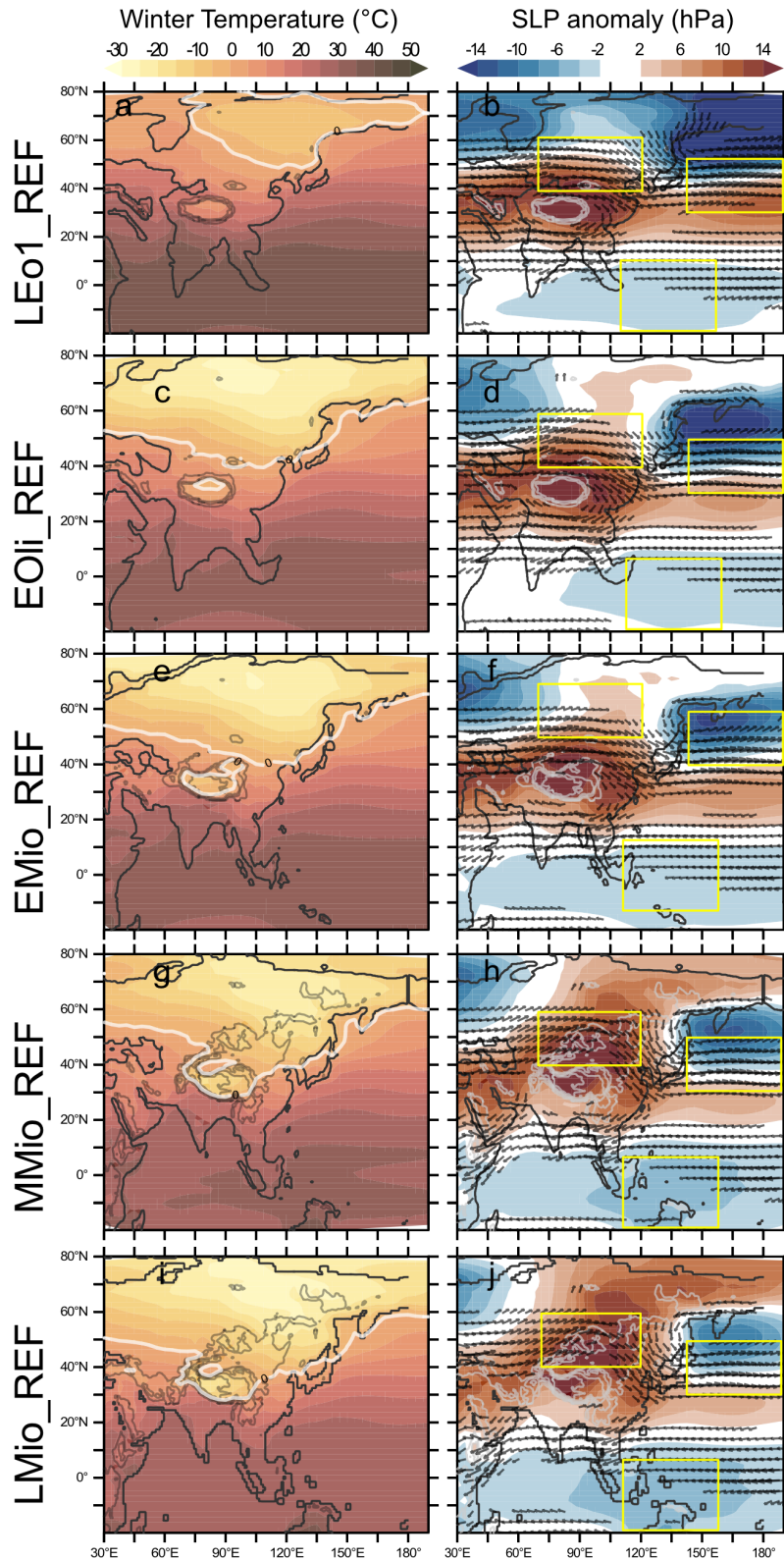


Figure 12. Evolution of the winter monsoon diagnostics throughout the Cenozoic. **Left column:** December-February (DJF) mean temperature at 2 m (shading, Celsius), and 0 °C isotherm (white contour); **Right column:** DJF normalized Sea Level Pressure anomaly (shading, hPa) and 850 hPa winds above 4 m/s (vectors). In all captions, topography is overlain in gray contour each 1000 m. Yellow boxes indicate the regions over which the sea level pressure gradients are calculated for the East Asian Winter Monsoon Index, presented in section 4.3

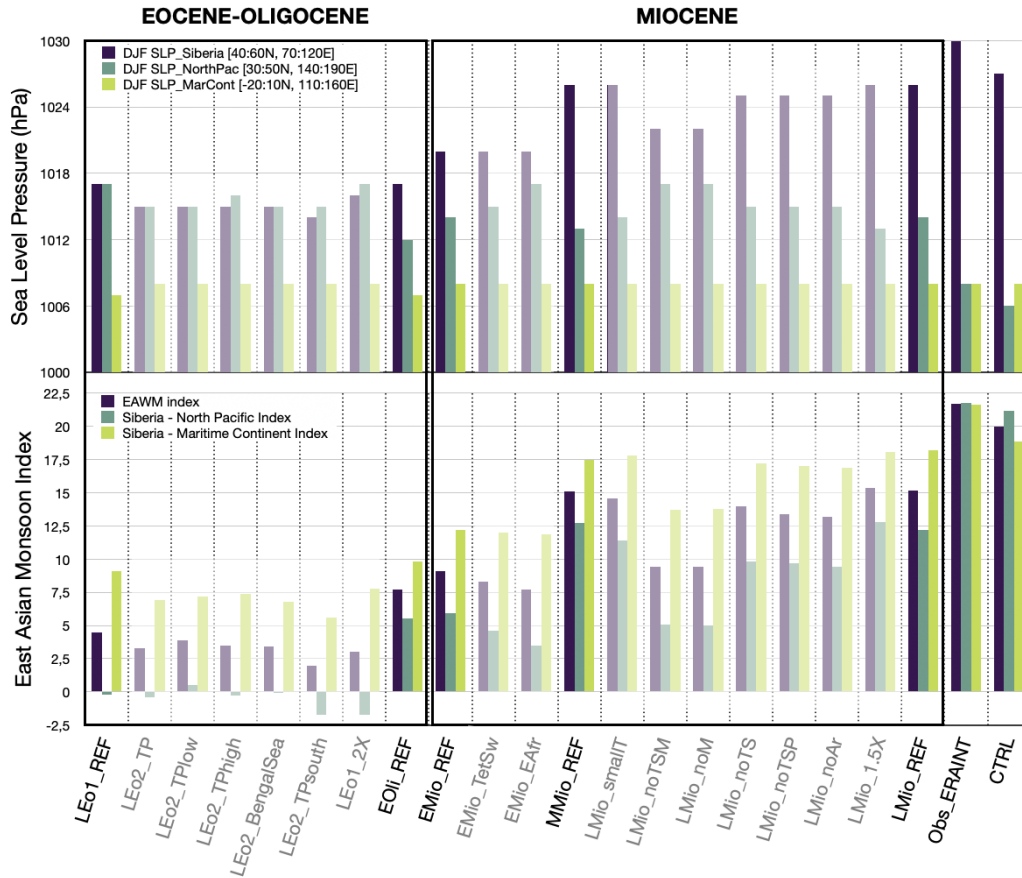


Figure 13. **Upper panel:** December-February (DJF) Sea Level Pressure (hPa) evolution over Siberia, North Pacific and the Maritime Continent ; **lower panel:** Evolution of the East Asian Winter Monsoon index (purple) and of the East-West and North-South regional indexes throughout the different reference and sensitivity experiments, after (L. Wang & Chen, 2014).

1124 6 Discussion

1125 A long-standing debate pits the effect of continentality against that of orography as
 1126 the main driver of Asian climate evolution (Prell & Kutzbach, 1992; Kutzbach et al., 1993;
 1127 Ramstein et al., 1997; Fluteau et al., 1999; Z. Zhang et al., 2007; Roe et al., 2016; Zoura
 1128 et al., 2019; R. Zhang et al., 2021). Our results (summarized in Table 2) suggest that
 1129 these two features impacted different climatic characteristics of the Asian monsoons and all
 1130 contributed to the emergence of current Asian climate. In the following sections, we put our
 1131 main findings in perspective with available paleoclimatic indicators and previous modeling
 1132 work, and tackle specific questions raised in section 2.4.

1133 6.1 Summer monsoons in the Eocene: driven by $p\text{CO}_2$, Tibetan paleo- 1134 geography or continentality ?

1135 Although the LEO1_REF experiment simulates the seasonally wet climate indicated
 1136 by eastern Chinese floras well (Meng et al., 2018; Y. Xie et al., 2022), it fails to identify the
 1137 subhumid to humid climate inferred from fossil paleoflora and paleofauna in northern India
 1138 (Saxena & Trivedi, 2009) and Tibet (T. Su et al., 2020; Sorrel et al., 2017). In a previous
 1139 study, this south Asian aridity bias in our experiment was interpreted as resulting from the
 1140 hot surface temperatures simulated in India, together with strong mid-tropospheric subsi-
 1141 dence that inhibits deep convection and condensation, especially over northern India (Tardif
 1142 et al., 2020). However, a previous study using the same model and paleogeography was able
 1143 to simulate monsoon-like climate in both the EAM and SAM domains, providing that or-
 1144 bital configurations induced summer solar maxima (Tardif et al., 2021). This orbitally-paced
 1145 wet/dry climate dichotomy is, at least qualitatively, in agreement with stratigraphic and pa-
 1146 leobotanic evidence from southern and eastern China (C. Huang & Hinnov, 2019; Licht et
 1147 al., 2014) and hints at a strong sensitivity of the South Asian region to surface tempera-
 1148 ture gradients in the Eocene. Such sensitivity seems further confirmed by the fact that, in
 1149 the present study, South Asian Eocene climate appears especially sensitive to experiments
 1150 affecting land-sea distribution and global temperature (LEO1_2X and LEO2_BengalSea, SI
 1151 Fig. 15 f, g).

1152 The East Asian monsoon domain, on the other hand, displays sensitivity to topo-
 1153 graphic changes in the Tibetan region. We simulate that an uplift of a proto-TP (LEO2_TP
 1154 - LEO2_TPLow) would result in an onset or increase in EAM monsoon-like precipitation
 1155 seasonality due to increased summer precipitation (up to 50%, Fig. 6 e, SI Fig. 15 b, c,
 1156 d), in agreement with previous modeling work (R. Zhang et al., 2018; R. Zhang, Jiang, &
 1157 Zhang, 2017; R. Zhang et al., 2021; Z. Zhang et al., 2007; X. Liu & Yin, 2002; X. Li et al.,
 1158 2017; Farnsworth et al., 2019; Thomson et al., 2021). Likewise, the decreased EAM intensity
 1159 and increased inland Asian aridity when the southern edge of the TP is situated at 30°N is
 1160 coherent with a previous study testing the impact of the latitudinal position of the incipient
 1161 TP (R. Zhang et al., 2018). Therefore, the inception or reinforcement of the East Asian
 1162 summer monsoon in the Eocene seems intertwined with the TP evolution history, as well
 1163 as with existing topography before the TP uplift (e.g. the Lhasa terrane), although their
 1164 paleoelevation and extent is not well constrained. Furthermore, we show that monsoon-like
 1165 rainfall seasonality may have occurred prior to the establishment of modern-like East Asian
 1166 winter monsoon circulation and Jet Stream summer migration, which were likely established
 1167 during the late Paleogene or the Neogene.

1168 6.2 Forcing factors of wintertime climate variability

1169 The observation of loess deposits in northeastern Tibet as early as 40 Ma was in-
 1170 terpreted as resulting from the periodic inception (or reinforcement) of the Siberian High
 1171 in winter due to enhanced continentality after the Paratethys Sea retreat (Meijer et al.,
 1172 2021). Other loess deposits reported during the Oligocene in the Chinese Loess Plateau
 1173 and Mongolia, apparently coeval with periods of cooling and ice-sheet expansion (J. Sun &

1174 Windley, 2015; Wasiljeff et al., 2022), further suggest the presence of a Siberian High and
 1175 corresponding dust transport in the late Paleogene. The potential forcing factors driving the
 1176 establishment of this winter pressure pattern have, however, been significantly less studied
 1177 than summer monsoons dynamics, with studies mostly focusing on the impact of orography
 1178 rather than continentality (White et al., 2017; Sha et al., 2015; Baldwin & Vecchi, 2016).
 1179 Our results suggest that both increased continentality and regional uplift contributed to-
 1180 gether to the progressive inception of the modern Siberian High, while $p\text{CO}_2$ decrease alone
 1181 had a lesser impact (Fig. 13). A modern-like Siberian High with typical EAWM wind
 1182 patterns is however not simulated until our middle and late Miocene simulations, when the
 1183 Tian Shan, but especially the Mongolian landforms, are set to their present-day elevation
 1184 in the model.

1185 Previous modeling work based on present-day geography that tested the effect of Mon-
 1186 golian landform uplift (Sha et al., 2015; Shi et al., 2015; Yu et al., 2018; R. Zhang, Jiang,
 1187 Zhang, Cheng, & Zhang, 2017) reproduced the same tendencies that we present here, namely
 1188 a strong increase of the winter sea level pressure over Siberia and typical deviation of the
 1189 westerlies towards northern latitudes resulting in a pronounced drying of eastern Asia and
 1190 EAWM amplification (Fig. 11 d). Other studies focusing more on the summer monsoon
 1191 simulate increased EASM precipitation and wind circulation, although they incorporate
 1192 Tian Shan uplift together with Mongolia (Yu et al., 2018; R. Zhang et al., 2012; H. Tang
 1193 et al., 2013; Zhisheng et al., 2001), which remains coherent with our findings testing the
 1194 uplift of both features (Fig. 11 h). Although the effect of Mongolian landforms has not
 1195 been explicitly tested in paleoclimate modeling studies using realistic paleogeographic re-
 1196 constructions, we can generally observe that when a modern-like Mongolian orography is
 1197 prescribed, the simulated winds and precipitation are close to the modern-like EAWM (Licht
 1198 et al., 2014; X. Li et al., 2017), while this is not the case with a reduced Mongolia eleva-
 1199 tion (Huber & Goldner, 2012). Given the large uncertainties related to the Hangay Dome
 1200 uplift history, performing additional experiments testing the impact of an early uplift in an
 1201 Oligocene configuration could enable one to evaluate the potential presence of a Siberian
 1202 High at that time, and therefore help interpret early loess-like deposits observed at that
 1203 time in the Chinese Loess Plateau and Mongolia (J. Sun & Windley, 2015; Wasiljeff et al.,
 1204 2022). Loess-like deposition in the Xining Basin at ~ 40 Ma, however, seems too old to
 1205 be attributed to the development of the modern Siberian High, given that Mongolia was
 1206 probably at low elevation and that continentality alone does not seem sufficient to trigger a
 1207 modern-like Siberian anticyclone. This suggests that alternative mechanisms for dust trans-
 1208 port should be explored for this period, although testing this hypothesis would require new
 1209 data such as daily to hourly wind speed model outputs (Aoki et al., 2005).

1210 **6.3 The critical role of peripheral landforms in the establishment of mon-** 1211 **soon seasonal features in the Miocene**

1212 In agreement with previous studies (R. Zhang, Jiang, & Zhang, 2017; Acosta & Huber,
 1213 2020; H. Tang et al., 2013), our results highlight the key role played by the Anatolian-
 1214 Iranian Plateau uplift in modern-like SAM establishment, as it reinforces both summer
 1215 rainfall and winter aridity (Fig. 9 j, k). The effect of the Tian Shan uplift on Asian climate
 1216 is less conspicuous, likely owing to the proximity of these mountains to other important
 1217 landforms (e.g. Pamir-Karakoram, Anatolian-Iranian Plateau, Mongolia), which may result
 1218 in competing effects on the regional climate. While a rigorous comparison between our
 1219 results and previous studies is hampered by many diverging boundary conditions, all tend
 1220 to indicate that the Tian Shan uplift would have: i) increased yearly orographic precipitation
 1221 on the ranges, ii) decreased precipitation in inland Asian mid-latitudes and iii) reinforced the
 1222 EAM through increased summer precipitation (Fig. 11 m, n, o) (Baldwin & Vecchi, 2016;
 1223 H. Tang et al., 2013; Yu et al., 2018; R. Zhang, Jiang, & Zhang, 2017; R. Zhang, Jiang,
 1224 Zhang, Cheng, & Zhang, 2017). The key role played by the Tian Shan ranges (together with
 1225 the Pamir and Mongolian landforms) in triggering the Jet Stream northward migration in
 1226 summer (SI Fig. 18 e, f, Fig. 9 e, h, k, n), as suggested by previous modeling work derived

1227 from present-day geography (Sha et al., 2020; Shi et al., 2015), likely contributes to this
1228 EASM intensification. Substantial differences are nevertheless noted with other modeling
1229 studies, especially regarding the impact of Tian Shan uplift on inland Asian and northeastern
1230 Indian climate, likely due to these regions' key location on the westerlies path. Westerlies
1231 may indeed be deviated either to the North or the South, depending on the respective
1232 degree of elevation of the Iranian-Anatolian Plateau and the Tian Shan. While we simulate
1233 a weakening of SAM rainfall seasonality due to increased winter precipitation after the Tian
1234 Shan uplift, the opposite trend is simulated in studies where the Anatolian-Iranian Plateau
1235 is already fully uplifted at the time of the Tian Shan uplift, thus preventing the westerlies
1236 from bringing moisture to India (Baldwin & Vecchi, 2016; H. Tang et al., 2013; Yu et al.,
1237 2018; R. Zhang, Jiang, & Zhang, 2017; X. Wang et al., 2020).

1238 Our set of simulations also highlights that East African topography can strongly impact
1239 the Neogene evolution of the SASM as it greatly contributes to the establishment of modern-
1240 like atmospheric circulation, as discussed by Sarr et al. (2022). The presence of intermediate
1241 to high elevation topography in East Africa in the early Miocene is for example crucial
1242 for the "early" bending of the Somali Jet, before the closure of the West Tethys Seaway
1243 and establishment of Anatolian-Iranian topography with modern-like elevation (Fig. 9 e).
1244 Increasing elevation in Eastern Africa is also responsible, in our simulations, for increasing
1245 SASM precipitation. This contrasts with previous studies that simulate reduced SASM
1246 precipitation, due to African topography blocking the advection of moisture from equatorial
1247 Africa towards India (H.-H. Wei & Bordoni, 2016; Chakraborty et al., 2009). We hypothesize
1248 that this difference may come from these studies using present-day paleogeography, and/or
1249 unchanged fixed sea surface temperatures for all the experiments, thereby neglecting the
1250 potential effect of the East African uplift on Indian Ocean surface temperature gradients.
1251 It is also very likely that the impact of East African highlands uplift on South Asian rainfall
1252 regime may be modulated by the degree of uplift in the Iranian-Anatolian region. Better
1253 constraints on the relative degree of uplift of these different mountain ranges in the past,
1254 although seldom taken into account, is therefore critical to interpreting paleoenvironmental
1255 indicators.

1256 **6.4 Continentality increase in the Miocene and acts as an amplifier of** 1257 **SAM, EAM and inland aridity**

1258 The northward motion of the ITCZ over the Arabian Sea and the stronger SASM
1259 precipitation in response to continentality increase in the Miocene is a feature clearly sim-
1260 ulated in our experiments, and which is obtained with either the Paratethys Sea retreat or
1261 an emerging Arabian Peninsula (Fig. 8 e, h). The role of the Paratethys Sea retreat as a
1262 vector of amplified summer low pressure and resulting moisture advection via a strength-
1263 ened Somali Jet is well established by modeling experiments (Ramstein et al., 1997; Fluteau
1264 et al., 1999; R. Zhang et al., 2021; Z. Zhang et al., 2007). The Paratethys Sea retreat
1265 also drastically dries the winter-time "westerly corridor" (centered around 40°N, Fig. 8 h),
1266 resulting in increased inland Asian aridity (Fig. 8 i), here again mostly in coherence with
1267 previous modeling studies (R. Zhang et al., 2021; Z. Zhang et al., 2007), and field evidence
1268 (Palcu et al., 2021). On the other hand, the effect of increased land exposure in the Arabian
1269 Peninsula region on Asian climate has been, to our knowledge, significantly less explored by
1270 modeling studies and is rarely mentioned as a potential forcing factor in proxy data studies.
1271 We tentatively attribute this to the lack of constraints and data in this region. Given the
1272 shallow depth and extension of the Arabian Peninsula (roughly comparable to India's area),
1273 it is very likely that the episodes of partial or complete flooding that occurred throughout
1274 the Oligocene to late Miocene (Barrier et al., 2018; Otero & Gayet, 2001) may have had
1275 great consequences on atmospheric circulation patterns. Following Sarr et al. (2022), our
1276 results show that increased peninsula exposure reinforces the Somali Jet in summer and en-
1277 hances summer precipitation in SAM and EAM domains (Fig. 8 e). Additionally, it drives
1278 the onset of upwelling in the Arabian Sea (see Sarr et al. (2022)), which is traditionally
1279 used as a proxy for the establishment of a monsoon wind regime in South Asia. Our simu-

1280 lations suggest that a proto Somali Jet and intense summer precipitation were most likely
1281 established in the middle Miocene, before the Arabian Peninsula emergence, and therefore
1282 before any strong upwelling activity initiated in the Arabian Sea. In addition, the onset of
1283 upwelling in the Arabian Sea was likely uncorrelated to potential Miocene uplift events in
1284 the Himalaya-Tibet region (Sarr et al., 2022).

1285 **6.5 Persistent uncertainties and directions for future work**

1286 Our study demonstrates the key role played by land-sea distribution and by all to-
1287 pographic features surrounding the Indian Ocean in shaping the modern SAM, EAM and
1288 inland Asia aridity. Nevertheless, additional work is required both from modeling and in the
1289 field to help refine our understanding of the mechanisms at play throughout the Cenozoic
1290 in Asia. By showing the influence of several geographical units on Asian climate during
1291 different geological periods, our results highlight the conceptual limitations of performing
1292 tests based on present-day geographies or assuming homogeneous Asian orographic uplift
1293 throughout geological history to evaluate past monsoon evolution. In that respect, it is not
1294 surprising that most of those type of studies simulate modern-like summer and winter mon-
1295 soons features when maintaining high-elevation African, Mongolian and Anatolian-Iranian
1296 landforms, as well as an emerged Arabian platform (Roe et al., 2016; Zoura et al., 2019;
1297 Acosta & Huber, 2020). Our results also suggest that some paleogeographic events consid-
1298 ered roughly coeval may have had opposite influences on the Asian climate’s seasonal fea-
1299 tures, for example the Tian Shan and Anatolian-Iranian Plateau uplift discussed in section
1300 6.2. Refining the relative chronology of these various uplift phases is therefore paramount to
1301 better interpret the variations in monsoon intensity recorded by proxy data. Additionally,
1302 paleoelevation thresholds are likely to be critical for constraining Asian climate evolution,
1303 due to interactions of the topography with either low level (e.g. the summer monsoon winds)
1304 or mid tropospheric (e.g. the Jet Stream) air masses (X. Liu & Yin, 2002; X. Wang et al.,
1305 2020; Zhisheng et al., 2001; Prell & Kutzbach, 1992).

1306 We also acknowledge that a better understanding of the seasonal monsoon mechanisms
1307 simulated here would benefit from additional simulations performed with increased spatial
1308 and temporal resolution. Previous work have for example demonstrated the importance of
1309 high spatial resolution in the full depiction of the SASM circulation (Acosta & Huber, 2017)
1310 or the study of the interplay between the summer Jet Stream behavior and the formation of
1311 the Meiyu-Bayu front in Eastern Asia (Kong et al., 2017; Sampe & Xie, 2010). Additional
1312 diagnostics at planetary-scale, may also provide interesting comparison with previous studies
1313 on the impact of monsoon dynamics on large scale circulation patterns and long-distance
1314 teleconnections (Rodwell & Hoskins, 1996; Merlis et al., 2013; Biasutti et al., 2018).

1315 A more precise view of land-sea distribution and regional seaway evolution is also
1316 paramount. Indeed, these factors influence SST gradients, thereby controlling sea level
1317 pressure patterns, low tropospheric circulation, and oceanic circulation. Although our re-
1318 sults point to a minimal effect of the mechanical closure of the Tethyan Seaway on regional
1319 climate, other features need to be tested. For example, a better understanding of the In-
1320 donesian Gateway and Indonesian throughflow evolution would be of great interest, as these
1321 control in part Indo-Pacific Warm Pool SST distribution (Cane & Molnar, 2001; Tan et
1322 al., 2022) and may thus have influenced Asian climate (Q. Su et al., 2019). While the final
1323 step of the Indonesian Gateway constriction likely occurred during the Pliocene (Auer et
1324 al., 2019), its paleobathymetry and complex geometric configuration remain largely undoc-
1325 umented between 17-3.5 Ma (Kuhnt et al., 2004). While no major tectonic deformation is
1326 thought to have occurred during this period, the shallow depth of the gateway likely made it
1327 sensitive to middle Miocene sea level fluctuations (Sosdian & Lear, 2020), with possible im-
1328 pact on the Eastern Indian and Western Pacific Oceans surface temperatures and therefore
1329 on SST gradients. Although more distant from Asia, studies have also pointed to a possible
1330 influence of the Central American Seaway (Prabhat et al., 2022) or Drake (Toumoulin et

1331 al., 2020) and Tasman (Scher et al., 2015) Gateway openings on oceanic circulation, which
1332 may have in turn impacted sea surface temperature gradients and monsoon activity.

1333 7 Conclusions

1334 In this study, we took advantage of recent work that extended the Asian paleo-
1335 monsoonal record back to the Paleogene and of the improved understanding of the physical
1336 concepts underpinning the monsoons derived from climate model sensitivity experiments.
1337 Overall, we simulate an intensification of monsoonal metrics throughout the Cenozoic, in
1338 response to evolving paleogeography and global climate trends. Our results suggest that
1339 modern-like monsoons likely existed since at least the mid-late Miocene when considering to-
1340 gether patterns of atmospheric circulation as well as seasonality and precipitation amounts,
1341 in agreement with paleoclimate indicators. However, we also show that high rainfall sea-
1342 sonality already existed since the Paleogene in both SAM and EAM domains, before the
1343 establishment of modern atmospheric circulation patterns. In accord with previous studies,
1344 our results highlight the limited effect of $p\text{CO}_2$ on monsoon dynamics, when compared to
1345 the effect of paleogeographic changes. A notable exception is the strong impact of a $p\text{CO}_2$
1346 drawdown at the EOT on the northward migration of the subtropical Jet Stream during
1347 summer, which increases precipitation in the EAM region.

1348 Our results also strongly suggest that any variations in the land-sea distribution,
1349 whether due to tectonic activity or sea level fluctuations, would have strongly impacted
1350 Asian climate, despite the fact that the exact shape and extent of coastal shallow-water
1351 environments remain poorly constrained. Many episodes of increased continentality are doc-
1352 umented over the course of the Cenozoic, including regional regressions of the Paratethys
1353 epicontinental Sea and periodic exposure of the Arabian Platform due to sea level fluctua-
1354 tions since the Eocene-Oligocene Transition. All of these events likely favored the enhance-
1355 ment of summer moisture penetration into Asia, by promoting the extension of the wide
1356 subtropical low pressure belt, thereby amplifying the seasonal latitudinal migration of the
1357 ITCZ on land.

1358 In addition, while the evolution of the Himalayan-TP complex is recurrently put for-
1359 ward as the leading phenomenon driving Asian climate evolution, our results rather point
1360 towards a combined effect of all landforms surrounding the modern Indian Ocean. We also
1361 emphasize that all paleogeographic features do not bear the same importance on the SASM,
1362 EASM or EAWM, respectively. Our simulations suggest that the Tibetan Plateau uplift
1363 likely favored the onset of monsoon-like precipitation seasonality in eastern Asia in the
1364 Eocene, by promoting the advection of moist air masses in summer and partially shielding
1365 the region from westerly moisture input during winter. Alongside that, we show that the up-
1366 lift of Eastern African and Anatolian-Iranian landforms was critical to intensify and redirect
1367 the Somali Jet towards the Indian subcontinent, thereby contributing to the development of
1368 a modern-like South Asian monsoon summer circulation and amplifying moisture advection
1369 towards Asia in summer. In addition, in our simulations, the uplift of the Anatolian-Iranian
1370 orogen contributed to enhancing winter aridity in most of southeastern Asia by blocking
1371 moisture advection from the westerlies to lower latitudes.

1372 Our simulations further show that uplift of the Tian Shan and the Mongolian moun-
1373 tains was key for the establishment of the winter Siberian High, and resulting aridification
1374 of inland and eastern Asia during winter. The summer Jet Stream migration north of the
1375 Tibetan Plateau was likely amplified in the mid-late Miocene, as the Pamir and Tian Shan
1376 landforms approached their modern elevations and contributed to channeling the jet towards
1377 higher latitudes. This relocation of the Jet Stream amplifies the penetration of moist air
1378 masses over eastern China, which contributes to increasing EAM precipitation seasonality.
1379 Overall, our results do suggest a fundamentally polygenetic history of monsoonal evolution,
1380 in agreement with available paleoclimate indicators and previous modeling studies. This
1381 suggests that the very concept of a "monsoon onset" is inappropriate. We also stress the

1382 need for more accurate constraints on the evolution of paleo-shorelines, the relative timing
1383 of peripheral mountain belts uplift, as well as on the paleo-elevation of landforms in order
1384 to better understand the evolution of Asian climate in the past.

1385 **Acronyms**

1386 **ITCZ** Inter Tropical Convergence Zone
1387 **SASM** South Asian Summer Monsoon
1388 **EASM** East Asian Summer Monsoon
1389 **EAWM** East Asian Winter Monsoon
1390 **TP** Tibetan Plateau
1391 **EOT** Eocene Oligocene Transition
1392 **CLAMP** Climate Leaf Analysis Multivariate Program

1393 **Acknowledgments**

1394 D.T., G.L.H., F.F., A.T., Y.D., P.S., J-B.L. and A-C.S. were granted access to the HPC
1395 resources of TGCC under the allocations 2018-A0050107601, 2018-A0030102212, 2019-
1396 A0070107601, 2019-A0050102212 and 2020-A0090107601 made by GENCI. D.T. has re-
1397 ceived funding from the European Research Council (ERC) under the European Union's
1398 Horizon 2020 research and innovation programme (grant agreement No 865787). Y.D. ac-
1399 knowledges support from ANR AMOR (ANR-16-CE31-0020). Most of the Figures were
1400 done using NOAA pyferret within Jupyter notebooks, thanks to the ferretmagic add-on
1401 developed at LSCE by Patrick Brockmann. Ferret is a product of NOAA's Pacific Marine
1402 Environmental Laboratory. Information is available at <http://ferret.pmel.noaa.gov/Ferret>
1403 (last access: 1 Jan 2022; NOAA's Pacific Marine Environmental Laboratory, 2020), dis-
1404 tributed under the Open Source Definition. The Jupyter notebook is an open-source
1405 web application. The paleogeographic configurations from F.P. were produced using the
1406 paleoenvironment online application (<https://map.paleoenvironment.eu/>). Other recon-
1407 structions were obtained with NetCDF editor online tools developed by the Paleoclimate
1408 modelling group at CEREGE laboratory ([https://paleoclim-cnrs.github.io/documentation-
1409 processing/IPSL_Boundary_Conditions/](https://paleoclim-cnrs.github.io/documentation-processing/IPSL_Boundary_Conditions/)). The scientific color maps (<https://www.fabiocrameri.ch/colourmaps/>)
1410 (Crameri, 2021) used in most of the Figures prevent visual distortion of the data and exclu-
1411 sion of readers with color vision deficiencies (Crameri et al., 2020).

1412

References

- 1413 Abels, H. A., Dupont-Nivet, G., Xiao, G., Bosboom, R., & Krijgsman, W. (2011, Jan-
 1414 uary). Step-wise change of Asian interior climate preceding the Eocene–Oligocene
 1415 Transition (EOT). *Palaeogeography, Palaeoclimatology, Palaeoecology*, *299*(3-4), 399–
 1416 412. Retrieved 2017-10-09, from [http://linkinghub.elsevier.com/retrieve/pii/
 1417 S0031018210007042](http://linkinghub.elsevier.com/retrieve/pii/S0031018210007042) doi: 10.1016/j.palaeo.2010.11.028
- 1418 Acosta, R. P., & Huber, M. (2017). The neglected Indo-Gangetic Plains low-level jet and its
 1419 importance for moisture transport and precipitation during the peak summer mon-
 1420 soon. *Geophysical Research Letters*, *44*(16), 8601–8610. Retrieved 2021-03-08, from
 1421 <https://agupubs.onlinelibrary.wiley.com/doi/abs/10.1002/2017GL074440>
 1422 (_eprint: <https://agupubs.onlinelibrary.wiley.com/doi/pdf/10.1002/2017GL074440>)
 1423 doi: <https://doi.org/10.1002/2017GL074440>
- 1424 Acosta, R. P., & Huber, M. (2020, February). Competing Topographic Mechanisms for the
 1425 Summer Indo-Asian Monsoon. *Geophysical Research Letters*, *47*(3). Retrieved 2020-
 1426 06-19, from <https://onlinelibrary.wiley.com/doi/abs/10.1029/2019GL085112>
 1427 doi: 10.1029/2019GL085112
- 1428 Agard, P., Omrani, J., Jolivet, L., Whitechurch, H., Vrielynck, B., Spakman, W., ... Wor-
 1429 tel, R. (2011, November). Zagros orogeny: a subduction-dominated process. *Geologi-
 1430 cal Magazine*, *148*(5-6), 692–725. Retrieved 2017-10-09, from [http://www.journals
 1431 .cambridge.org/abstract.S001675681100046X](http://www.journals) doi: 10.1017/S001675681100046X
- 1432 Ali, J. R., & Aitchison, J. C. (2005, October). Greater India. *Earth-Science Reviews*,
 1433 *72*(3-4), 169–188. Retrieved 2022-09-13, from [https://linkinghub.elsevier.com/
 1434 retrieve/pii/S0012825205001042](https://linkinghub.elsevier.com/retrieve/pii/S0012825205001042) doi: 10.1016/j.earscirev.2005.07.005
- 1435 Ali, S., Hathorne, E. C., & Frank, M. (2021). Persistent Provenance of South
 1436 Asian Monsoon-Induced Silicate Weathering Over the Past 27 Million Years. *Pa-
 1437 leoceanography and Paleoclimatology*, *36*(3), e2020PA003909. Retrieved 2022-
 1438 05-02, from <https://onlinelibrary.wiley.com/doi/abs/10.1029/2020PA003909>
 1439 (_eprint: <https://onlinelibrary.wiley.com/doi/pdf/10.1029/2020PA003909>) doi: 10.
 1440 1029/2020PA003909
- 1441 Anderson, C., Murray, R., Dunlea, A., Giosan, L., Kinsley, C., McGee, D., & Tada, R.
 1442 (2020, May). Aeolian delivery to Ulleung Basin, Korea (Japan Sea), during devel-
 1443 opment of the East Asian Monsoon through the last 12 Ma. *Geological Magazine*,
 1444 *157*(5), 806–817. Retrieved 2022-11-14, from [https://www.cambridge.org/core/
 1445 product/identifier/S001675681900013X/type/journal_article](https://www.cambridge.org/core/product/identifier/S001675681900013X/type/journal_article) doi: 10.1017/
 1446 S001675681900013X
- 1447 Ao, H., Roberts, A. P., Dekkers, M. J., Liu, X., Rohling, E. J., Shi, Z., ... Zhao, X. (2016,
 1448 June). Late Miocene–Pliocene Asian monsoon intensification linked to Antarctic ice-
 1449 sheet growth. *Earth and Planetary Science Letters*, *444*, 75–87. Retrieved 2022-05-03,
 1450 from <https://linkinghub.elsevier.com/retrieve/pii/S0012821X16301157> doi:
 1451 10.1016/j.epsl.2016.03.028
- 1452 Ao, H., Rohling, E. J., Zhang, R., Roberts, A. P., Holbourn, A. E., Ladant, J.-B., ... An,
 1453 Z. (2021, November). Global warming-induced Asian hydrological climate transition
 1454 across the Miocene–Pliocene boundary. *Nature Communications*, *12*(1), 6935. Re-
 1455 trieved 2022-05-03, from <http://www.nature.com/articles/s41467-021-27054-5>
 1456 (Number: 1 Publisher: Nature Publishing Group) doi: 10.1038/s41467-021-27054-5
- 1457 Aoki, I., Kurosaki, Y., Osada, R., Sato, T., & Kimura, F. (2005). Dust
 1458 storms generated by mesoscale cold fronts in the Tarim Basin, Northwest
 1459 China. *Geophysical Research Letters*, *32*(6). Retrieved 2022-02-21, from
 1460 <http://onlinelibrary.wiley.com/doi/abs/10.1029/2004GL021776> (_eprint:
 1461 <https://agupubs.onlinelibrary.wiley.com/doi/pdf/10.1029/2004GL021776>) doi: 10.
 1462 1029/2004GL021776
- 1463 Auer, G., Vleeschouwer, D. D., Smith, R. A., Bogus, K., Groeneveld, J., Grunert,
 1464 P., ... Henderiks, J. (2019). Timing and Pacing of Indonesian Throughflow
 1465 Restriction and Its Connection to Late Pliocene Climate Shifts. *Paleoceanogra-
 1466 phy and Paleoclimatology*, *34*(4), 635–657. Retrieved 2021-09-02, from <http://>

- 1467 agupubs.onlinelibrary.wiley.com/doi/abs/10.1029/2018PA003512 (eprint:
1468 https://onlinelibrary.wiley.com/doi/pdf/10.1029/2018PA003512) doi: 10.1029/
1469 2018PA003512
- 1470 Averyanova, A., Tarasevich, V., Popova, S., Utescher, T., Li, S.-F., Mosbrugger, V., & Xing,
1471 Y. (2021, February). Rupelian Kazakhstan floras in the context of early Oligocene
1472 climate and vegetation in Central Asia. *Terra Nova*, 33. doi: 10.1111/ter.12523
- 1473 Baldermann, A., Wasser, O., Abdullayev, E., Bernasconi, S., Löhr, S., Wemmer, K., ...
1474 Richoz, S. (2021, September). Palaeo-environmental evolution of Central Asia during
1475 the Cenozoic: new insights from the continental sedimentary archive of the Valley
1476 of Lakes (Mongolia). *Climate of the Past*, 17(5), 1955–1972. Retrieved 2022-03-09,
1477 from <https://cp.copernicus.org/articles/17/1955/2021/> doi: 10.5194/cp-17-
1478 -1955-2021
- 1479 Baldwin, J., & Vecchi, G. (2016, August). Influence of the Tian Shan on Arid Ex-
1480 tratropical Asia. *Journal of Climate*, 29(16), 5741–5762. Retrieved 2021-09-
1481 23, from [https://journals.ametsoc.org/view/journals/clim/29/16/jcli-d-15-](https://journals.ametsoc.org/view/journals/clim/29/16/jcli-d-15-0490.1.xml)
1482 [-0490.1.xml](https://journals.ametsoc.org/view/journals/clim/29/16/jcli-d-15-0490.1.xml) (Publisher: American Meteorological Society Section: Journal of Cli-
1483 mate) doi: 10.1175/JCLI-D-15-0490.1
- 1484 Ballato, P., Landgraf, A., Schildgen, T. F., Stockli, D. F., Fox, M., Ghassemi, M. R.,
1485 ... Strecker, M. R. (2015, September). The growth of a mountain belt forced
1486 by base-level fall: Tectonics and surface processes during the evolution of the Al-
1487 borz Mountains, N Iran. *Earth and Planetary Science Letters*, 425, 204–218. Re-
1488 trieved 2021-03-10, from [https://www.sciencedirect.com/science/article/pii/](https://www.sciencedirect.com/science/article/pii/S0012821X15003490)
1489 [S0012821X15003490](https://www.sciencedirect.com/science/article/pii/S0012821X15003490) doi: 10.1016/j.epsl.2015.05.051
- 1490 Ballato, P., Mulch, A., Landgraf, A., Strecker, M. R., Dalconi, M. C., Friedrich, A., &
1491 Tabatabaei, S. H. (2010, November). Middle to late Miocene Middle Eastern climate
1492 from stable oxygen and carbon isotope data, southern Alborz mountains, N Iran. *Earth*
1493 *and Planetary Science Letters*, 300(1), 125–138. Retrieved 2021-04-07, from [https://](https://www.sciencedirect.com/science/article/pii/S0012821X10006308)
1494 www.sciencedirect.com/science/article/pii/S0012821X10006308 doi: 10.1016/
1495 j.epsl.2010.09.043
- 1496 Bande, A., Sobel, E. R., Mikolaichuk, A., Schmidt, A., & Stockli, D. F. (2017). Ex-
1497 humation history of the western Kyrgyz Tien Shan: Implications for intramontane
1498 basin formation. *Tectonics*, 36(1), 163–180. Retrieved 2021-03-26, from [http://](http://agupubs.onlinelibrary.wiley.com/doi/abs/10.1002/2016TC004284)
1499 agupubs.onlinelibrary.wiley.com/doi/abs/10.1002/2016TC004284 (eprint:
1500 <https://onlinelibrary.wiley.com/doi/pdf/10.1002/2016TC004284>) doi: [https://doi](https://doi.org/10.1002/2016TC004284)
1501 [.org/10.1002/2016TC004284](https://doi.org/10.1002/2016TC004284)
- 1502 Bannon, P. R. (1979, November). On the Dynamics of the East African Jet. I: Simu-
1503 lation of Mean Conditions for July. *Journal of the Atmospheric Sciences*, 36(11),
1504 2139–2152. Retrieved 2019-07-05, from [http://journals.ametsoc.org/doi/abs/](http://journals.ametsoc.org/doi/abs/10.1175/1520-0469%281979%29036%3C2139%3AOTDOTE%3E2.0.CO%3B2)
1505 [10.1175/1520-0469%281979%29036%3C2139%3AOTDOTE%3E2.0.CO%3B2](http://journals.ametsoc.org/doi/abs/10.1175/1520-0469%281979%29036%3C2139%3AOTDOTE%3E2.0.CO%3B2) doi: 10.1175/
1506 1520-0469(1979)036(2139:OTDOTE)2.0.CO;2
- 1507 Barbolini, N., Woutersen, A., Dupont-Nivet, G., Silvestro, D., Tardif, D., Coster, P. M. C.,
1508 ... Hoorn, C. (2020). Cenozoic evolution of the steppe-desert biome in Central
1509 Asia. *Science Advances*, 6(41), eabb8227. Retrieved 2022-05-03, from [https://www](https://www.science.org/doi/10.1126/sciadv.abb8227)
1510 [.science.org/doi/10.1126/sciadv.abb8227](https://www.science.org/doi/10.1126/sciadv.abb8227) (Publisher: American Association for
1511 the Advancement of Science) doi: 10.1126/sciadv.abb8227
- 1512 Barrier, , Vrielynck, B., & Brunet-Lourdin, M.-F. (2018). *Paleotectonic Reconstruction*
1513 *of the Central Tethyan Realm: Tectono-Sedimentary-Palinspastic Maps from Late*
1514 *Permian to Pliocene: Atlas of 20 Maps.*
- 1515 Beasley, C., Kender, S., Giosan, L., Bolton, C. T., Anand, P., Leng, M. J.,
1516 ... Littler, K. (2021). Evidence of a South Asian Proto-Monsoon Dur-
1517 ing the Oligocene-Miocene Transition. *Paleoceanography and Paleocli-*
1518 *matology*, 36(9), e2021PA004278. Retrieved 2022-05-03, from [https://](https://onlinelibrary.wiley.com/doi/abs/10.1029/2021PA004278)
1519 onlinelibrary.wiley.com/doi/abs/10.1029/2021PA004278 (eprint:
1520 <https://onlinelibrary.wiley.com/doi/pdf/10.1029/2021PA004278>) doi: 10.1029/
1521 2021PA004278

- 1522 Bershaw, J., Garziona, C. N., Schoenbohm, L., Gehrels, G., & Tao, L. (2012, January).
 1523 Cenozoic evolution of the Pamir plateau based on stratigraphy, zircon provenance,
 1524 and stable isotopes of foreland basin sediments at Oyttag (Wuyitake) in the Tarim
 1525 Basin (west China). *Journal of Asian Earth Sciences*, *44*, 136–148. Retrieved 2017-
 1526 10-09, from <http://linkinghub.elsevier.com/retrieve/pii/S1367912011001878>
 1527 doi: 10.1016/j.jseaes.2011.04.020
- 1528 Betzler, C., Eberli, G. P., Kroon, D., Wright, J. D., Swart, P. K., Nath, B. N., ... Young,
 1529 J. R. (2016, July). The abrupt onset of the modern South Asian Monsoon winds.
 1530 *Scientific Reports*, *6*(1), 29838. Retrieved 2022-05-03, from [http://www.nature.com/](http://www.nature.com/articles/srep29838)
 1531 [articles/srep29838](http://www.nature.com/articles/srep29838) (Number: 1 Publisher: Nature Publishing Group) doi: 10
 1532 .1038/srep29838
- 1533 Betzler, C., Eberli, G. P., Lüdmann, T., Reolid, J., Kroon, D., Reijmer, J. J. G., ... Yao,
 1534 Z. (2018, January). Refinement of Miocene sea level and monsoon events from the
 1535 sedimentary archive of the Maldives (Indian Ocean). *Progress in Earth and Planetary*
 1536 *Science*, *5*(1), 5. Retrieved 2021-03-17, from [https://doi.org/10.1186/s40645-018-](https://doi.org/10.1186/s40645-018-0165-x)
 1537 [-0165-x](https://doi.org/10.1186/s40645-018-0165-x) doi: 10.1186/s40645-018-0165-x
- 1538 Bhatia, H., Khan, M. A., Srivastava, G., Hazra, T., Spicer, R., Hazra, M., ... Roy, K. (2021,
 1539 May). Late Cretaceous–Paleogene Indian monsoon climate vis-à-vis movement of the
 1540 Indian plate, and the birth of the South Asian Monsoon. *Gondwana Research*, *93*,
 1541 89–100. Retrieved 2022-05-03, from [https://linkinghub.elsevier.com/retrieve/](https://linkinghub.elsevier.com/retrieve/pii/S1342937X21000289)
 1542 [pii/S1342937X21000289](https://linkinghub.elsevier.com/retrieve/pii/S1342937X21000289) doi: 10.1016/j.jgr.2021.01.010
- 1543 Bhatia, H., Srivastava, G., Adhikari, P., Tao, S., Utescher, T., Paudyal, K. N., &
 1544 Mehrotra, R. C. (2022, April). Asian monsoon and vegetation shift: evidence
 1545 from the Siwalik succession of India. *Geological Magazine*, 1–18. Retrieved 2022-
 1546 05-02, from [http://www.cambridge.org/core/journals/geological-magazine/](http://www.cambridge.org/core/journals/geological-magazine/article/asian-monsoon-and-vegetation-shift-evidence-from-the-siwalik-succesion-of-india/C11DD05BB2C70B0BA4ED7930A80219D2)
 1547 [article/asian-monsoon-and-vegetation-shift-evidence-from-the-siwalik](http://www.cambridge.org/core/journals/geological-magazine/article/asian-monsoon-and-vegetation-shift-evidence-from-the-siwalik-succesion-of-india/C11DD05BB2C70B0BA4ED7930A80219D2)
 1548 [-succesion-of-india/C11DD05BB2C70B0BA4ED7930A80219D2](http://www.cambridge.org/core/journals/geological-magazine/article/asian-monsoon-and-vegetation-shift-evidence-from-the-siwalik-succesion-of-india/C11DD05BB2C70B0BA4ED7930A80219D2) (Publisher: Cam-
 1549 bridge University Press) doi: 10.1017/S0016756822000243
- 1550 Bhatia, H., Srivastava, G., Spicer, R., Farnsworth, A., Spicer, T., Mehrotra, R., ... Valdes,
 1551 P. (2021, January). Leaf physiognomy records the Miocene intensification of the South
 1552 Asia Monsoon. *Global and Planetary Change*, *196*, 103365. Retrieved 2022-05-03,
 1553 from <https://linkinghub.elsevier.com/retrieve/pii/S0921818120302563> doi:
 1554 10.1016/j.gloplacha.2020.103365
- 1555 Bialik, O. M., Auer, G., Ogawa, N. O., Kroon, D., Waldmann, N. D., & Ohkouchi, N.
 1556 (2020). Monsoons, Upwelling, and the Deoxygenation of the Northwestern Indian
 1557 Ocean in Response to Middle to Late Miocene Global Climatic Shifts. *Paleoceanogra-*
 1558 *phy and Paleoclimatology*, *35*(2), e2019PA003762. Retrieved 2021-03-17, from [http://](http://agupubs.onlinelibrary.wiley.com/doi/abs/10.1029/2019PA003762)
 1559 agupubs.onlinelibrary.wiley.com/doi/abs/10.1029/2019PA003762 (eprint:
 1560 <https://onlinelibrary.wiley.com/doi/pdf/10.1029/2019PA003762>) doi: [https://doi](https://doi.org/10.1029/2019PA003762)
 1561 [.org/10.1029/2019PA003762](https://doi.org/10.1029/2019PA003762)
- 1562 Bialik, O. M., Frank, M., Betzler, C., Zammit, R., & Waldmann, N. D. (2019, June).
 1563 Two-step closure of the Miocene Indian Ocean Gateway to the Mediterranean. *Sci-*
 1564 *entific Reports*, *9*(1), 8842. Retrieved 2021-03-09, from [https://www.nature.com/](https://www.nature.com/articles/s41598-019-45308-7)
 1565 [articles/s41598-019-45308-7](https://www.nature.com/articles/s41598-019-45308-7) (Number: 1 Publisher: Nature Publishing Group)
 1566 doi: 10.1038/s41598-019-45308-7
- 1567 Biasutti, M., Voigt, A., Boos, W. R., Braconnot, P., Hargreaves, J. C., Harrison, S. P.,
 1568 ... Xie, S.-P. (2018, June). Global energetics and local physics as drivers of past,
 1569 present and future monsoons. *Nature Geoscience*, *11*(6), 392–400. Retrieved 2019-
 1570 01-22, from <http://www.nature.com/articles/s41561-018-0137-1> doi: 10.1038/
 1571 [s41561-018-0137-1](http://www.nature.com/articles/s41561-018-0137-1)
- 1572 Bierman, P. R., Shakun, J. D., Corbett, L. B., Zimmerman, S. R., & Rood, D. H.
 1573 (2016, December). A persistent and dynamic East Greenland Ice Sheet over the
 1574 past 7.5 million years. *Nature*, *540*(7632), 256–260. Retrieved 2021-06-21, from
 1575 <http://www.nature.com/articles/nature20147> (Bandiera.abtest: a Cg_type: Na-
 1576 ture Research Journals Number: 7632 Primary_atype: Research Publisher: Nature

- 1577 Publishing Group Subject_term: Cryospheric science;Nuclear chemistry;Palaeoclimate
 1578 Subject_term_id: cryospheric-science;nuclear-chemistry;palaeoclimate) doi: 10.1038/
 1579 nature20147
- 1580 Blayney, T., Najman, Y., Dupont-Nivet, G., Carter, A., Millar, I., Garzanti, E., ... Vezzoli,
 1581 G. (2016, October). Indentation of the Pamirs with respect to the northern margin
 1582 of Tibet: Constraints from the Tarim basin sedimentary record: INDENTATION OF
 1583 THE PAMIRS. *Tectonics*, *35*(10), 2345–2369. Retrieved 2017-10-09, from [http://](http://doi.wiley.com/10.1002/2016TC004222)
 1584 doi.wiley.com/10.1002/2016TC004222 doi: 10.1002/2016TC004222
- 1585 Bolton, C. T., Gray, E., Kuhnt, W., Holbourn, A. E., Lübbers, J., Grant, K., ... Andersen,
 1586 N. (2022, April). Secular and orbital-scale variability of equatorial Indian Ocean
 1587 summer monsoon winds during the late Miocene. *Climate of the Past*, *18*(4), 713–738.
 1588 Retrieved 2022-06-02, from <https://cp.copernicus.org/articles/18/713/2022/>
 1589 doi: 10.5194/cp-18-713-2022
- 1590 Boos, W. R., & Kuang, Z. (2010, January). Dominant control of the South Asian monsoon by
 1591 orographic insulation versus plateau heating. *Nature*, *463*(7278), 218–222. Retrieved
 1592 2017-10-09, from <http://www.nature.com/doi/10.1038/nature08707> doi:
 1593 10.1038/nature08707
- 1594 Boos, W. R., & Kuang, Z. (2013, February). Sensitivity of the South Asian monsoon to
 1595 elevated and non-elevated heating. *Scientific Reports*, *3*(1), 1192. Retrieved 2023-
 1596 03-31, from <https://www.nature.com/articles/srep01192> (Number: 1 Publisher:
 1597 Nature Publishing Group) doi: 10.1038/srep01192
- 1598 Bosboom, R., Dupont-Nivet, G., Grothe, A., Brinkhuis, H., Villa, G., Mandic, O., ...
 1599 Krijgsman, W. (2014a, October). Linking Tarim Basin sea retreat (west China) and
 1600 Asian aridification in the late Eocene. *Basin Research*, *26*(5), 621–640. Retrieved 2017-
 1601 10-09, from <http://doi.wiley.com/10.1111/bre.12054> doi: 10.1111/bre.12054
- 1602 Bosboom, R., Dupont-Nivet, G., Grothe, A., Brinkhuis, H., Villa, G., Mandic, O., ... Guo,
 1603 Z. (2014b, June). Timing, cause and impact of the late Eocene stepwise sea retreat
 1604 from the Tarim Basin (west China). *Palaeogeography, Palaeoclimatology, Palaeoecol-*
 1605 *ogy*, *403*, 101–118. Retrieved 2017-10-09, from [http://linkinghub.elsevier.com/](http://linkinghub.elsevier.com/retrieve/pii/S0031018214001709)
 1606 [retrieve/pii/S0031018214001709](http://linkinghub.elsevier.com/retrieve/pii/S0031018214001709) doi: 10.1016/j.palaeo.2014.03.035
- 1607 Bosboom, R., Mandic, O., Dupont-Nivet, G., Proust, J.-N., Ormukov, C., & Aminov, J.
 1608 (2017). Late Eocene palaeogeography of the proto-Paratethys Sea in Central Asia
 1609 (NW China, southern Kyrgyzstan and SW Tajikistan). *Geological Society, Lon-*
 1610 *don, Special Publications*, *427*(1), 565–588. Retrieved 2019-11-22, from [http://](http://sp.lyellcollection.org/lookup/doi/10.1144/SP427.11)
 1611 sp.lyellcollection.org/lookup/doi/10.1144/SP427.11 doi: 10.1144/SP427.11
- 1612 Botsyun, S., Sepulchre, P., Donnadieu, Y., Risi, C., Licht, A., & Caves Rugenstein,
 1613 J. K. (2019, March). Revised paleoaltimetry data show low Tibetan Plateau el-
 1614 evation during the Eocene. *Science*, *363*(6430), eaaq1436. Retrieved 2019-07-23,
 1615 from <http://www.sciencemag.org/lookup/doi/10.1126/science.aaq1436> doi:
 1616 10.1126/science.aaq1436
- 1617 Botsyun, S., Sepulchre, P., Risi, C., & Donnadieu, Y. (2016, June). Impacts of Tibetan
 1618 Plateau uplift on atmospheric dynamics and associated precipitation ¹⁸O. *Climate of*
 1619 *the Past*, *12*(6), 1401–1420. Retrieved 2017-10-09, from [http://www.clim-past.net/](http://www.clim-past.net/12/1401/2016/)
 1620 [12/1401/2016/](http://www.clim-past.net/12/1401/2016/) doi: 10.5194/cp-12-1401-2016
- 1621 Boucot, A. J., Xu, C., Scotese, C. R., & Morley, R. J. (2013). *Phanerozoic Paleoclimate: An*
 1622 *Atlas of Lithologic Indicators of Climate*. Tulsa, Oklahoma, U.S.A.: SEPM (Society for
 1623 Sedimentary Geology). Retrieved 2019-11-04, from [https://pubs.geoscienceworld](https://pubs.geoscienceworld.org/books/book/1966/)
 1624 [.org/books/book/1966/](https://pubs.geoscienceworld.org/books/book/1966/) doi: 10.2110/sepmcsp.11
- 1625 Bougeois, L., Dupont-Nivet, G., de Rafélis, M., Tindall, J. C., Proust, J.-N., Reichart,
 1626 G.-J., ... Ormukov, C. (2018, March). Asian monsoons and aridification response
 1627 to Paleogene sea retreat and Neogene westerly shielding indicated by seasonality in
 1628 Paratethys oysters. *Earth and Planetary Science Letters*, *485*, 99–110. Retrieved 2018-
 1629 04-03, from <http://linkinghub.elsevier.com/retrieve/pii/S0012821X17307483>
 1630 doi: 10.1016/j.epsl.2017.12.036
- 1631 Bullen, M., Burbank, D., & Garver, J. (2003, March). Building the Northern Tien Shan: In-

- 1632 tegrated Thermal, Structural, and Topographic Constraints. *The Journal of Geology*,
1633 111(2), 149–165. Retrieved 2021-03-26, from [https://www.journals.uchicago.edu/](https://www.journals.uchicago.edu/doi/10.1086/345840)
1634 doi/10.1086/345840 doi: 10.1086/345840
- 1635 Burls, N. J., Bradshaw, C. D., Boer, A. M. D., Herold, N., Huber, M., Pound,
1636 M., ... Zhang, Z. (2021). Simulating Miocene Warmth: Insights From
1637 an Opportunistic Multi-Model Ensemble (MioMIP1). *Paleoceanography and Pa-*
1638 *leoclimatology*, 36(5), e2020PA004054. Retrieved 2021-06-21, from [http://](http://agupubs.onlinelibrary.wiley.com/doi/abs/10.1029/2020PA004054)
1639 agupubs.onlinelibrary.wiley.com/doi/abs/10.1029/2020PA004054 (_eprint:
1640 <https://onlinelibrary.wiley.com/doi/pdf/10.1029/2020PA004054>) doi: 10.1029/
1641 2020PA004054
- 1642 Cane, M. A., & Molnar, P. (2001, May). Closing of the Indonesian seaway as a
1643 precursor to east African aridification around 3–4 million years ago. *Nature*,
1644 411(6834), 157–162. Retrieved 2021-09-09, from [http://www.nature.com/articles/](http://www.nature.com/articles/35075500)
1645 35075500 (Bandiera.abtest: a Cg_type: Nature Research Journals Number: 6834 Pri-
1646 mary_atype: Research Publisher: Nature Publishing Group) doi: 10.1038/35075500
- 1647 Carrapa, B., DeCelles, P. G., Wang, X., Clementz, M. T., Mancin, N., Stoica, M., ... Chen,
1648 F. (2015, August). Tectono-climatic implications of Eocene Paratethys regression in
1649 the Tajik basin of central Asia. *Earth and Planetary Science Letters*, 424, 168–178. Re-
1650 trieved 2022-03-21, from [https://www.sciencedirect.com/science/article/pii/](https://www.sciencedirect.com/science/article/pii/S0012821X15003325)
1651 S0012821X15003325 doi: 10.1016/j.epsl.2015.05.034
- 1652 Cavazza, W., Cattò, S., Zattin, M., Okay, A. I., & Reiners, P. (2018, August). Ther-
1653 mochronology of the Miocene Arabia-Eurasia collision zone of southeastern Turkey.
1654 *Geosphere*, 14(5), 2277–2293. Retrieved 2022-03-04, from [https://doi.org/10](https://doi.org/10.1130/GES01637.1)
1655 .1130/GES01637.1 doi: 10.1130/GES01637.1
- 1656 Caves Rugenstein, J., Bayshashov, B., Zhamangara, A., Ritch, A., Ibarra, D., Mix, H.,
1657 ... Chamberlain, C. (2017, February). Late Miocene Uplift of the Tian Shan and
1658 Altai and Reorganization of Central Asia Climate. *GSA Today*, 27. doi: 10.1130/
1659 GSATG305A.1
- 1660 Caves Rugenstein, J., Sjostrom, D., Mix, H., Winnick, M., & Chamberlain, C. (2014,
1661 September). Aridification of Central Asia and Uplift of the Altai and Hangay Moun-
1662 tains, Mongolia: Stable Isotope Evidence. *American Journal of Science*, 314, 1171–
1663 1201. doi: 10.2475/08.2014.01]
- 1664 Chakraborty, A., Nanjundiah, R. S., & Srinivasan, J. (2009). Impact of African
1665 orography and the Indian summer monsoon on the low-level Somali jet. *In-*
1666 *ternational Journal of Climatology*, 29(7), 983–992. Retrieved 2022-06-28,
1667 from <http://onlinelibrary.wiley.com/doi/abs/10.1002/joc.1720> (_eprint:
1668 <https://rmets.onlinelibrary.wiley.com/doi/pdf/10.1002/joc.1720>) doi: 10.1002/joc
1669 .1720
- 1670 Charreau, J., Chen, Y., Gilder, S., Dominguez, S., Avouac, J.-P., Sen, S., ... Wang,
1671 W.-M. (2005, January). Magnetostratigraphy and rock magnetism of the Neogene
1672 Kuitun He section (northwest China): implications for Late Cenozoic uplift of the
1673 Tianshan mountains. *Earth and Planetary Science Letters*, 230(1), 177–192. Re-
1674 trieved 2021-03-29, from [https://www.sciencedirect.com/science/article/pii/](https://www.sciencedirect.com/science/article/pii/S0012821X04006739)
1675 S0012821X04006739 doi: 10.1016/j.epsl.2004.11.002
- 1676 Charreau, J., Kent-Corson, M. L., Barrier, L., Augier, R., Ritts, B. D., Chen, Y., ... Guil-
1677 mette, C. (2012, August). A high-resolution stable isotopic record from the Junggar
1678 Basin (NW China): Implications for the paleotopographic evolution of the Tianshan
1679 Mountains. *Earth and Planetary Science Letters*, 341-344, 158–169. Retrieved 2017-
1680 10-09, from <http://linkinghub.elsevier.com/retrieve/pii/S0012821X12002622>
1681 doi: 10.1016/j.epsl.2012.05.033
- 1682 Cheng, Y.-M., & Yang, X.-N. (2016, February). Miocene woods from the Qaidam
1683 Basin on northern Qinghai-Tibet Plateau with implications for paleoenvironmen-
1684 tal change. *Journal of Asian Earth Sciences*, 116, 198–207. Retrieved 2023-01-03,
1685 from <https://linkinghub.elsevier.com/retrieve/pii/S1367912015301516> doi:
1686 10.1016/j.jseaes.2015.11.022

- 1687 Clark, M., House, M., Royden, L., Whipple, K., Burchfiel, B., Zhang, X., & Tang, W. (2005,
1688 June). Late Cenozoic uplift of southeastern Tibet. *Geology*, *33*(6), 525–528. Retrieved
1689 2022-03-03, from <https://doi.org/10.1130/G21265.1> doi: 10.1130/G21265.1
- 1690 Clift, P. D. (2020, June). Asian monsoon dynamics and sediment transport in SE
1691 Asia. *Journal of Asian Earth Sciences*, *195*, 104352. Retrieved 2022-05-02, from
1692 <https://linkinghub.elsevier.com/retrieve/pii/S1367912020301334> doi: 10
1693 .1016/j.jseaes.2020.104352
- 1694 Clift, P. D., Betzler, C., Christensen, B., Clemens, S., Eberli, G., France-Lanord, C., ...
1695 Wan, S. (2022, July). A synthesis of monsoon exploration in the Asian marginal seas.
1696 *Scientific Drilling*, *10*, 1–29. doi: 10.5194/sd-10-1-2022
- 1697 Clift, P. D., Hodges, K., Heslop, Hannigan, R., Hoang, L., & Calves, G. (2008, Novem-
1698 ber). Correlation of Himalayan exhumation rates and Asia monsoon intensity. *Nature*
1699 *Geoscience*, *1*, doi:10.1038/ngeo351. doi: 10.1038/ngeo351
- 1700 Clift, P. D., Kulhanek, D. K., Zhou, P., Bowen, M. G., Vincent, S. M., Lyle, M., & Hahn,
1701 A. (2019, June). Chemical weathering and erosion responses to changing monsoon
1702 climate in the Late Miocene of Southwest Asia. *Geological Magazine*, *157*(6), 939–955.
1703 Retrieved 2021-05-27, from <https://doi.org/10.1017/S0016756819000608> doi:
1704 10.1017/S0016756819000608
- 1705 Clift, P. D., Wan, S., & Blusztajn, J. (2014, March). Reconstructing chemical weath-
1706 ering, physical erosion and monsoon intensity since 25Ma in the northern South
1707 China Sea: A review of competing proxies. *Earth-Science Reviews*, *130*, 86–102. Re-
1708 trieved 2022-09-13, from <https://www.sciencedirect.com/science/article/pii/S0012825214000051> doi: 10.1016/j.earscirev.2014.01.002
- 1709
1710 Cohen, J., Saito, K., & Entekhabi, D. (2001, January). The role of the Siberian high in
1711 northern hemisphere climate variability. *Geophysical Research Letters*, *28*(2), 299–302.
1712 Retrieved 2020-06-20, from <http://doi.wiley.com/10.1029/2000GL011927> doi:
1713 10.1029/2000GL011927
- 1714 Cook, K. L., & Royden, L. H. (2008). The role of crustal strength varia-
1715 tions in shaping orogenic plateaus, with application to Tibet. *Journal of Geo-*
1716 *physical Research: Solid Earth*, *113*(B8). Retrieved 2021-03-29, from [http://](http://agupubs.onlinelibrary.wiley.com/doi/abs/10.1029/2007JB005457)
1717 agupubs.onlinelibrary.wiley.com/doi/abs/10.1029/2007JB005457 (eprint:
1718 <https://onlinelibrary.wiley.com/doi/pdf/10.1029/2007JB005457>) doi: [https://doi](https://doi.org/10.1029/2007JB005457)
1719 [.org/10.1029/2007JB005457](https://doi.org/10.1029/2007JB005457)
- 1720 Couvreur, T. L. P., Dauby, G., Blach-Overgaard, A., Deblauwe, V., Dessein, S., Drois-
1721 sart, V., ... Sepulchre, P. (2021). Tectonics, climate and the diversification of
1722 the tropical African terrestrial flora and fauna. *Biological Reviews*, *96*(1), 16–51.
1723 Retrieved 2021-03-09, from [https://onlinelibrary.wiley.com/doi/abs/10.1111/](https://onlinelibrary.wiley.com/doi/abs/10.1111/brv.12644)
1724 [brv.12644](https://onlinelibrary.wiley.com/doi/abs/10.1111/brv.12644) (eprint: <https://onlinelibrary.wiley.com/doi/pdf/10.1111/brv.12644>)
1725 doi: <https://doi.org/10.1111/brv.12644>
- 1726 Crameri, F. (2021, February). *Scientific colour maps*. Zenodo. Retrieved 2021-04-15,
1727 from <https://zenodo.org/record/4491293> (Language: eng) doi: 10.5281/zenodo
1728 .4491293
- 1729 Crameri, F., Shephard, G. E., & Heron, P. J. (2020, October). The misuse of colour
1730 in science communication. *Nature Communications*, *11*(1), 5444. Retrieved 2021-
1731 04-15, from <http://www.nature.com/articles/s41467-020-19160-7> (Number: 1
1732 Publisher: Nature Publishing Group) doi: 10.1038/s41467-020-19160-7
- 1733 Cunningham, W. D. (2001, February). Cenozoic normal faulting and regional doming in the
1734 southern Hangay region, Central Mongolia: implications for the origin of the Baikal
1735 rift province. *Tectonophysics*, *331*(4), 389–411. Retrieved 2021-03-26, from [https://](https://www.sciencedirect.com/science/article/pii/S0040195100002286)
1736 www.sciencedirect.com/science/article/pii/S0040195100002286 doi: 10.1016/
1737 S0040-1951(00)00228-6
- 1738 Curry, W. B., Ostermann, D. R., Guptha, M. V. S., & Ittekkot, V. (1992, January).
1739 Foraminiferal production and monsoonal upwelling in the Arabian Sea: evidence
1740 from sediment traps. *Geological Society, London, Special Publications*, *64*(1), 93–
1741 106. Retrieved 2023-03-30, from <https://www.lyellcollection.org/doi/10.1144/>

- 1742 GSL.SP.1992.064.01.06 doi: 10.1144/GSL.SP.1992.064.01.06
- 1743 Daradich, A., Mitrovica, J. X., Pysklywec, R. N., Willett, S. D., & Forte, A. M. (2003).
1744 Mantle flow, dynamic topography, and rift-flank uplift of Arabia. *Geology*, *31*(10),
1745 901–904.
- 1746 Darin, M. H., Umhoefer, P. J., & Thomson, S. N. (2018). Rapid Late Eocene
1747 Exhumation of the Sivas Basin (Central Anatolia) Driven by Initial Arabia-
1748 Eurasia Collision. *Tectonics*, *37*(10), 3805–3833. Retrieved 2022-03-04, from
1749 <http://onlinelibrary.wiley.com/doi/abs/10.1029/2017TC004954> (eprint:
1750 <https://agupubs.onlinelibrary.wiley.com/doi/pdf/10.1029/2017TC004954>) doi: 10
1751 .1029/2017TC004954
- 1752 DeConto, R. M., & Pollard, D. (2003, September). A coupled climate–ice sheet mod-
1753 eling approach to the Early Cenozoic history of the Antarctic ice sheet. *Palaeo-
1754 geography, Palaeoclimatology, Palaeoecology*, *198*(1-2), 39–52. Retrieved 2018-01-08,
1755 from <http://linkinghub.elsevier.com/retrieve/pii/S0031018203003936> doi:
1756 10.1016/S0031-0182(03)00393-6
- 1757 De Grave, J., Buslov, M. M., & Van den haute, P. (2007, February). Distant effects
1758 of India–Eurasia convergence and Mesozoic intracontinental deformation in Central
1759 Asia: Constraints from apatite fission-track thermochronology. *Journal of Asian Earth
1760 Sciences*, *29*(2), 188–204. Retrieved 2021-03-26, from [https://www.sciencedirect
1761 .com/science/article/pii/S136791200600071X](https://www.sciencedirect.com/science/article/pii/S136791200600071X) doi: 10.1016/j.jseas.2006.03.001
- 1762 De Grave, J., Buslov, M. M., Van Den Haute, P., Metcalf, J., Dehandschutter, B., &
1763 McWilliams, M. O. (2009). Multi-method chronometry of the Teletskoye graben and
1764 its basement, Siberian Altai Mountains: new insights on its thermo-tectonic evolution.
1765 *Geological Society, London, Special Publications*, *324*(1), 237–259. Retrieved 2021-04-
1766 20, from <http://sp.lyellcollection.org/lookup/doi/10.1144/SP324.17> doi:
1767 10.1144/SP324.17
- 1768 Ding, L., Spicer, R., Yang, J., Xu, Q., Cai, F., Li, S., ... Mehrotra, R. (2017, March).
1769 Quantifying the rise of the Himalaya orogen and implications for the South Asian
1770 monsoon. *Geology*, *45*(3), 215–218. Retrieved 2017-10-09, from [https://pubs
1771 .geoscienceworld.org/geology/article/45/3/215-218/195254](https://pubs.geoscienceworld.org/geology/article/45/3/215-218/195254) doi: 10.1130/
1772 G38583.1
- 1773 Ding, L., Xu, Q., Yue, Y., Wang, H., Cai, F., & Li, S. (2014, April). The Andean-
1774 type Gangdese Mountains: Paleoelevation record from the Paleocene–Eocene Linzhou
1775 Basin. *Earth and Planetary Science Letters*, *392*, 250–264. Retrieved 2017-10-09,
1776 from <http://linkinghub.elsevier.com/retrieve/pii/S0012821X14000612> doi:
1777 10.1016/j.epsl.2014.01.045
- 1778 Ding, W., Hou, D., Gan, J., Wu, P., Zhang, M., & George, S. C. (2021, April).
1779 Palaeovegetation variation in response to the late Oligocene-early Miocene East
1780 Asian summer monsoon in the Ying-Qiong Basin, South China Sea. *Palaeogeog-
1781 raphy, Palaeoclimatology, Palaeoecology*, *567*, 110205. Retrieved 2022-05-03, from
1782 <https://linkinghub.elsevier.com/retrieve/pii/S0031018220306532> doi: 10
1783 .1016/j.palaeo.2020.110205
- 1784 Ding, Z., Huang, G., Liu, F., Wu, R., & Wang, P. (2021, June). Responses of global mon-
1785 soon and seasonal cycle of precipitation to precession and obliquity forcing. *Climate
1786 Dynamics*, *56*. doi: 10.1007/s00382-021-05663-6
- 1787 Dowsett, H., Dolan, A., Rowley, D., Moucha, R., Forte, A. M., Mitrovica, J. X., ... Hay-
1788 wood, A. (2016, July). The PRISM4 (mid-Piacenzian) paleoenvironmental reconstruc-
1789 tion. *Climate of the Past*, *12*(7), 1519–1538. Retrieved 2022-04-15, from [https://
1790 cp.copernicus.org/articles/12/1519/2016/](https://cp.copernicus.org/articles/12/1519/2016/) doi: 10.5194/cp-12-1519-2016
- 1791 Dufresne, J.-L., Foujols, M.-A., Denvil, S., Caubel, A., Marti, O., Aumont, O., ... Vuichard,
1792 N. (2013, May). Climate change projections using the IPSL-CM5 Earth System
1793 Model: from CMIP3 to CMIP5. *Climate Dynamics*, *40*(9-10), 2123–2165. Retrieved
1794 2019-11-22, from <http://link.springer.com/10.1007/s00382-012-1636-1> doi:
1795 10.1007/s00382-012-1636-1
- 1796 Faccenna, C., Glišović, P., Forte, A., Becker, T. W., Garzanti, E., Sembroni, A., & Gvirtz-

- 1797 man, Z. (2019, December). Role of dynamic topography in sustaining the Nile River
1798 over 30 million years. *Nature Geoscience*, *12*(12), 1012–1017. Retrieved 2021-03-10,
1799 from <http://www.nature.com/articles/s41561-019-0472-x> (Number: 12 Pub-
1800 lisher: Nature Publishing Group) doi: 10.1038/s41561-019-0472-x
- 1801 Fang, X., Galy, A., Yang, Y., Zhang, W., Ye, C., & Song, C. (2019, October). Paleogene
1802 global cooling–induced temperature feedback on chemical weathering, as recorded
1803 in the northern Tibetan Plateau. *Geology*, *47*(10), 992–996. Retrieved 2022-10-
1804 03, from [https://pubs.geoscienceworld.org/gsa/geology/article/47/10/992/
1805 573474/Paleogene-global-cooling-induced-temperature](https://pubs.geoscienceworld.org/gsa/geology/article/47/10/992/573474/Paleogene-global-cooling-induced-temperature) doi: 10.1130/G46422.1
- 1806 Fang, X., Yan, M., Zhang, W., Nie, J., Han, W., Wu, F., ... Yang, Y. (2021, Novem-
1807 ber). Paleogeography control of Indian monsoon intensification and expansion at
1808 41 Ma. *Science Bulletin*, *66*(22), 2320–2328. Retrieved 2022-05-02, from [https://
1809 linkinghub.elsevier.com/retrieve/pii/S2095927321005041](https://linkinghub.elsevier.com/retrieve/pii/S2095927321005041) doi: 10.1016/j.scib
1810 .2021.07.023
- 1811 Farnsworth, A., Lunt, D. J., Robinson, S. A., Valdes, P. J., Roberts, W. H. G., Clift,
1812 P. D., ... Pancost, R. D. (2019, October). Past East Asian monsoon evolution
1813 controlled by paleogeography, not CO₂. *Science Advances*, *5*(10), eaax1697. doi:
1814 10.1126/sciadv.aax1697
- 1815 Feakins, S. J., Liddy, H. M., Tauxe, L., Galy, V., Feng, X., Tierney, J. E., ... Warny,
1816 S. (2020). Miocene C4 Grassland Expansion as Recorded by the Indus Fan. *Paleo-
1817 ceanography and Paleoclimatology*, *35*(6), e2020PA003856. Retrieved 2022-06-07, from
1818 <http://onlinelibrary.wiley.com/doi/abs/10.1029/2020PA003856> (eprint:
1819 <https://agupubs.onlinelibrary.wiley.com/doi/pdf/10.1029/2020PA003856>) doi: 10
1820 .1029/2020PA003856
- 1821 Feng, R., & Poulsen, C. J. (2016, February). Refinement of Eocene lapse rates, fossil-
1822 leaf altimetry, and North American Cordilleran surface elevation estimates. *Earth
1823 and Planetary Science Letters*, *436*, 130–141. Retrieved 2020-03-23, from [https://
1824 linkinghub.elsevier.com/retrieve/pii/S0012821X15007852](https://linkinghub.elsevier.com/retrieve/pii/S0012821X15007852) doi: 10.1016/j.epsl
1825 .2015.12.022
- 1826 Fichefet, T., & Maqueda, M. A. M. (1997). Sensitivity of a global sea ice model to the
1827 treatment of ice thermodynamics and dynamics. *Journal of Geophysical Research:
1828 Oceans*, *102*(C6), 12609–12646.
- 1829 Fluteau, F., Ramstein, G., & Besse, J. (1999, May). Simulating the evolution of the
1830 Asian and African monsoons during the past 30 Myr using an atmospheric general
1831 circulation model. *Journal of Geophysical Research: Atmospheres*, *104*(D10), 11995–
1832 12018. Retrieved 2019-05-10, from <http://doi.wiley.com/10.1029/1999JD900048>
1833 doi: 10.1029/1999JD900048
- 1834 Foster, G. L., Royer, D. L., & Lunt, D. J. (2017, April). Future climate forcing poten-
1835 tially without precedent in the last 420 million years. *Nature Communications*, *8*(1).
1836 Retrieved 2020-05-28, from <http://www.nature.com/articles/ncomms14845> doi:
1837 10.1038/ncomms14845
- 1838 François, T., Burov, E., Agard, P., & Meyer, B. (2014). Buildup of a dynamically supported
1839 orogenic plateau: Numerical modeling of the Zagros/Central Iran case study. *Geo-
1840 chemistry, Geophysics, Geosystems*, *15*(6), 2632–2654. Retrieved 2021-03-09, from
1841 <https://agupubs.onlinelibrary.wiley.com/doi/abs/10.1002/2013GC005223>
1842 (eprint: <https://agupubs.onlinelibrary.wiley.com/doi/pdf/10.1002/2013GC005223>)
1843 doi: <https://doi.org/10.1002/2013GC005223>
- 1844 Frisch, K., Voigt, S., Verestek, V., Appel, E., Albert, R., Gerdes, A., ... Batenburg, S. (2019,
1845 November). Long-Period Astronomical Forcing of Westerlies’ Strength in Central Asia
1846 During Miocene Climate Cooling. *Paleoceanography and Paleoclimatology*, *34*. doi:
1847 10.1029/2019PA003642
- 1848 Garziona, C. N., Ikari, M. J., & Basu, A. R. (2005, September). Source of Oligocene
1849 to Pliocene sedimentary rocks in the Linxia basin in northeastern Tibet from Nd
1850 isotopes: Implications for tectonic forcing of climate. *GSA Bulletin*, *117*(9-10), 1156–
1851 1166. Retrieved 2021-09-07, from <https://doi.org/10.1130/B25743.1> doi: 10

- 1852 .1130/B25743.1
- 1853 Golonka, J. (2009). Phanerozoic paleoenvironment and paleolithofacies maps : Cenozoic.
1854 *Geologia / Akademia Górniczo-Hutnicza im. Stanisława Staszica w Krakowie, T. 35, z.*
1855 *4*, 507–587. Retrieved 2021-04-06, from [http://yadda.icm.edu.pl/yadda/element/](http://yadda.icm.edu.pl/yadda/element/bwmeta1.element.baztech-article-AGHM-0011-0001)
1856 [bwmeta1.element.baztech-article-AGHM-0011-0001](http://yadda.icm.edu.pl/yadda/element/bwmeta1.element.baztech-article-AGHM-0011-0001)
- 1857 Gough, D. O. (1981). Solar Interior Structure and Luminosity Variations. In V. Domingo
1858 (Ed.), *Physics of Solar Variations* (pp. 21–34). Dordrecht: Springer Netherlands.
1859 Retrieved 2019-10-03, from [http://link.springer.com/10.1007/978-94-010-9633-](http://link.springer.com/10.1007/978-94-010-9633-1_4)
1860 [-1_4](http://link.springer.com/10.1007/978-94-010-9633-1_4) doi: 10.1007/978-94-010-9633-1_4
- 1861 Gourbet, L., Leloup, P. H., Paquette, J.-L., Sorrel, P., Maheo, G., Wang, G., ... Shen, T.
1862 (2017, March). Reappraisal of the Jianchuan Cenozoic basin stratigraphy and its impli-
1863 cations on the SE Tibetan plateau evolution. *Tectonophysics*, *700-701*, 162–179. Re-
1864 trieved 2021-03-29, from [https://www.sciencedirect.com/science/article/pii/](https://www.sciencedirect.com/science/article/pii/S0040195117300537)
1865 [S0040195117300537](https://www.sciencedirect.com/science/article/pii/S0040195117300537) doi: 10.1016/j.tecto.2017.02.007
- 1866 Guillocheau, F., Simon, B., Baby, G., Bessin, P., Robin, C., & Dauteuil, O. (2018, January).
1867 Planation surfaces as a record of mantle dynamics: The case example of Africa. *Gond-*
1868 *wana Research*, *53*, 82–98. Retrieved 2021-04-07, from [https://www.sciencedirect](https://www.sciencedirect.com/science/article/pii/S1342937X17302496)
1869 [.com/science/article/pii/S1342937X17302496](https://www.sciencedirect.com/science/article/pii/S1342937X17302496) doi: 10.1016/j.gr.2017.05.015
- 1870 Guo, Z. T., Ruddiman, W. F., Hao, Q. Z., Wu, H. B., Qiao, Y. S., Zhu, R. X., ... Liu,
1871 T. S. (2002, March). Onset of Asian desertification by 22 Myr ago inferred from
1872 loess deposits in China. *Nature*, *416*(6877), 159–163. Retrieved 2020-04-24, from
1873 <http://www.nature.com/articles/416159a> doi: 10.1038/416159a
- 1874 Guo, Z. T., Sun, B., Zhang, Z. S., Peng, S. Z., Xiao, G. Q., Ge, J. Y., ... Liu, J. F. (2008).
1875 A major reorganization of Asian climate by the early Miocene. *Climate of the Past*,
1876 *4*(3), 153–174.
- 1877 Gupta, A. K., Yuvaraja, A., Prakasam, M., Clemens, S. C., & Velu, A. (2015, Novem-
1878 ber). Evolution of the South Asian monsoon wind system since the late Middle
1879 Miocene. *Palaeogeography, Palaeoclimatology, Palaeoecology*, *438*, 160–167. Re-
1880 trieved 2021-09-07, from [https://www.sciencedirect.com/science/article/pii/](https://www.sciencedirect.com/science/article/pii/S0031018215004332)
1881 [S0031018215004332](https://www.sciencedirect.com/science/article/pii/S0031018215004332) doi: 10.1016/j.palaeo.2015.08.006
- 1882 Gébelin, A., Mulch, A., Teyssier, C., Jessup, M. J., Law, R. D., & Brunel, M.
1883 (2013, July). The Miocene elevation of Mount Everest. *Geology*, *41*(7), 799–
1884 802. Retrieved 2017-10-09, from [http://pubs.geoscienceworld.org/geology/](http://pubs.geoscienceworld.org/geology/article/41/7/799/131318/The-Miocene-elevation-of-Mount-Everest)
1885 [article/41/7/799/131318/The-Miocene-elevation-of-Mount-Everest](http://pubs.geoscienceworld.org/geology/article/41/7/799/131318/The-Miocene-elevation-of-Mount-Everest) doi: 10
1886 .1130/G34331.1
- 1887 Gülyüz, E., Durak, H., Özkaptan, M., & Krijgsman, W. (2020, January). Paleomagnetic
1888 constraints on the early Miocene closure of the southern Neo-Tethys (Van region; East
1889 Anatolia): Inferences for the timing of Eurasia-Arabia collision. *Global and Planetary*
1890 *Change*, *185*, 103089. Retrieved 2022-03-04, from [https://www.sciencedirect.com/](https://www.sciencedirect.com/science/article/pii/S0921818119305740)
1891 [science/article/pii/S0921818119305740](https://www.sciencedirect.com/science/article/pii/S0921818119305740) doi: 10.1016/j.gloplacha.2019.103089
- 1892 Hall, R., Gower, D., Johnson, K., Richardson, J., Rosen, B., Rüber, L., & Williams, S.
1893 (2012). Sundaland and Wallacea: geology, plate tectonics and palaeogeography. *Biotic*
1894 *evolution and environmental change in Southeast Asia*, *82*, 32. (Publisher: Cambridge
1895 University Press Cambridge)
- 1896 Han, Z., Jia, H., Meng, X., Ferguson, D., Luo, M., Liu, P., ... Quan, C. (2022, October).
1897 A New Clue for the Late Eocene Freshwater Ecosystem of Central China Evidenced
1898 by New Fossils of *Trapa* L. and *Hemitrapa* Miki (Lythraceae). *Biology*, *11*, 1442. doi:
1899 10.3390/biology11101442
- 1900 Harzhauser, M., & Piller, W. E. (2007, September). Benchmark data of a changing sea
1901 — Palaeogeography, Palaeobiogeography and events in the Central Paratethys during
1902 the Miocene. *Palaeogeography, Palaeoclimatology, Palaeoecology*, *253*(1), 8–31. Re-
1903 trieved 2021-04-01, from [https://www.sciencedirect.com/science/article/pii/](https://www.sciencedirect.com/science/article/pii/S0031018207001927)
1904 [S0031018207001927](https://www.sciencedirect.com/science/article/pii/S0031018207001927) doi: 10.1016/j.palaeo.2007.03.031
- 1905 Haywood, A. M., Tindall, J. C., Dowsett, H. J., Dolan, A. M., Foley, K. M., Hunter, S. J., ...
1906 Lunt, D. J. (2020, November). The Pliocene Model Intercomparison Project Phase 2:

- 1907 large-scale climate features and climate sensitivity. *Climate of the Past*, 16(6), 2095–
 1908 2123. Retrieved 2021-03-09, from [https://cp.copernicus.org/articles/16/2095/](https://cp.copernicus.org/articles/16/2095/2020/)
 1909 2020/ (Publisher: Copernicus GmbH) doi: <https://doi.org/10.5194/cp-16-2095-2020>
- 1910 He, B. (2017, May). Influences of elevated heating effect by the Himalaya on the changes
 1911 in Asian summer monsoon. *Theoretical and Applied Climatology*, 128(3-4), 905–917.
 1912 Retrieved 2017-10-09, from [http://link.springer.com/10.1007/s00704-016-1746-](http://link.springer.com/10.1007/s00704-016-1746-5)
 1913 [5](http://link.springer.com/10.1007/s00704-016-1746-5) doi: 10.1007/s00704-016-1746-5
- 1914 Heermance, R., Pearson, J., Moe, A., Langtao, L., Jianhong, X., Chen, J., ... Bogue,
 1915 S. (2018, September). Erg deposition and development of the ancestral Taklimakan
 1916 Desert (western China) between 12.2 and 7.0 Ma. *Geology*, 46. doi: 10.1130/G45085.1
- 1917 Hellwig, A., Voigt, S., Mulch, A., Frisch, K., Bartenstein, A., Pross, J., ...
 1918 Voigt, T. (2018). Late Oligocene to early Miocene humidity change
 1919 recorded in terrestrial sequences in the Ili Basin (south-eastern Kazakhstan,
 1920 Central Asia). *Sedimentology*, 65(2), 517–539. Retrieved 2022-03-22,
 1921 from <http://onlinelibrary.wiley.com/doi/abs/10.1111/sed.12390> (eprint:
 1922 <https://onlinelibrary.wiley.com/doi/pdf/10.1111/sed.12390>) doi: 10.1111/sed.12390
- 1923 Herman, A. B., Spicer, R. A., Aleksandrova, G. N., Yang, J., Kodrul, T. M., Maslova,
 1924 N. P., ... Jin, J.-H. (2017, August). Eocene–early Oligocene climate and veg-
 1925 etation change in southern China: Evidence from the Maoming Basin. *Palaeoge-*
 1926 *ography, Palaeoclimatology, Palaeoecology*, 479, 126–137. Retrieved 2017-10-09,
 1927 from <http://linkinghub.elsevier.com/retrieve/pii/S0031018217300664> doi:
 1928 10.1016/j.palaeo.2017.04.023
- 1929 Holbourn, A., Kuhnt, W., Clemens, S. C., & Heslop, D. (2021). A 12 Myr Miocene Record
 1930 of East Asian Monsoon Variability From the South China Sea. *Paleoceanography*
 1931 *and Paleoclimatology*, 36(7), e2021PA004267. Retrieved 2021-09-08, from [http://](http://agupubs.onlinelibrary.wiley.com/doi/abs/10.1029/2021PA004267)
 1932 agupubs.onlinelibrary.wiley.com/doi/abs/10.1029/2021PA004267 (eprint:
 1933 <https://onlinelibrary.wiley.com/doi/pdf/10.1029/2021PA004267>) doi: 10.1029/
 1934 2021PA004267
- 1935 Holbourn, A., Kuhnt, W., Clemens, S. C., Kochhann, K. G. D., Jöhnck, J., Lübbers, J., &
 1936 Andersen, N. (2018, December). Late Miocene climate cooling and intensification of
 1937 southeast Asian winter monsoon. *Nature Communications*, 9(1). Retrieved 2020-10-
 1938 09, from <http://www.nature.com/articles/s41467-018-03950-1> doi: 10.1038/
 1939 s41467-018-03950-1
- 1940 Hoorn, C., Ohja, T., & Quade, J. (2000, November). Palynological evidence for veg-
 1941 etation development and climatic change in the Sub-Himalayan Zone (Neogene,
 1942 Central Nepal). *Palaeogeography, Palaeoclimatology, Palaeoecology*, 163(3-4), 133–
 1943 161. Retrieved 2022-06-07, from [https://linkinghub.elsevier.com/retrieve/](https://linkinghub.elsevier.com/retrieve/pii/S0031018200001498)
 1944 [pii/S0031018200001498](https://linkinghub.elsevier.com/retrieve/pii/S0031018200001498) doi: 10.1016/S0031-0182(00)00149-8
- 1945 Hoorn, C., Straathof, J., Abels, H. A., Xu, Y., Utescher, T., & Dupont-Nivet, G. (2012, Au-
 1946 gust). A late Eocene palynological record of climate change and Tibetan Plateau uplift
 1947 (Xining Basin, China). *Palaeogeography, Palaeoclimatology, Palaeoecology*, 344-345,
 1948 16–38. Retrieved 2017-10-09, from [http://linkinghub.elsevier.com/retrieve/](http://linkinghub.elsevier.com/retrieve/pii/S0031018212002775)
 1949 [pii/S0031018212002775](http://linkinghub.elsevier.com/retrieve/pii/S0031018212002775) doi: 10.1016/j.palaeo.2012.05.011
- 1950 Hourdin, F., Foujols, M.-A., Codron, F., Guemas, V., Dufresne, J.-L., Bony, S., ... Bopp,
 1951 L. (2013, May). Impact of the LMDZ atmospheric grid configuration on the climate
 1952 and sensitivity of the IPSL-CM5A coupled model. *Climate Dynamics*, 40(9-10), 2167–
 1953 2192. Retrieved 2018-06-05, from [http://link.springer.com/10.1007/s00382-012-](http://link.springer.com/10.1007/s00382-012-1411-3)
 1954 [1411-3](http://link.springer.com/10.1007/s00382-012-1411-3) doi: 10.1007/s00382-012-1411-3
- 1955 Huang, C., & Hinnov, L. (2019, December). Astronomically forced climate evolution in a
 1956 saline lake record of the middle Eocene to Oligocene, Jiangnan Basin, China. *Earth*
 1957 *and Planetary Science Letters*, 528, 115846. Retrieved 2020-09-07, from [https://](https://linkinghub.elsevier.com/retrieve/pii/S0012821X19305382)
 1958 linkinghub.elsevier.com/retrieve/pii/S0012821X19305382 doi: 10.1016/j.epsl
 1959 .2019.115846
- 1960 Huang, H., Pérez-Pinedo, D., Morley, R. J., Dupont-Nivet, G., Philip, A., Win, Z., ...
 1961 Hoorn, C. (2021, April). At a crossroads: The late Eocene flora of central Myanmar

- owes its composition to plate collision and tropical climate. *Review of Palaeobotany and Palynology*, 104441. Retrieved 2021-05-06, from <https://www.sciencedirect.com/science/article/pii/S0034666721000658> doi: 10.1016/j.revpalbo.2021.104441
- Huang, W., Dupont-Nivet, G., Lippert, P. C., van Hinsbergen, D. J. J., Dekkers, M. J., Waldrip, R., ... Kapp, P. (2015, March). What was the Paleogene latitude of the Lhasa terrane? A reassessment of the geochronology and paleomagnetism of Linzizong volcanic rocks (Linzhou basin, Tibet). *Tectonics*, 34(3), 594–622. Retrieved 2017-10-09, from <http://doi.wiley.com/10.1002/2014TC003787> doi: 10.1002/2014TC003787
- Huang, Y., Clemens, S., Liu, W., Wang, Y., & Prell, W. (2007, June). Large-scale hydrological change drove the late Miocene C4 plant expansion in the Himalayan foreland and Arabian Peninsula. *Geology*, 35. doi: 10.1130/G23666A.1
- Huber, M., & Goldner, A. (2012, January). Eocene monsoons. *Journal of Asian Earth Sciences*, 44, 3–23. Retrieved 2017-10-09, from <http://linkinghub.elsevier.com/retrieve/pii/S1367912011003725> doi: 10.1016/j.jseaes.2011.09.014
- Hui, Z., Zhou, X., Chevalier, M., Wei, X., Pan, Y., & Chen, Y. (2021, August). Miocene East Asia summer monsoon precipitation variability and its possible driving forces. *Palaeogeography, Palaeoclimatology, Palaeoecology*, 110609. Retrieved 2021-09-22, from <https://www.sciencedirect.com/science/article/pii/S0031018221003941> doi: 10.1016/j.palaeo.2021.110609
- Ingalls, M., Rowley, D. B., Currie, B., & Colman, A. S. (2016, November). Large-scale subduction of continental crust implied by India–Asia mass-balance calculation. *Nature Geoscience*, 9(11), 848–853. Retrieved 2020-10-16, from <http://www.nature.com/articles/ngeo2806> (Number: 11 Publisher: Nature Publishing Group) doi: 10.1038/ngeo2806
- Jacques, F. M., Guo, S.-X., Su, T., Xing, Y.-W., Huang, Y.-J., Liu, Y.-S. C., ... Zhou, Z.-K. (2011, May). Quantitative reconstruction of the Late Miocene monsoon climates of southwest China: A case study of the Lincang flora from Yunnan Province. *Palaeogeography, Palaeoclimatology, Palaeoecology*, 304(3-4), 318–327. Retrieved 2022-05-03, from <https://linkinghub.elsevier.com/retrieve/pii/S0031018210002233> doi: 10.1016/j.palaeo.2010.04.014
- Jacques, F. M., Su, T., Spicer, R. A., Xing, Y., Huang, Y., Wang, W., & Zhou, Z. (2011, March). Leaf physiognomy and climate: Are monsoon systems different? *Global and Planetary Change*, 76(1-2), 56–62. Retrieved 2022-05-06, from <https://linkinghub.elsevier.com/retrieve/pii/S0921818110002560> doi: 10.1016/j.gloplacha.2010.11.009
- Jagoutz, O., Royden, L., Holt, A. F., & Becker, T. W. (2015, June). Anomalously fast convergence of India and Eurasia caused by double subduction. *Nature Geoscience*, 8(6), 475–478. Retrieved 2019-11-22, from <http://www.nature.com/articles/ngeo2418> doi: 10.1038/ngeo2418
- Jeong, J.-H., Ou, T., Linderholm, H. W., Kim, B.-M., Kim, S.-J., Kug, J.-S., & Chen, D. (2011, December). Recent recovery of the Siberian High intensity: RECOVERY OF THE SIBERIAN HIGH INTENSITY. *Journal of Geophysical Research: Atmospheres*, 116(D23), n/a–n/a. Retrieved 2020-06-20, from <http://doi.wiley.com/10.1029/2011JD015904> doi: 10.1029/2011JD015904
- Jhun, J.-G., & Lee, E.-J. (2004, February). A New East Asian Winter Monsoon Index and Associated Characteristics of the Winter Monsoon. *Journal of Climate*, 17(4), 711–726. Retrieved 2021-11-10, from https://journals.ametsoc.org/view/journals/clim/17/4/1520-0442_2004_017_0711_aneawm_2.0.co_2.xml (Publisher: American Meteorological Society Section: Journal of Climate) doi: 10.1175/1520-0442(2004)017<0711:ANEAWM>2.0.CO;2
- Jia, G., Peng, P., Zhao, Q., & Jian, Z. (2003, December). Changes in terrestrial ecosystem since 30 Ma in East Asia: Stable isotope evidence from black carbon in the South China Sea. *Geology*, 31(12), 1093–1096. Retrieved 2022-05-02, from <https://doi.org/10.1130/G19992.1> doi: 10.1130/G19992.1

- 2017 Jiang, H., & Ding, Z. (2008, July). A 20 Ma pollen record of East-Asian summer monsoon
2018 evolution from Guyuan, Ningxia, China. *Palaeogeography, Palaeoclimatology, Palaeoecology*,
2019 *265*(1-2), 30–38. Retrieved 2022-06-14, from [https://linkinghub.elsevier](https://linkinghub.elsevier.com/retrieve/pii/S0031018208002629)
2020 [.com/retrieve/pii/S0031018208002629](https://linkinghub.elsevier.com/retrieve/pii/S0031018208002629) doi: 10.1016/j.palaeo.2008.04.016
- 2021 Jiang, H., Wan, S., Ma, X., Zhong, N., & Zhao, D. (2017, October). End-member modeling
2022 of the grain-size record of Sikouzi fine sediments in Ningxia (China) and implica-
2023 tions for temperature control of Neogene evolution of East Asian winter monsoon.
2024 *PLOS ONE*, *12*(10), e0186153. Retrieved 2022-06-14, from [https://dx.plos.org/](https://dx.plos.org/10.1371/journal.pone.0186153)
2025 [10.1371/journal.pone.0186153](https://dx.plos.org/10.1371/journal.pone.0186153) doi: 10.1371/journal.pone.0186153
- 2026 Jolivet, M., Dominguez, S., Charreau, J., Chen, Y., Li, Y., & Wang, Q. (2010). Mesozoic and
2027 Cenozoic tectonic history of the central Chinese Tian Shan: Reactivated tectonic struc-
2028 tures and active deformation. *Tectonics*, *29*(6). Retrieved 2021-03-29, from [http://](http://agupubs.onlinelibrary.wiley.com/doi/abs/10.1029/2010TC002712)
2029 agupubs.onlinelibrary.wiley.com/doi/abs/10.1029/2010TC002712 (eprint:
2030 <https://onlinelibrary.wiley.com/doi/pdf/10.1029/2010TC002712>) doi: [https://doi](https://doi.org/10.1029/2010TC002712)
2031 [.org/10.1029/2010TC002712](https://doi.org/10.1029/2010TC002712)
- 2032 Jolivet, M., Ritz, J.-F., Vassallo, R., Larroque, C., Braucher, R., Todbileg, M., ...
2033 Arzhanikov, S. (2007, October). Mongolian summits: An uplifted, flat, old
2034 but still preserved erosion surface. *Geology*, *35*(10), 871–874. Retrieved 2021-03-
2035 29, from [http://pubs.geoscienceworld.org/gsa/geology/article/35/10/871/](http://pubs.geoscienceworld.org/gsa/geology/article/35/10/871/129664/Mongolian-summits-An-uplifted-flat-old-but-still)
2036 [129664/Mongolian-summits-An-uplifted-flat-old-but-still](http://pubs.geoscienceworld.org/gsa/geology/article/35/10/871/129664/Mongolian-summits-An-uplifted-flat-old-but-still) (Publisher: Geo-
2037 ScienceWorld) doi: 10.1130/G23758A.1
- 2038 Kaakinen, A., Sonninen, E., & Lunkka, J. P. (2006, August). Stable isotope record in
2039 paleosol carbonates from the Chinese Loess Plateau: Implications for late Neogene
2040 paleoclimate and paleovegetation. *Palaeogeography, Palaeoclimatology, Palaeoecology*,
2041 *237*(2-4), 359–369. Retrieved 2022-06-16, from [https://linkinghub.elsevier.com/](https://linkinghub.elsevier.com/retrieve/pii/S0031018205007315)
2042 [retrieve/pii/S0031018205007315](https://linkinghub.elsevier.com/retrieve/pii/S0031018205007315) doi: 10.1016/j.palaeo.2005.12.011
- 2043 Kapp, P., & DeCelles, P. G. (2019, March). Mesozoic–Cenozoic geological evolution of the
2044 Himalayan–Tibetan orogen and working tectonic hypotheses. *American Journal of*
2045 *Science*, *319*(3), 159–254. Retrieved 2019-11-15, from [http://www.ajsonline.org/](http://www.ajsonline.org/lookup/doi/10.2475/03.2019.01)
2046 [lookup/doi/10.2475/03.2019.01](http://www.ajsonline.org/lookup/doi/10.2475/03.2019.01) doi: 10.2475/03.2019.01
- 2047 Karaođlan, F., Parlak, O., Hejl, E., Neubauer, F., & Klötzli, U. (2016, May). The tempo-
2048 ral evolution of the active margin along the Southeast Anatolian Orogenic Belt (SE
2049 Turkey): Evidence from U–Pb, Ar–Ar and fission track chronology. *Gondwana Re-*
2050 *search*, *33*, 190–208. Retrieved 2022-03-04, from [https://www.sciencedirect.com/](https://www.sciencedirect.com/science/article/pii/S1342937X16000599)
2051 [science/article/pii/S1342937X16000599](https://www.sciencedirect.com/science/article/pii/S1342937X16000599) doi: 10.1016/j.gr.2015.12.011
- 2052 Kaya, M. Y., Dupont-Nivet, G., Proust, J., Roperch, P., Bougeois, L., Meijer, N., ...
2053 Zhaojie, G. (2019, June). Paleogene evolution and demise of the proto-Paratethys
2054 Sea in Central Asia (Tarim and Tajik basins): Role of intensified tectonic activity at
2055 ca. 41 Ma. *Basin Research*, *31*(3), 461–486. Retrieved 2019-11-22, from [https://](https://onlinelibrary.wiley.com/doi/abs/10.1111/bre.12330)
2056 onlinelibrary.wiley.com/doi/abs/10.1111/bre.12330 doi: 10.1111/bre.12330
- 2057 Kent-Corson, M. L., Ritts, B. D., Zhuang, G., Bovet, P. M., Graham, S. A., &
2058 Page Chamberlain, C. (2009, May). Stable isotopic constraints on the tectonic, to-
2059 pographic, and climatic evolution of the northern margin of the Tibetan Plateau.
2060 *Earth and Planetary Science Letters*, *282*(1-4), 158–166. Retrieved 2017-10-09,
2061 from <http://linkinghub.elsevier.com/retrieve/pii/S0012821X0900154X> doi:
2062 [10.1016/j.epsl.2009.03.011](http://linkinghub.elsevier.com/retrieve/pii/S0012821X0900154X)
- 2063 Khan, M. A., Spicer, R. A., Bera, S., Ghosh, R., Yang, J., Spicer, T. E. V., ... Grote,
2064 P. J. (2014, February). Miocene to Pleistocene floras and climate of the Eastern
2065 Himalayan Siwaliks, and new palaeoelevation estimates for the Namling–Oiyug Basin,
2066 Tibet. *Global and Planetary Change*, *113*, 1–10. Retrieved 2022-05-02, from [https://](https://www.sciencedirect.com/science/article/pii/S0921818113002749)
2067 www.sciencedirect.com/science/article/pii/S0921818113002749 doi: 10.1016/
2068 [j.gloplacha.2013.12.003](https://www.sciencedirect.com/science/article/pii/S0921818113002749)
- 2069 Kong, W., Swenson, L. M., & Chiang, J. C. H. (2017, May). Seasonal Transitions and
2070 the Westerly Jet in the Holocene East Asian Summer Monsoon. *Journal of Climate*,
2071 *30*(9), 3343–3365. Retrieved 2020-03-04, from <http://journals.ametsoc.org/doi/>

- 2072 10.1175/JCLI-D-16-0087.1 doi: 10.1175/JCLI-D-16-0087.1
- 2073 Krinner, G., Viovy, N., de Noblet-Ducoudré, N., Ogée, J., Polcher, J., Friedlingstein, P.,
2074 ... Prentice, I. C. (2005, March). A dynamic global vegetation model for studies
2075 of the coupled atmosphere-biosphere system: DVGMM FOR COUPLED CLIMATE
2076 STUDIES. *Global Biogeochemical Cycles*, 19(1). Retrieved 2018-10-22, from <http://doi.wiley.com/10.1029/2003GB002199> doi: 10.1029/2003GB002199
- 2077
- 2078 Kroon, D., Steens, T., & Troelstra, S. R. (1991). Onset of monsoonal related upwelling in
2079 the western Arabian sea as revealed by planktonic foraminifers. In *Proceedings of the*
2080 *ocean drilling program, scientific results* (Vol. 11).
- 2081 Kuhnt, W., Holbourn, A., Hall, R., Zuvela, M., & Käse, R. (2004). Neogene history of the In-
2082 donesian Throughflow. In P. Clift, W. Kuhnt, P. Wang, & D. Hayes (Eds.), *Geophysical*
2083 *Monograph Series* (Vol. 149, pp. 299–320). Washington, D. C.: American Geophys-
2084 ical Union. Retrieved 2021-09-02, from <https://onlinelibrary.wiley.com/doi/10.1029/149GM16> doi: 10.1029/149GM16
- 2085
- 2086 Kutzbach, J. E., Prell, W. L., & Ruddiman, W. F. (1993, March). Sensitivity of Eurasian
2087 Climate to Surface Uplift of the Tibetan Plateau. *The Journal of Geology*, 101(2),
2088 177–190. Retrieved 2020-05-11, from <https://www.journals.uchicago.edu/doi/10.1086/648215> doi: 10.1086/648215
- 2089
- 2090 Käßner, A., Ratschbacher, L., Jonckheere, R., Enkelmann, E., Khan, J., Sonntag, B.-L., ...
2091 Oimahmadov, I. (2016). Cenozoic intracontinental deformation and exhumation at
2092 the northwestern tip of the India-Asia collision—southwestern Tian Shan, Tajikistan,
2093 and Kyrgyzstan. *Tectonics*, 35(9), 2171–2194. Retrieved 2021-03-26, from <http://agupubs.onlinelibrary.wiley.com/doi/abs/10.1002/2015TC003897> (eprint:
2094 <https://onlinelibrary.wiley.com/doi/pdf/10.1002/2015TC003897>) doi: <https://doi.org/10.1002/2015TC003897>
- 2095
- 2096
- 2097 Ladant, J.-B., Donnadiou, Y., Lefebvre, V., & Dumas, C. (2014, August). The respec-
2098 tive role of atmospheric carbon dioxide and orbital parameters on ice sheet evolution
2099 at the Eocene-Oligocene transition: Ice sheet evolution at the EOT. *Paleoceanogra-*
2100 *phy*, 29(8), 810–823. Retrieved 2019-05-10, from <http://doi.wiley.com/10.1002/2013PA002593> doi: 10.1002/2013PA002593
- 2101
- 2102 Laugié, M., Donnadiou, Y., Ladant, J.-B., Green, J. A. M., Bopp, L., & Raison, F.
2103 (2020, June). Stripping back the modern to reveal the Cenomanian–Turonian cli-
2104 mate and temperature gradient underneath. *Climate of the Past*, 16(3), 953–971.
2105 Retrieved 2021-03-09, from <https://cp.copernicus.org/articles/16/953/2020/>
2106 (Publisher: Copernicus GmbH) doi: <https://doi.org/10.5194/cp-16-953-2020>
- 2107
- 2108 Lee, J., Kim, S., Lee, J. I., Cho, H. G., Phillips, S. C., & Khim, B.-K. (2020, January).
2109 Monsoon-influenced variation of clay mineral compositions and detrital Nd-Sr isotopes
2110 in the western Andaman Sea (IODP Site U1447) since the late Miocene. *Palaeo-*
2111 *geography, Palaeoclimatology, Palaeoecology*, 538, 109339. Retrieved 2022-06-02,
2112 from <https://linkinghub.elsevier.com/retrieve/pii/S0031018219303773> doi:
10.1016/j.palaeo.2019.109339
- 2113
- 2114 Lee, J.-Y., Wang, B., Seo, K.-H., Ha, K.-J., Kitoh, A., & Liu, J. (2015, August). Effects of
2115 mountain uplift on global monsoon precipitation. *Asia-Pacific Journal of Atmospheric*
2116 *Sciences*, 51(3), 275–290. Retrieved 2017-10-09, from <http://link.springer.com/10.1007/s13143-015-0077-2> doi: 10.1007/s13143-015-0077-2
- 2117
- 2118 Li, B., Sun, D., Wang, X., Zhang, Y., Hu, W., Wang, F., ... Liang, B. (2016, Au-
2119 gust). 18O and 13C records from a Cenozoic sedimentary sequence in the Lanzhou
2120 Basin, Northwestern China: Implications for palaeoenvironmental and palaeoecolog-
2121 ical changes. *Journal of Asian Earth Sciences*, 125, 22–36. Retrieved 2022-05-12,
2122 from <https://linkinghub.elsevier.com/retrieve/pii/S1367912016301249> doi:
10.1016/j.jseaes.2016.05.010
- 2123
- 2124 Li, F., Rousseau, D.-D., Wu, N., Hao, Q., & Pei, Y. (2008, October). Late Neogene
2125 evolution of the East Asian monsoon revealed by terrestrial mollusk record in Western
2126 Chinese Loess Plateau: From winter to summer dominated sub-regime. *Earth and Planetary Science Letters*, 274(3-4), 439–447. Retrieved 2022-06-16, from <https://>

- 2127 linkinghub.elsevier.com/retrieve/pii/S0012821X08004986 doi: 10.1016/j.epsl
2128 .2008.07.038
- 2129 Li, L., Dupont-Nivet, G., Najman, Y., Kaya, M., Meijer, N., Pujol, M., & Aminov, J.
2130 (2021). Middle to late Miocene growth of the North Pamir. *Basin Research*, *n/a*(*n/a*).
2131 Retrieved 2021-11-09, from [http://onlinelibrary.wiley.com/doi/abs/10.1111/](http://onlinelibrary.wiley.com/doi/abs/10.1111/bre.12629)
2132 [bre.12629](http://onlinelibrary.wiley.com/doi/abs/10.1111/bre.12629) (eprint: <https://onlinelibrary.wiley.com/doi/pdf/10.1111/bre.12629>) doi:
2133 10.1111/bre.12629
- 2134 Li, Q., Utescher, T., Liu, Y. C., Ferguson, D., Jia, H., & Quan, C. (2022, Septem-
2135 ber). Monsoonal climate of East Asia in Eocene times inferred from an analysis
2136 of plant functional types. *Palaeogeography, Palaeoclimatology, Palaeoecology*, *601*,
2137 111138. Retrieved 2022-10-24, from [https://linkinghub.elsevier.com/retrieve/](https://linkinghub.elsevier.com/retrieve/pii/S003101822200308X)
2138 [pii/S003101822200308X](https://linkinghub.elsevier.com/retrieve/pii/S003101822200308X) doi: 10.1016/j.palaeo.2022.111138
- 2139 Li, S., Xing, Y., Valdes, P. J., Huang, Y., Su, T., Farnsworth, A., ... Zhou, Z. (2018,
2140 September). Oligocene climate signals and forcings in Eurasia revealed by plant macro-
2141 fossil and modelling results. *Gondwana Research*, *61*, 115–127. Retrieved 2019-10-18,
2142 from <https://linkinghub.elsevier.com/retrieve/pii/S1342937X18301473> doi:
2143 10.1016/j.gr.2018.04.015
- 2144 Li, X., Zhang, R., Zhang, Z., & Yan, Q. (2017, October). What enhanced the aridity in
2145 Eocene Asian inland: Global cooling or early Tibetan Plateau uplift? *Palaeogeography,*
2146 *Palaeoclimatology, Palaeoecology*. Retrieved 2018-01-16, from [http://linkinghub](http://linkinghub.elsevier.com/retrieve/pii/S0031018217306922)
2147 [.elsevier.com/retrieve/pii/S0031018217306922](http://linkinghub.elsevier.com/retrieve/pii/S0031018217306922) doi: 10.1016/j.palaeo.2017.10
2148 .029
- 2149 Liang, J.-q., Leng, Q., Xiao, L., Höfig, D. F., Royer, D. L., Zhang, Y. G., & Yang, H. (2022,
2150 October). Early Miocene redwood fossils from Inner Mongolia: CO₂ reconstructions
2151 and paleoclimate effects of a low Mongolian plateau. *Review of Palaeobotany and*
2152 *Palynology*, *305*, 104743. Retrieved 2022-08-21, from [https://linkinghub.elsevier](https://linkinghub.elsevier.com/retrieve/pii/S0034666722001415)
2153 [.com/retrieve/pii/S0034666722001415](https://linkinghub.elsevier.com/retrieve/pii/S0034666722001415) doi: 10.1016/j.revpalbo.2022.104743
- 2154 Licht, A., Dupont-Nivet, G., Win, Z., Swe, H. H., Kaythi, M., Roperch, P., ... Sein, K.
2155 (2018, November). Paleogene evolution of the Burmese forearc basin and implications
2156 for the history of India-Asia convergence. *GSA Bulletin*, *131*(5-6), 730–748. Retrieved
2157 2021-03-29, from <https://doi.org/10.1130/B35002.1> doi: 10.1130/B35002.1
- 2158 Licht, A., van Cappelle, M., Abels, H. A., Ladant, J.-B., Trabucho-Alexandre, J., France-
2159 Lanord, C., ... Jaeger, J.-J. (2014, September). Asian monsoons in a late Eocene
2160 greenhouse world. *Nature*, *513*(7519), 501–506. Retrieved 2017-10-09, from [http://](http://www.nature.com/doi/10.1038/nature13704)
2161 www.nature.com/doi/10.1038/nature13704 doi: 10.1038/nature13704
- 2162 Ling, C.-C., Ma, F.-J., Dong, J.-L., Zhou, G.-H., Wang, Q.-J., & Sun, B.-N. (2021, Oc-
2163 tober). A mid-altitude area in southwestern China experienced a humid subtropical
2164 climate with subtle monsoon signatures during the early Oligocene: Evidence from the
2165 Ningming flora of Guangxi. *Palaeogeography, Palaeoclimatology, Palaeoecology*, *579*,
2166 110601. Retrieved 2022-05-03, from [https://linkinghub.elsevier.com/retrieve/](https://linkinghub.elsevier.com/retrieve/pii/S0031018221003862)
2167 [pii/S0031018221003862](https://linkinghub.elsevier.com/retrieve/pii/S0031018221003862) doi: 10.1016/j.palaeo.2021.110601
- 2168 Liu, D., Li, H., Sun, Z., Cao, Y., Wang, L., Pan, J., ... Ye, X. (2017, August). Cenozoic
2169 episodic uplift and kinematic evolution between the Pamir and Southwestern Tien
2170 Shan. *Tectonophysics*, *712-713*, 438–454. Retrieved 2021-03-26, from [https://www](https://www.sciencedirect.com/science/article/pii/S004019511730255X)
2171 [.sciencedirect.com/science/article/pii/S004019511730255X](https://www.sciencedirect.com/science/article/pii/S004019511730255X) doi: 10.1016/j
2172 .tecto.2017.06.009
- 2173 Liu, J., Li, J., Song, C., Yu, H., Peng, T., Hui, Z., & Ye, X. (2016, July). Palynological
2174 evidence for late Miocene stepwise aridification on the northeastern Tibetan Plateau.
2175 *Climate of the Past*, *12*, 1473–1484. doi: 10.5194/cp-12-1473-2016
- 2176 Liu, W., Liu, Z., An, Z., Sun, J., Chang, H., Wang, N., ... Wang, H. (2014, Novem-
2177 ber). Late Miocene episodic lakes in the arid Tarim Basin, western China. *Proceed-*
2178 *ings of the National Academy of Sciences*, *111*(46), 16292–16296. Retrieved 2022-06-
2179 17, from <https://www.pnas.org/doi/full/10.1073/pnas.1410890111> (Publisher:
2180 Proceedings of the National Academy of Sciences) doi: 10.1073/pnas.1410890111
- 2181 Liu, X., Guo, Q., Guo, Z., Yin, J., Dong, B., & Smith, R. (2015, October). Where were the

- 2182 monsoon regions and arid zones in Asia prior to the Tibetan Plateau uplift? *National*
 2183 *Science Review*, 2, nrv068. doi: 10.1093/nsr/nrv068
- 2184 Liu, X., Sun, H., Miao, Y., Dong, B., & Yin, Z.-Y. (2015, May). Impacts of uplift of northern
 2185 Tibetan Plateau and formation of Asian inland deserts on regional climate and environ-
 2186 ment. *Quaternary Science Reviews*, 116, 1–14. Retrieved 2022-06-22, from [https://](https://www.sciencedirect.com/science/article/pii/S0277379115001171)
 2187 www.sciencedirect.com/science/article/pii/S0277379115001171 doi: 10.1016/
 2188 [j.quascirev.2015.03.010](https://www.sciencedirect.com/science/article/pii/S0277379115001171)
- 2189 Liu, X., & Yin, Z.-Y. (2002, July). Sensitivity of East Asian monsoon climate to the uplift
 2190 of the Tibetan Plateau. *Palaeogeography, Palaeoclimatology, Palaeoecology*, 183(3),
 2191 223–245. Retrieved 2021-04-14, from [https://www.sciencedirect.com/science/](https://www.sciencedirect.com/science/article/pii/S0031018201004886)
 2192 [article/pii/S0031018201004886](https://www.sciencedirect.com/science/article/pii/S0031018201004886) doi: 10.1016/S0031-0182(01)00488-6
- 2193 Liu, Z., Zhang, K., Sun, Y., Liu, W., Liu, Y. C., & Quan, C. (2014). Cenozoic Environ-
 2194 mental Changes in the Northern Qaidam Basin Inferred from n-alkane Records. *Acta*
 2195 *Geologica Sinica - English Edition*, 88(5), 1547–1555. Retrieved 2022-06-17, from
 2196 <http://onlinelibrary.wiley.com/doi/abs/10.1111/1755-6724.12317> (eprint:
 2197 <https://onlinelibrary.wiley.com/doi/pdf/10.1111/1755-6724.12317>) doi: 10.1111/1755-
 2198 -6724.12317
- 2199 Lu, H., & Guo, Z. (2014, January). Evolution of the monsoon and dry climate in East Asia
 2200 during late Cenozoic: A review. *Science China Earth Sciences*, 57(1), 70–79. Retrieved
 2201 2017-10-09, from <http://link.springer.com/10.1007/s11430-013-4790-3> doi:
 2202 10.1007/s11430-013-4790-3
- 2203 Lu, H., Wang, X., & li, l. (2010, August). Aeolian sediment evidence that global cooling has
 2204 driven late Cenozoic stepwise aridification in Central Asia. *Geological Society London*
 2205 *Special Publications*, 342, 29–44. doi: 10.1144/SP342.4
- 2206 Luo, M., Jia, H., Li, Q., Meng, X., Ferguson, D., Liu, P., ... Quan, C. (2022, August).
 2207 Middle Miocene lotus (Nelumbonaceae, Nelumbo) from the Qaidam Basin, Northern
 2208 Tibet Plateau. *Biology*, 11, 1261. doi: 10.3390/biology11091261
- 2209 Lévy, M., Shankar, D., André, J.-M., Shenoi, S. S. C., Durand, F., & de Boyer Montégut, C.
 2210 (2007, December). Basin-wide seasonal evolution of the Indian Ocean’s phytoplankton
 2211 blooms. *Journal of Geophysical Research*, 112(C12). Retrieved 2020-07-30, from
 2212 <http://doi.wiley.com/10.1029/2007JC004090> doi: 10.1029/2007JC004090
- 2213 Ma, X., & Jiang, H. (2015, June). Combined tectonics and climate forcing for the widespread
 2214 aeolian dust accumulation in the Chinese Loess Plateau since the early late Miocene.
 2215 *International Geology Review*, 57, 1861–1876. doi: 10.1080/00206814.2015.1027305
- 2216 Ma, X., Jiang, H., Cheng, J., & Xu, H. (2012, September). Spatiotemporal evolution
 2217 of Paleogene palynoflora in China and its implication for development of the ex-
 2218 tensional basins in East China. *Review of Palaeobotany and Palynology*, 184, 24–
 2219 35. Retrieved 2019-02-10, from [https://linkinghub.elsevier.com/retrieve/pii/](https://linkinghub.elsevier.com/retrieve/pii/S0034666712001935)
 2220 [S0034666712001935](https://linkinghub.elsevier.com/retrieve/pii/S0034666712001935) doi: 10.1016/j.revpalbo.2012.07.013
- 2221 Ma, Y., Fang, X., Li, J., Wu, F., & Zhang, J. (2005, May). The vegetation and cli-
 2222 mate change during Neocene and Early Quaternary in Jiuxi Basin, China. *Sci-*
 2223 *ence in China Series D: Earth Sciences*, 48(5), 676. Retrieved 2022-06-16, from
 2224 <http://link.springer.com/10.1360/03yd0110> doi: 10.1360/03yd0110
- 2225 Macaulay, E. A., Sobel, E. R., Mikolaichuk, A., Kohn, B., & Stuart, F. M.
 2226 (2014). Cenozoic deformation and exhumation history of the Central Kyr-
 2227 gyz Tien Shan. *Tectonics*, 33(2), 135–165. Retrieved 2022-03-22, from
 2228 <http://onlinelibrary.wiley.com/doi/abs/10.1002/2013TC003376> (eprint:
 2229 <https://agupubs.onlinelibrary.wiley.com/doi/pdf/10.1002/2013TC003376>) doi: 10
 2230 .1002/2013TC003376
- 2231 Macaulay, E. A., Sobel, E. R., Mikolaichuk, A., Wack, M., Gilder, S. A., Mulch, A., ...
 2232 Apayarov, F. (2016). The sedimentary record of the Issyk Kul basin, Kyrgyzstan:
 2233 climatic and tectonic inferences. *Basin Research*, 28(1), 57–80. Retrieved 2022-03-22,
 2234 from <http://onlinelibrary.wiley.com/doi/abs/10.1111/bre.12098> (eprint:
 2235 <https://onlinelibrary.wiley.com/doi/pdf/10.1111/bre.12098>) doi: 10.1111/bre.12098
- 2236 Madec, G. (2016). NEMO ocean engine. *Note du P\`ole de modélisation de l’Institut*

- 2237 *Pierre-Simon Laplace*(27), 396.
- 2238 Madec, G., & Imbard, M. (1996, May). A global ocean mesh to overcome the North
2239 Pole singularity. *Climate Dynamics*, 12(6), 381–388. Retrieved 2021-03-09, from
2240 <https://doi.org/10.1007/BF00211684> doi: 10.1007/BF00211684
- 2241 Matsuzaki, K. M., Suzuki, N., & Tada, R. (2020, June). An intensified East Asian winter
2242 monsoon in the Japan Sea between 7.9 and 6.6 Ma. *Geology*, 48(9), 919–923. Retrieved
2243 2022-12-20, from <https://doi.org/10.1130/G47393.1> doi: 10.1130/G47393.1
- 2244 Maurin, T., & Rangin, C. (2009). Structure and kinematics of the Indo-Burmese Wedge: Re-
2245 cent and fast growth of the outer wedge. *Tectonics*, 28(2). Retrieved 2021-03-29, from
2246 <http://agupubs.onlinelibrary.wiley.com/doi/abs/10.1029/2008TC002276>
2247 (_eprint: <https://onlinelibrary.wiley.com/doi/pdf/10.1029/2008TC002276>) doi:
2248 <https://doi.org/10.1029/2008TC002276>
- 2249 McQuarrie, N., & Hinsbergen, D. J. J. v. (2013, March). Retrodeform-
2250 ing the Arabia-Eurasia collision zone: Age of collision versus magnitude of
2251 continental subduction. *Geology*, 41(3), 315–318. Retrieved 2021-04-06,
2252 from [http://pubs.geoscienceworld.org/gsa/geology/article-abstract/41/3/
2253 315/131120/Retrodeforming-the-Arabia-Eurasia-collision-zone](http://pubs.geoscienceworld.org/gsa/geology/article-abstract/41/3/315/131120/Retrodeforming-the-Arabia-Eurasia-collision-zone) (Publisher:
2254 GeoScienceWorld) doi: 10.1130/G33591.1
- 2255 Meijer, N., Dupont-Nivet, G., Abels, H. A., Kaya, M. Y., Licht, A., Xiao, M., ... Guo,
2256 Z. (2019, March). Central Asian moisture modulated by proto-Paratethys Sea in-
2257 cursions since the early Eocene. *Earth and Planetary Science Letters*, 510, 73–
2258 84. Retrieved 2019-04-25, from [https://linkinghub.elsevier.com/retrieve/pii/
2259 S0012821X19300019](https://linkinghub.elsevier.com/retrieve/pii/S0012821X19300019) doi: 10.1016/j.epsl.2018.12.031
- 2260 Meijer, N., Dupont-Nivet, G., Barbolini, N., Woutersen, A., Rohrmann, A., Yang, Z., ...
2261 Nowaczyk, N. (2021, February). Loess-Like Dust Appearance at 40 Ma in Central
2262 China. *Paleoceanography and Paleoclimatology*, 36. doi: 10.1029/2020PA003993
- 2263 Meng, Q.-t., Bruch, A. A., Sun, G., Liu, Z.-j., Hu, F., & Sun, P.-c. (2018, December). Quan-
2264 titative reconstruction of Middle and Late Eocene paleoclimate based on palynological
2265 records from the Huadian Basin, northeastern China: Evidence for monsoonal influ-
2266 ence on oil shale formation. *Palaeogeography, Palaeoclimatology, Palaeoecology*, 510,
2267 63–77. Retrieved 2020-07-10, from [https://linkinghub.elsevier.com/retrieve/
2268 pii/S0031018217304741](https://linkinghub.elsevier.com/retrieve/pii/S0031018217304741) doi: 10.1016/j.palaeo.2017.11.036
- 2269 Merlis, T. M., Schneider, T., Bordoni, S., & Eisenman, I. (2013, Febru-
2270 ary). HadleyII Circulation Response to Orbital Precession. Part II: Subtrop-
2271 ical Continent. *Journal of Climate*, 26(3), 754–771. Retrieved 2020-09-
2272 07, from [https://journals.ametsoc.org/jcli/article/26/3/754/33493/Hadley
2273 -Circulation-Response-to-Orbital-Precession](https://journals.ametsoc.org/jcli/article/26/3/754/33493/Hadley-Circulation-Response-to-Orbital-Precession) (Publisher: American Meteorolo-
2274 gical Society) doi: 10.1175/JCLI-D-12-00149.1
- 2275 Metcalfe, I. (2013, April). Gondwana dispersion and Asian accretion: Tectonic and palaeo-
2276 geographic evolution of eastern Tethys. *Journal of Asian Earth Sciences*, 66, 1–
2277 33. Retrieved 2020-10-14, from [https://linkinghub.elsevier.com/retrieve/pii/
2278 S1367912012005779](https://linkinghub.elsevier.com/retrieve/pii/S1367912012005779) doi: 10.1016/j.jseas.2012.12.020
- 2279 Meulenkamp, J. E., & Sissingh, W. (2003, July). Tertiary palaeogeography and
2280 tectonostratigraphic evolution of the Northern and Southern Peri-Tethys platforms
2281 and the intermediate domains of the African–Eurasian convergent plate boundary
2282 zone. *Palaeogeography, Palaeoclimatology, Palaeoecology*, 196(1), 209–228. Re-
2283 trieved 2021-04-06, from [https://www.sciencedirect.com/science/article/pii/
2284 S0031018203003195](https://www.sciencedirect.com/science/article/pii/S0031018203003195) doi: 10.1016/S0031-0182(03)00319-5
- 2285 Miao, Y., Fang, X., Herrmann, M., Wu, F., Zhang, Y., & Liu, D. (2011, January). Miocene
2286 pollen record of KC-1 core in the Qaidam Basin, NE Tibetan Plateau and implications
2287 for evolution of the East Asian monsoon. *Palaeogeography, Palaeoclimatology, Palaeoe-
2288 cology*, 299(1-2), 30–38. Retrieved 2022-05-04, from [https://linkinghub.elsevier
2289 .com/retrieve/pii/S0031018210006425](https://linkinghub.elsevier.com/retrieve/pii/S0031018210006425) doi: 10.1016/j.palaeo.2010.10.026
- 2290 Miao, Y., Herrmann, M., Wu, F., Yan, X., & Yang, S. (2012, May). What controlled
2291 Mid–Late Miocene long-term aridification in Central Asia? — Global cooling or

- 2292 Tibetan Plateau uplift: A review. *Earth-Science Reviews*, 112(3), 155–172. Re-
 2293 trieved 2022-03-22, from [https://www.sciencedirect.com/science/article/pii/](https://www.sciencedirect.com/science/article/pii/S0012825212000141)
 2294 [S0012825212000141](https://www.sciencedirect.com/science/article/pii/S0012825212000141) doi: 10.1016/j.earscirev.2012.02.003
- 2295 Miao, Y., Song, C., Fang, X., Meng, Q., Zhang, P., Wu, F., & Yan, X. (2016, January).
 2296 Late Cenozoic genus Fupingopollenites development and its implications for the Asian
 2297 summer monsoon evolution. *Gondwana Research*, 29(1), 320–333. Retrieved 2017-
 2298 10-09, from <http://linkinghub.elsevier.com/retrieve/pii/S1342937X15000040>
 2299 doi: 10.1016/j.gr.2014.12.007
- 2300 Miao, Y., Warny, S., Clift, P. D., Liu, C., & Gregory, M. (2017, December). Evidence
 2301 of continuous Asian summer monsoon weakening as a response to global cooling over
 2302 the last 8 Ma. *Gondwana Research*, 52, 48–58. Retrieved 2022-07-05, from [https://](https://linkinghub.elsevier.com/retrieve/pii/S1342937X16304294)
 2303 linkinghub.elsevier.com/retrieve/pii/S1342937X16304294 doi: 10.1016/j.gr.
 2304 .2017.09.003
- 2305 Miao, Y., Wu, F., Chang, H., Fang, X., Deng, T., Sun, J., & Jin, C. (2016, March). A
 2306 Late-Eocene palynological record from the Hoh Xil Basin, northern Tibetan Plateau,
 2307 and its implications for stratigraphic age, paleoclimate and paleoelevation. *Gondwana*
 2308 *Research*, 31, 241–252. Retrieved 2017-10-09, from [http://linkinghub.elsevier](http://linkinghub.elsevier.com/retrieve/pii/S1342937X15000374)
 2309 [.com/retrieve/pii/S1342937X15000374](http://linkinghub.elsevier.com/retrieve/pii/S1342937X15000374) doi: 10.1016/j.gr.2015.01.007
- 2310 Miao, Y., Wu, F., Herrmann, M., Yan, X., & Meng, Q. (2013, October). Late early
 2311 Oligocene East Asian summer monsoon in the NE Tibetan Plateau: Evidence from a
 2312 palynological record from the Lanzhou Basin, China. *Journal of Asian Earth Sciences*,
 2313 75, 46–57. Retrieved 2022-04-14, from [https://www.sciencedirect.com/science/](https://www.sciencedirect.com/science/article/pii/S1367912013003507)
 2314 [article/pii/S1367912013003507](https://www.sciencedirect.com/science/article/pii/S1367912013003507) doi: 10.1016/j.jseaes.2013.07.003
- 2315 Miller, K. G., Browning, J. V., Schmelz, W. J., Kopp, R. E., Mountain, G. S., & Wright, J. D.
 2316 (2020, May). Cenozoic sea-level and cryospheric evolution from deep-sea geochemical
 2317 and continental margin records. *Science Advances*, 6(20), eaaz1346. Retrieved 2021-
 2318 03-09, from <https://advances.sciencemag.org/content/6/20/eaaz1346> (Pub-
 2319 lisher: American Association for the Advancement of Science Section: Review) doi:
 2320 10.1126/sciadv.aaz1346
- 2321 Molnar, P., Boos, W. R., & Battisti, D. S. (2010, April). Orographic Controls on Climate
 2322 and Paleoclimate of Asia: Thermal and Mechanical Roles for the Tibetan Plateau.
 2323 *Annual Review of Earth and Planetary Sciences*, 38(1), 77–102. Retrieved 2018-
 2324 03-09, from [http://www.annualreviews.org/doi/10.1146/annurev-earth-040809-](http://www.annualreviews.org/doi/10.1146/annurev-earth-040809-152456)
 2325 [-152456](http://www.annualreviews.org/doi/10.1146/annurev-earth-040809-152456) doi: 10.1146/annurev-earth-040809-152456
- 2326 Molnar, P., England, P., & Martinod, J. (1993). Mantle dynamics, uplift of the Tibetan
 2327 Plateau, and the Indian Monsoon. *Reviews of Geophysics*, 31(4), 357. Retrieved 2020-
 2328 07-27, from <http://doi.wiley.com/10.1029/93RG02030> doi: 10.1029/93RG02030
- 2329 Morley, R. J. (2018, July). Assembly and division of the South and South-East Asian
 2330 flora in relation to tectonics and climate change. *Journal of Tropical Ecology*,
 2331 34(4), 209–234. Retrieved 2022-06-23, from [https://www.cambridge.org/core/](https://www.cambridge.org/core/product/identifier/S0266467418000202/type/journal_article)
 2332 [product/identifier/S0266467418000202/type/journal_article](https://www.cambridge.org/core/product/identifier/S0266467418000202/type/journal_article) doi: 10.1017/
 2333 S0266467418000202
- 2334 Moucha, R., & Forte, A. M. (2011, October). Changes in African topography driven
 2335 by mantle convection. *Nature Geoscience*, 4(10), 707–712. Retrieved 2021-04-07,
 2336 from <http://www.nature.com/articles/ngeo1235> (Number: 10 Publisher: Nature
 2337 Publishing Group) doi: 10.1038/ngeo1235
- 2338 Mouthereau, F. (2011, November). Timing of uplift in the Zagros belt/Iranian plateau and
 2339 accommodation of late Cenozoic Arabia–Eurasia convergence. *Geological Magazine*,
 2340 148(5-6), 726–738. Retrieved 2020-06-22, from [https://www.cambridge.org/core/](https://www.cambridge.org/core/product/identifier/S0016756811000306/type/journal_article)
 2341 [product/identifier/S0016756811000306/type/journal_article](https://www.cambridge.org/core/product/identifier/S0016756811000306/type/journal_article) doi: 10.1017/
 2342 S0016756811000306
- 2343 Mouthereau, F., Lacombe, O., & Vergés, J. (2012, April). Building the Zagros collisional
 2344 orogen: Timing, strain distribution and the dynamics of Arabia/Eurasia plate con-
 2345 vergence. *Tectonophysics*, 532-535, 27–60. Retrieved 2021-09-15, from [https://](https://www.sciencedirect.com/science/article/pii/S0040195112000509)
 2346 www.sciencedirect.com/science/article/pii/S0040195112000509 doi: 10.1016/

- 2347 j.tecto.2012.01.022
- 2348 Najman, Y., Sobel, E. R., Millar, I., Stockli, D. F., Govin, G., Lisker, F., ... Kahn, A.
2349 (2020, January). The exhumation of the Indo-Burman Ranges, Myanmar. *Earth*
2350 *and Planetary Science Letters*, 530, 115948. Retrieved 2021-03-29, from [https://](https://www.sciencedirect.com/science/article/pii/S0012821X19306405)
2351 www.sciencedirect.com/science/article/pii/S0012821X19306405 doi: 10.1016/
2352 j.epsl.2019.115948
- 2353 Ninomiya, K., & Shibagaki, Y. (2007). Multi-Scale Features of the Meiyu-Baiu Front and
2354 Associated Precipitation Systems. *Journal of the Meteorological Society of Japan.*
2355 *Ser. II, 85B*, 103–122. Retrieved 2022-09-13, from [http://www.jstage.jst.go.jp/](http://www.jstage.jst.go.jp/article/jmsj/85B/0/85B_0_103/article)
2356 [article/jmsj/85B/0/85B_0_103/article](http://www.jstage.jst.go.jp/article/jmsj/85B/0/85B_0_103/article) doi: 10.2151/jmsj.85B.103
- 2357 Okay, A. I., Zattin, M., & Cavazza, W. (2010, January). Apatite fission-track data for the
2358 Miocene Arabia-Eurasia collision. *Geology*, 38(1), 35–38. Retrieved 2022-03-04, from
2359 <https://doi.org/10.1130/G30234.1> doi: 10.1130/G30234.1
- 2360 Otero, O., & Gayet, M. (2001, January). Palaeoichthyofaunas from the Lower Oligocene
2361 and Miocene of the Arabian Plate: palaeoecological and palaeobiogeographical im-
2362 plications. *Palaeogeography, Palaeoclimatology, Palaeoecology*, 165(1), 141–169. Re-
2363 trieved 2021-04-06, from [https://www.sciencedirect.com/science/article/pii/](https://www.sciencedirect.com/science/article/pii/S0031018200001589)
2364 [S0031018200001589](https://www.sciencedirect.com/science/article/pii/S0031018200001589) doi: 10.1016/S0031-0182(00)00158-9
- 2365 Ozsvárt, P., Kocsis, L., Nyerges, A., Györi, O., & Pálffy, J. (2016, October). The
2366 Eocene-Oligocene climate transition in the Central Paratethys. *Palaeogeography,*
2367 *Palaeoclimatology, Palaeoecology*, 459, 471–487. Retrieved 2021-04-01, from [https://](https://www.sciencedirect.com/science/article/pii/S0031018216302899)
2368 www.sciencedirect.com/science/article/pii/S0031018216302899 doi: 10.1016/
2369 j.palaeo.2016.07.034
- 2370 Page, M., Licht, A., Dupont-Nivet, G., Meijer, N., Barbolini, N., Hoorn, C., ... Guo, Z.
2371 (2019, March). Synchronous cooling and decline in monsoonal rainfall in northeastern
2372 Tibet during the fall into the Oligocene icehouse. *Geology*, 47(3), 203–206. Retrieved
2373 2020-01-21, from [https://pubs.geoscienceworld.org/gsa/geology/article/47/](https://pubs.geoscienceworld.org/gsa/geology/article/47/3/203/568396/Synchronous-cooling-and-decline-in-monsoonal)
2374 [3/203/568396/Synchronous-cooling-and-decline-in-monsoonal](https://pubs.geoscienceworld.org/gsa/geology/article/47/3/203/568396/Synchronous-cooling-and-decline-in-monsoonal) doi: 10.1130/
2375 G45480.1
- 2376 Palcu, D. V., Patina, I. S., Şandric, I., Lazarev, S., Vasiliev, I., Stoica, M., & Krijgsman,
2377 W. (2021, December). Late Miocene megalake regressions in Eurasia. *Scientific Re-*
2378 *ports*, 11(1), 11471. Retrieved 2021-06-11, from [http://www.nature.com/articles/](http://www.nature.com/articles/s41598-021-91001-z)
2379 [s41598-021-91001-z](http://www.nature.com/articles/s41598-021-91001-z) doi: 10.1038/s41598-021-91001-z
- 2380 Peng, T., Li, J., Song, C., Guo, B., Liu, J., Zhao, Z., & Zhang, J. (2016, April).
2381 An integrated biomarker perspective on Neogene–Quaternary climatic evolution in
2382 NE Tibetan Plateau: Implications for the Asian aridification. *Quaternary Interna-*
2383 *tional*, 399, 174–182. Retrieved 2022-06-09, from [https://www.sciencedirect.com/](https://www.sciencedirect.com/science/article/pii/S104061821500422X)
2384 [science/article/pii/S104061821500422X](https://www.sciencedirect.com/science/article/pii/S104061821500422X) doi: 10.1016/j.quaint.2015.04.020
- 2385 Pettke, T., Halliday, A. N., & Rea, D. K. (2002). Cenozoic evolution of Asian climate
2386 and sources of Pacific seawater Pb and Nd derived from eolian dust of sediment
2387 core LL44-GPC3. *Paleoceanography*, 17(3), 3–1–3–13. Retrieved 2022-03-25, from
2388 <http://onlinelibrary.wiley.com/doi/abs/10.1029/2001PA000673> (eprint:
2389 <https://agupubs.onlinelibrary.wiley.com/doi/pdf/10.1029/2001PA000673>) doi: 10
2390 .1029/2001PA000673
- 2391 Pillot, Q., Donnadieu, Y., Sarr, A.-C., Ladant, J.-B., & Suchéras-Marx, B. (2022).
2392 Evolution of Ocean Circulation in the North Atlantic Ocean During the Miocene:
2393 Impact of the Greenland Ice Sheet and the Eastern Tethys Seaway. *Paleoceanog-*
2394 *raphy and Paleoclimatology*, 37(8), e2022PA004415. Retrieved 2022-09-13, from
2395 <http://onlinelibrary.wiley.com/doi/abs/10.1029/2022PA004415> (eprint:
2396 <https://agupubs.onlinelibrary.wiley.com/doi/pdf/10.1029/2022PA004415>) doi: 10
2397 .1029/2022PA004415
- 2398 Pirouz, M., Avouac, J.-P., Hassanzadeh, J., Kirschvink, J. L., & Bahroudi, A. (2017,
2399 November). Early Neogene foreland of the Zagros, implications for the initial closure
2400 of the Neo-Tethys and kinematics of crustal shortening. *Earth and Planetary Science*
2401 *Letters*, 477, 168–182. Retrieved 2020-10-20, from <https://linkinghub.elsevier>

- 2400 .com/retrieve/pii/S0012821X17304302 doi: 10.1016/j.epsl.2017.07.046
- 2403 Poblete, F., Dupont-Nivet, G., Licht, A., van Hinsbergen, D. J. J., Roperch, P., Miha-
- 2404 lynuk, M. G., ... Baatsen, M. L. J. (2021, March). Towards interactive global
- 2405 paleogeographic maps, new reconstructions at 60, 40 and 20Ma. *Earth-Science Re-*
- 2406 *views*, 214, 103508. Retrieved 2021-04-07, from [https://www.sciencedirect.com/](https://www.sciencedirect.com/science/article/pii/S0012825221000076)
- 2407 [science/article/pii/S0012825221000076](https://www.sciencedirect.com/science/article/pii/S0012825221000076) doi: 10.1016/j.earscirev.2021.103508
- 2408 Polissar, P. J., Uno, K. T., Phelps, S. R., Karp, A. T., Freeman, K. H., &
- 2409 Pensky, J. L. (2021). Hydrologic Changes Drove the Late Miocene Expan-
- 2410 sion of C4 Grasslands on the Northern Indian Subcontinent. *Paleoceanogra-*
- 2411 *phy and Paleoclimatology*, 36(4), e2020PA004108. Retrieved 2022-06-07, from
- 2412 <http://onlinelibrary.wiley.com/doi/abs/10.1029/2020PA004108> (.eprint:
- 2413 <https://agupubs.onlinelibrary.wiley.com/doi/pdf/10.1029/2020PA004108>) doi: 10
- 2414 .1029/2020PA004108
- 2415 Poulsen, C. J., & Jeffery, M. L. (2011, June). Climate change imprint-
- 2416 ing on stable isotopic compositions of high-elevation meteoric water cloaks
- 2417 past surface elevations of major orogens. *Geology*, 39(6), 595–598. Re-
- 2418 trieved 2022-04-11, from [http://pubs.geoscienceworld.org/geology/article/](http://pubs.geoscienceworld.org/geology/article/39/6/595/130636/Climate-change-imprinting-on-stable-isotopic)
- 2419 [39/6/595/130636/Climate-change-imprinting-on-stable-isotopic](http://pubs.geoscienceworld.org/geology/article/39/6/595/130636/Climate-change-imprinting-on-stable-isotopic) doi: 10
- 2420 .1130/G32052.1
- 2421 Pound, M. J., & Salzmann, U. (2017, February). Heterogeneity in global vegetation and ter-
- 2422 restrial climate change during the late Eocene to early Oligocene transition. *Scientific*
- 2423 *Reports*, 7, 43386. Retrieved 2017-11-23, from [http://www.nature.com/articles/](http://www.nature.com/articles/srep43386)
- 2424 [srep43386](http://www.nature.com/articles/srep43386) doi: 10.1038/srep43386
- 2425 Prabhat, P., Rahaman, W., Lathika, N., Tarique, M., Mishra, R., & Thamban, M. (2022,
- 2426 December). Modern-like deep water circulation in Indian Ocean caused by Central
- 2427 American Seaway closure. *Nature Communications*, 13(1), 7561. Retrieved 2022-12-
- 2428 09, from <https://www.nature.com/articles/s41467-022-35145-0> doi: 10.1038/
- 2429 [s41467-022-35145-0](https://www.nature.com/articles/s41467-022-35145-0)
- 2430 Prell, W. L., & Kutzbach, J. E. (1992). Sensitivity of the Indian monsoon to forcing
- 2431 parameters and implications for its evolution. *Nature*, 360(6405), 647–652.
- 2432 Qiang, X., An, Z., Song, Y., Chang, H., Sun, Y., Liu, W., ... Ai, L. (2011, January).
- 2433 New eolian red clay sequence on the western Chinese Loess Plateau linked to onset of
- 2434 Asian desertification about 25 Ma ago. *Science China Earth Sciences*, 54(1), 136–144.
- 2435 Retrieved 2017-10-09, from [http://link.springer.com/10.1007/s11430-010-4126-](http://link.springer.com/10.1007/s11430-010-4126-5)
- 2436 [-5](http://link.springer.com/10.1007/s11430-010-4126-5) doi: 10.1007/s11430-010-4126-5
- 2437 Rae, J. W., Zhang, Y. G., Liu, X., Foster, G. L., Stoll, H. M., & Whiteford, R. D.
- 2438 (2021, May). Atmospheric CO₂ over the Past 66 Million Years from Marine
- 2439 Archives. *Annual Review of Earth and Planetary Sciences*, 49(1), 609–641. Re-
- 2440 trieved 2021-06-01, from [https://www.annualreviews.org/doi/10.1146/annurev](https://www.annualreviews.org/doi/10.1146/annurev-earth-082420-063026)
- 2441 [-earth-082420-063026](https://www.annualreviews.org/doi/10.1146/annurev-earth-082420-063026) doi: 10.1146/annurev-earth-082420-063026
- 2442 Ramstein, G., Fluteau, F., Besse, J., & Joussaume, S. (1997, April). Effect of orogeny,
- 2443 plate motion and land–sea distribution on Eurasian climate change over the past
- 2444 30 million years. *Nature*, 386(6627), 788–795. Retrieved 2017-12-05, from [http://](http://www.nature.com/doi/10.1038/386788a0)
- 2445 www.nature.com/doi/10.1038/386788a0 doi: 10.1038/386788a0
- 2446 Rea, D., Leinen, M., & Janecek, T. (1985, March). Geologic Approach to the Long-Term
- 2447 History of Atmospheric Circulation. *Science (New York, N.Y.)*, 227, 721–5. doi:
- 2448 10.1126/science.227.4688.721
- 2449 Rea, D. K. (1994). The paleoclimatic record provided by eolian deposition in the deep
- 2450 sea: The geologic history of wind. *Reviews of Geophysics*, 32(2), 159–195. Retrieved
- 2451 2022-05-16, from <http://onlinelibrary.wiley.com/doi/abs/10.1029/93RG03257>
- 2452 (.eprint: <https://agupubs.onlinelibrary.wiley.com/doi/pdf/10.1029/93RG03257>) doi:
- 2453 10.1029/93RG03257
- 2454 Ren, J., Schubert, B. A., Lukens, W. E., & Quan, C. (2021, September). Low oxy-
- 2455 gen isotope values of fossil cellulose indicate an intense monsoon in East Asia dur-
- 2456 ing the late Oligocene. *Palaeogeography, Palaeoclimatology, Palaeoecology*, 577,

- 2457 110556. Retrieved 2022-02-22, from [https://linkinghub.elsevier.com/retrieve/](https://linkinghub.elsevier.com/retrieve/pii/S0031018221003412)
 2458 [pii/S0031018221003412](https://linkinghub.elsevier.com/retrieve/pii/S0031018221003412) doi: 10.1016/j.palaeo.2021.110556
- 2459 Ren, X., Nie, J., Saylor, J. E., Wang, X., Liu, F., & Horton, B. K. (2020). Temperature Con-
 2460 trol on Silicate Weathering Intensity and Evolution of the Neogene East Asian Summer
 2461 Monsoon. *Geophysical Research Letters*, *47*(15), e2020GL088808. Retrieved 2022-
 2462 06-09, from <http://onlinelibrary.wiley.com/doi/abs/10.1029/2020GL088808>
 2463 (_eprint: <https://agupubs.onlinelibrary.wiley.com/doi/pdf/10.1029/2020GL088808>)
 2464 doi: 10.1029/2020GL088808
- 2465 Roberts, E. M., Stevens, N. J., O'Connor, P. M., Dirks, P. H. G. M., Gottfried, M. D.,
 2466 Clyde, W. C., ... Hemming, S. (2012, April). Initiation of the western branch of the
 2467 East African Rift coeval with the eastern branch. *Nature Geoscience*, *5*(4), 289–294.
 2468 Retrieved 2021-04-07, from <http://www.nature.com/articles/ngeo1432> (Number:
 2469 4 Publisher: Nature Publishing Group) doi: 10.1038/ngeo1432
- 2470 Rodwell, M. J., & Hoskins, B. J. (1995, May). A Model of the Asian Summer Monsoon.Part
 2471 II: Cross-Equatorial Flow and PV Behavior. *Journal of the Atmospheric Sciences*,
 2472 *52*(9), 1341–1356. Retrieved 2019-07-05, from [http://journals.ametsoc.org/doi/](http://journals.ametsoc.org/doi/abs/10.1175/1520-0469%281995%29052%3C1341%3AAMOTAS%3E2.0.CO%3B2)
 2473 [abs/10.1175/1520-0469%281995%29052%3C1341%3AAMOTAS%3E2.0.CO%3B2](http://journals.ametsoc.org/doi/abs/10.1175/1520-0469%281995%29052%3C1341%3AAMOTAS%3E2.0.CO%3B2) doi: 10
 2474 .1175/1520-0469(1995)052(1341:AMOTAS)2.0.CO;2
- 2475 Rodwell, M. J., & Hoskins, B. J. (1996, July). Monsoons and the dynamics of deserts.
 2476 *Quarterly Journal of the Royal Meteorological Society*, *122*(534), 1385–1404. Retrieved
 2477 2019-07-03, from <http://doi.wiley.com/10.1002/qj.49712253408> doi: 10.1002/
 2478 [qj.49712253408](http://doi.wiley.com/10.1002/qj.49712253408)
- 2479 Roe, G. H., Ding, Q., Battisti, D. S., Molnar, P., Clark, M. K., & Garzione, C. N. (2016,
 2480 May). A modeling study of the response of Asian summertime climate to the largest
 2481 geologic forcings of the past 50 Ma: geological controls on Asian climate. *Journal of*
 2482 *Geophysical Research: Atmospheres*, *121*(10), 5453–5470. Retrieved 2018-01-11, from
 2483 <http://doi.wiley.com/10.1002/2015JD024370> doi: 10.1002/2015JD024370
- 2484 Rowley, D. B., & Currie, B. S. (2006, February). Palaeo-altimetry of the late Eocene
 2485 to Miocene Lunpola basin, central Tibet. *Nature*, *439*(7077), 677–681. Retrieved
 2486 2020-10-17, from <https://www.nature.com/articles/nature04506> (Number: 7077
 2487 Publisher: Nature Publishing Group) doi: 10.1038/nature04506
- 2488 Rögl, F. (1997). Palaeogeographic Considerations for Mediterranean and Paratethys Sea-
 2489 ways (Oligocene to Miocene). *Annalen des Naturhistorischen Museums in Wien. Se-
 2490 rie A für Mineralogie und Petrographie, Geologie und Paläontologie, Anthropologie*
 2491 *und Prähistorie*, *99*, 279–310. Retrieved 2021-03-09, from [http://www.jstor.org/](http://www.jstor.org/stable/41702129)
 2492 [stable/41702129](http://www.jstor.org/stable/41702129) (Publisher: Naturhistorisches Museum)
- 2493 Rögl, F. (1999). MEDITERRANEAN AND PARATETHYS. FACTS AND HY-
 2494 POTHESSES OF AN OLIGOCENE TO MIOCENE PALEO GEOGRAPHY (SHORT
 2495 OVERVIEW). *Geologica carpathica*, *50*(4), 339–349.
- 2496 Sampe, T., & Xie, S.-P. (2010, January). Large-Scale Dynamics of the Meiyu-Baiu Rain-
 2497 band: Environmental Forcing by the Westerly Jet*. *Journal of Climate*, *23*(1), 113–
 2498 134. Retrieved 2020-07-25, from [https://journals.ametsoc.org/jcli/article/](https://journals.ametsoc.org/jcli/article/23/1/113/32279/LargeScale-Dynamics-of-the-MeiyuBaiu-Rainband)
 2499 [23/1/113/32279/LargeScale-Dynamics-of-the-MeiyuBaiu-Rainband](https://journals.ametsoc.org/jcli/article/23/1/113/32279/LargeScale-Dynamics-of-the-MeiyuBaiu-Rainband) doi: 10
 2500 .1175/2009JCLI3128.1
- 2501 Sanyal, P., Bhattacharya, S., Kumar, R., Ghosh, S., & Sangode, S. (2004, March).
 2502 Mio–Pliocene monsoonal record from Himalayan foreland basin (Indian Siwalik) and
 2503 its relation to vegetational change. *Palaeogeography, Palaeoclimatology, Palaeoecology*,
 2504 *205*, 23–41. doi: 10.1016/j.palaeo.2003.11.013
- 2505 Sarr, A.-C., Donnadieu, Y., Bolton, C. T., Ladant, J.-B., Licht, A., Fluteau, F., ... Dupont-
 2506 Nivet, G. (2022, April). Neogene South Asian monsoon rainfall and wind histories
 2507 diverged due to topographic effects. *Nature Geoscience*, 1–6. Retrieved 2022-04-12,
 2508 from <http://www.nature.com/articles/s41561-022-00919-0> (Publisher: Nature
 2509 Publishing Group) doi: 10.1038/s41561-022-00919-0
- 2510 Sato, T. (2009, February). Influences of subtropical jet and Tibetan Plateau on precipitation
 2511 pattern in Asia: Insights from regional climate modeling. *Quaternary International*,

- 2512 194(1-2), 148–158. Retrieved 2022-02-21, from <https://linkinghub.elsevier.com/retrieve/pii/S1040618208002176> doi: 10.1016/j.quaint.2008.07.008
- 2513
- 2514 Saxena, R. K., & Trivedi, G. K. (2009). Palynological investigation of the Kopili Formation
2515 (Late Eocene) in North Cachar Hills, Assam, India. *Acta Palaeobotanica*, 49(2), 25.
- 2516 Scher, H. D., Whittaker, J. M., Williams, S. E., Latimer, J. C., Kordesch, W. E. C., &
2517 Delaney, M. L. (2015, July). Onset of Antarctic Circumpolar Current 30 million
2518 years ago as Tasmanian Gateway aligned with westerlies. *Nature*, 523(7562), 580–
2519 583. Retrieved 2022-12-09, from <http://www.nature.com/articles/nature14598>
2520 (Number: 7562 Publisher: Nature Publishing Group) doi: 10.1038/nature14598
- 2521 Schiemann, R., Lüthi, D., & Schär, C. (2009, June). Seasonality and Interannual Variability
2522 of the Westerly Jet in the Tibetan Plateau Region. *Journal of Climate*, 22(11), 2940–
2523 2957. Retrieved 2022-12-09, from <https://journals.ametsoc.org/view/journals/clim/22/11/2008jcli2625.1.xml> (Publisher: American Meteorological Society Sec-
2524 tion: Journal of Climate) doi: 10.1175/2008JCLI2625.1
- 2525
- 2526 Schott, F. A., & McCreary, J. P. (2001, January). The monsoon circulation of the Indian
2527 Ocean. *Progress in Oceanography*, 51(1), 1–123. Retrieved 2020-07-23, from <https://linkinghub.elsevier.com/retrieve/pii/S0079661101000830> doi: 10.1016/S0079-
2528 -6611(01)00083-0
- 2529
- 2530 Sembroni, A., Faccenna, C., Becker, T. W., Molin, P., & Abebe, B. (2016).
2531 Long-term, deep-mantle support of the Ethiopia-Yemen Plateau. *Tec-
2532 tonics*, 35(2), 469–488. Retrieved 2021-09-02, from [http://agupubs
2533 .onlinelibrary.wiley.com/doi/abs/10.1002/2015TC004000](http://agupubs.onlinelibrary.wiley.com/doi/abs/10.1002/2015TC004000) (_eprint:
2534 <https://onlinelibrary.wiley.com/doi/pdf/10.1002/2015TC004000>) doi: 10.1002/
2535 2015TC004000
- 2536 Sepulchre, P., Caubel, A., Ladant, J.-B., Bopp, L., Boucher, O., Braconnot, P., ... Tardif,
2537 D. (2020, July). IPSL-CM5A2 – an Earth system model designed for multi-millennial
2538 climate simulations. *Geoscientific Model Development*, 13(7), 3011–3053. Retrieved
2539 2020-11-27, from <https://gmd.copernicus.org/articles/13/3011/2020/> doi: 10
2540 .5194/gmd-13-3011-2020
- 2541 Sepulchre, P., Ramstein, G., Fluteau, F., Schuster, M., Tiercelin, J.-J., & Brunet, M. (2006,
2542 September). Tectonic Uplift and Eastern Africa Aridification. *Science*, 313(5792),
2543 1419–1423. Retrieved 2020-06-22, from [https://www.sciencemag.org/lookup/doi/
2544 10.1126/science.1129158](https://www.sciencemag.org/lookup/doi/10.1126/science.1129158) doi: 10.1126/science.1129158
- 2545 Sha, Y., Ren, X., Shi, Z., Zhou, P., Li, X., & Liu, X. (2020, April). Influence of the
2546 Tibetan Plateau and its northern margins on the mid-latitude Westerly Jet over
2547 Central Asia in summer. *Palaeogeography, Palaeoclimatology, Palaeoecology*, 544,
2548 109611. Retrieved 2022-06-27, from [https://linkinghub.elsevier.com/retrieve/
2549 pii/S0031018219306819](https://linkinghub.elsevier.com/retrieve/pii/S0031018219306819) doi: 10.1016/j.palaeo.2020.109611
- 2550 Sha, Y., Shi, Z., Liu, X., & An, Z. (2015). Distinct impacts of the Mongolian and Ti-
2551 betan Plateaus on the evolution of the East Asian monsoon. *Journal of Geophysical
2552 Research: Atmospheres*, 120(10), 4764–4782. Retrieved 2021-04-19, from [http://
2553 agupubs.onlinelibrary.wiley.com/doi/abs/10.1002/2014JD022880](http://agupubs.onlinelibrary.wiley.com/doi/abs/10.1002/2014JD022880) (_eprint:
2554 <https://onlinelibrary.wiley.com/doi/pdf/10.1002/2014JD022880>) doi: [https://doi
2555 .org/10.1002/2014JD022880](https://doi.org/10.1002/2014JD022880)
- 2556 Shen, X., Wan, S., France-Lanord, C., Clift, P. D., Tada, R., Révillon, S., ... Li, A. (2017,
2557 September). History of Asian eolian input to the Sea of Japan since 15 Ma: Links
2558 to Tibetan uplift or global cooling? *Earth and Planetary Science Letters*, 474, 296–
2559 308. Retrieved 2017-10-09, from [http://linkinghub.elsevier.com/retrieve/pii/
2560 S0012821X17303771](http://linkinghub.elsevier.com/retrieve/pii/S0012821X17303771) doi: 10.1016/j.epsl.2017.06.053
- 2561 Shi, Z., Liu, X., Liu, Y., Sha, Y., & Xu, T. (2015). Impact of Mongolian Plateau versus
2562 Tibetan Plateau on the westerly jet over North Pacific Ocean. *Climate Dynamics*,
2563 44(11-12), 3067–3076. (ISBN: 0930-7575 Publisher: Springer)
- 2564 Shukla, A., Mehrotra, R. C., Spicer, R. A., Spicer, T. E., & Kumar, M. (2014, Oc-
2565 tober). Cool equatorial terrestrial temperatures and the South Asian monsoon in
2566 the Early Eocene: Evidence from the Gurha Mine, Rajasthan, India. *Palaeo-*

- 2567 *geography, Palaeoclimatology, Palaeoecology*, 412, 187–198. Retrieved 2017-10-09,
 2568 from <http://linkinghub.elsevier.com/retrieve/pii/S003101821400399X> doi:
 2569 10.1016/j.palaeo.2014.08.004
- 2570 Smith, S. G., Wegmann, K. W., Ancuta, L. D., Gosse, J. C., & Hopkins, C. E. (2016,
 2571 August). Paleotopography and erosion rates in the central Hangay Dome, Mongo-
 2572 lia: Landscape evolution since the mid-Miocene. *Journal of Asian Earth Sciences*,
 2573 125, 37–57. Retrieved 2021-03-29, from [https://www.sciencedirect.com/science/
 2574 article/pii/S1367912016301274](https://www.sciencedirect.com/science/article/pii/S1367912016301274) doi: 10.1016/j.jseaes.2016.05.013
- 2575 Song, B., Spicer, R. A., Zhang, K., Ji, J., Farnsworth, A., Hughes, A. C., ... Shi, G.
 2576 (2020, May). Qaidam Basin leaf fossils show northeastern Tibet was high, wet and
 2577 cool in the early Oligocene. *Earth and Planetary Science Letters*, 537, 116175. Re-
 2578 trieved 2021-05-27, from [https://www.sciencedirect.com/science/article/pii/
 2579 S0012821X20301187](https://www.sciencedirect.com/science/article/pii/S0012821X20301187) doi: 10.1016/j.epsl.2020.116175
- 2580 Sorrel, P., Eymard, I., Leloup, P.-H., Maheo, G., Olivier, N., Sterb, M., ... Replumaz, A.
 2581 (2017, December). Wet tropical climate in SE Tibet during the Late Eocene. *Scien-
 2582 tific Reports*, 7(1). Retrieved 2018-04-03, from [http://www.nature.com/articles/
 2583 s41598-017-07766-9](http://www.nature.com/articles/s41598-017-07766-9) doi: 10.1038/s41598-017-07766-9
- 2584 Sosdian, S. M., & Lear, C. H. (2020). Initiation of the Western Pacific
 2585 Warm Pool at the Middle Miocene Climate Transition? *Paleoceanogra-
 2586 phy and Paleoclimatology*, 35(12), e2020PA003920. Retrieved 2021-09-20, from
 2587 <http://onlinelibrary.wiley.com/doi/abs/10.1029/2020PA003920> (eprint:
 2588 <https://onlinelibrary.wiley.com/doi/pdf/10.1029/2020PA003920>) doi: 10.1029/
 2589 2020PA003920
- 2590 Spicer, R., Su, T., Valdes, P. J., Farnsworth, A., Wu, F.-X., Shi, G., ... Zhou, Z. (2020,
 2591 May). Why ‘the uplift of the Tibetan Plateau’ is a myth? *National Science Review*,
 2592 19. Retrieved 2020-11-27, from [https://academic.oup.com/nsr/advance-article/
 2593 doi/10.1093/nsr/nwaa091/5829861](https://academic.oup.com/nsr/advance-article/doi/10.1093/nsr/nwaa091/5829861) doi: 10.1093/nsr/nwaa091
- 2594 Spicer, R., Yang, J., Herman, A., Kodrul, T., Aleksandrova, G., Maslova, N., ... Jin, J.-
 2595 H. (2017, September). Paleogene monsoons across India and South China: Drivers of
 2596 biotic change. *Gondwana Research*, 49, 350–363. Retrieved 2022-05-03, from [https://
 2597 linkinghub.elsevier.com/retrieve/pii/S1342937X16304385](https://linkinghub.elsevier.com/retrieve/pii/S1342937X16304385) doi: 10.1016/j.gr
 2598 .2017.06.006
- 2599 Spicer, R., Yang, J., Herman, A. B., Kodrul, T., Maslova, N., Spicer, T. E., ... Jin, J. (2016,
 2600 September). Asian Eocene monsoons as revealed by leaf architectural signatures.
 2601 *Earth and Planetary Science Letters*, 449, 61–68. Retrieved 2017-10-09, from [http://
 2602 linkinghub.elsevier.com/retrieve/pii/S0012821X16302618](http://linkinghub.elsevier.com/retrieve/pii/S0012821X16302618) doi: 10.1016/j.epsl
 2603 .2016.05.036
- 2604 Srivastava, G., Paudyal, K. N., Utescher, T., & Mehrotra, R. (2018, February). Miocene
 2605 vegetation shift and climate change: Evidence from the Siwalik of Nepal. *Global and
 2606 Planetary Change*, 161, 108–120. Retrieved 2022-05-30, from [https://linkinghub
 2607 .elsevier.com/retrieve/pii/S092181811730317X](https://linkinghub.elsevier.com/retrieve/pii/S092181811730317X) doi: 10.1016/j.gloplacha.2017
 2608 .12.001
- 2609 Srivastava, G., Spicer, R. A., Spicer, T. E., Yang, J., Kumar, M., Mehrotra, R., & Mehro-
 2610 tra, N. (2012, July). Megafloora and palaeoclimate of a Late Oligocene tropical
 2611 delta, Makum Coalfield, Assam: Evidence for the early development of the South
 2612 Asia Monsoon. *Palaeogeography, Palaeoclimatology, Palaeoecology*, 342-343, 130–
 2613 142. Retrieved 2018-06-22, from [http://linkinghub.elsevier.com/retrieve/pii/
 2614 S0031018212002532](http://linkinghub.elsevier.com/retrieve/pii/S0031018212002532) doi: 10.1016/j.palaeo.2012.05.002
- 2615 Straume, E. O., Gaina, C., Medvedev, S., & Nisancioglu, K. H. (2020, October). Global
 2616 Cenozoic Paleobathymetry with a focus on the Northern Hemisphere Oceanic Gate-
 2617 ways. *Gondwana Research*, 86, 126–143. Retrieved 2021-04-08, from [https://
 2618 www.sciencedirect.com/science/article/pii/S1342937X20301659](https://www.sciencedirect.com/science/article/pii/S1342937X20301659) doi: 10.1016/
 2619 j.gr.2020.05.011
- 2620 Su, H., & Zhou, J. (2020, June). Timing of Arabia-Eurasia collision: Constraints
 2621 from restoration of crustal-scale cross-sections. *Journal of Structural Geology*, 135,

104041. Retrieved 2022-03-04, from <https://www.sciencedirect.com/science/article/pii/S0191814119304456> doi: 10.1016/j.jsg.2020.104041
- 2622
2623
2624 Su, Q., Nie, J., Meng, Q., Heermance, R., Gong, L., Luo, Z., ... Garziona, C. (2019,
2625 September). Central Asian Drying at 3.3 Ma Linked to Tropical Forcing? *Geophysical*
2626 *Research Letters*, *46*. doi: 10.1029/2019GL084648
- 2627 Su, T., Farnsworth, A., Spicer, R., & Huang, J. (2019). No high Tibetan Plateau until the
2628 Neogene. *Science Advances*, *9*.
- 2629 Su, T., Spicer, R. A., Li, S.-H., Xu, H., Huang, J., Sherlock, S., ... Zhou, Z.-K. (2019, May).
2630 Uplift, climate and biotic changes at the Eocene–Oligocene transition in south-eastern
2631 Tibet. *National Science Review*, *6*(3), 495–504. Retrieved 2019-10-24, from [https://](https://academic.oup.com/nsr/article/6/3/495/5036537)
2632 academic.oup.com/nsr/article/6/3/495/5036537 doi: 10.1093/nsr/nwy062
- 2633 Su, T., Spicer, R. A., Wu, F.-X., Farnsworth, A., Huang, J., Del Rio, C., ... Zhou,
2634 Z.-K. (2020, December). A Middle Eocene lowland humid subtropical “Shangri-
2635 La” ecosystem in central Tibet. *Proceedings of the National Academy of Sciences*,
2636 *117*(52), 32989–32995. Retrieved 2021-02-01, from [http://www.pnas.org/lookup/](http://www.pnas.org/lookup/doi/10.1073/pnas.2012647117)
2637 [doi/10.1073/pnas.2012647117](http://www.pnas.org/lookup/doi/10.1073/pnas.2012647117) doi: 10.1073/pnas.2012647117
- 2638 Suarez, M. B., Passey, B. H., & Kaakinen, A. (2011, December). Paleosol carbonate
2639 multiple isotopologue signature of active East Asian summer monsoons during the
2640 late Miocene and Pliocene. *Geology*, *39*(12), 1151–1154. Retrieved 2022-06-09,
2641 from [http://pubs.geoscienceworld.org/geology/article/39/12/1151/130458/](http://pubs.geoscienceworld.org/geology/article/39/12/1151/130458/Paleosol-carbonate-multiple-isotopologue-signature)
2642 [Paleosol-carbonate-multiple-isotopologue-signature](http://pubs.geoscienceworld.org/geology/article/39/12/1151/130458/Paleosol-carbonate-multiple-isotopologue-signature) doi: 10.1130/G32350.1
- 2643 Sun, J., Liu, W., Guo, Z., Qi, L., & Zhang, Z. (2022, April). Enhanced aridifi-
2644 cation across the Eocene/Oligocene transition evidenced by geochemical record in
2645 the Tajik Basin, Central Asia. *Global and Planetary Change*, *211*, 103789. Re-
2646 trieved 2022-03-22, from [https://www.sciencedirect.com/science/article/pii/](https://www.sciencedirect.com/science/article/pii/S092181812200056X)
2647 [S092181812200056X](https://www.sciencedirect.com/science/article/pii/S092181812200056X) doi: 10.1016/j.gloplacha.2022.103789
- 2648 Sun, J., Sheykh, M., Ahmadi, N., Cao, M., Zhang, Z., Tian, S., ... Talebian, M.
2649 (2021, February). Permanent closure of the Tethyan Seaway in the northwest-
2650 ern Iranian Plateau driven by cyclic sea-level fluctuations in the late Middle
2651 Miocene. *Palaeogeography, Palaeoclimatology, Palaeoecology*, *564*, 110172. Re-
2652 trieved 2021-05-03, from [https://www.sciencedirect.com/science/article/pii/](https://www.sciencedirect.com/science/article/pii/S0031018220306209)
2653 [S0031018220306209](https://www.sciencedirect.com/science/article/pii/S0031018220306209) doi: 10.1016/j.palaeo.2020.110172
- 2654 Sun, J., & Windley, B. (2015, October). Onset of aridification by 34 Ma across the Eocene-
2655 Oligocene transition in Central Asia. *Geology*, *43*, G37165.1. doi: 10.1130/G37165.1
- 2656 Sun, J., Ye, J., Wu, W., Ni, X., Bi, S., Zhang, Z., ... Meng, J. (2010, June). Late
2657 Oligocene–Miocene mid-latitude aridification and wind patterns in the Asian interior.
2658 *Geology*, *38*(6), 515–518. Retrieved 2022-04-06, from [https://doi.org/10.1130/](https://doi.org/10.1130/G30776.1)
2659 [G30776.1](https://doi.org/10.1130/G30776.1) doi: 10.1130/G30776.1
- 2660 Sun, J., Zhang, L., Deng, C., & Zhu, R. (2008, May). Evidence for enhanced aridity in
2661 the Tarim Basin of China since 5.3Ma. *Quaternary Science Reviews*, *27*(9-10), 1012–
2662 1023. Retrieved 2022-06-16, from [https://linkinghub.elsevier.com/retrieve/](https://linkinghub.elsevier.com/retrieve/pii/S0277379108000310)
2663 [pii/S0277379108000310](https://linkinghub.elsevier.com/retrieve/pii/S0277379108000310) doi: 10.1016/j.quascirev.2008.01.011
- 2664 Sun, J., & Zhang, Z. (2008, November). Palynological evidence for the Mid-Miocene Cli-
2665 matic Optimum recorded in Cenozoic sediments of the Tian Shan Range, northwest-
2666 ern China. *Global and Planetary Change*, *64*(1-2), 53–68. Retrieved 2022-05-04,
2667 from [https://linkinghub.elsevier.com/retrieve/pii/](https://linkinghub.elsevier.com/retrieve/pii/S0921818108001045)
2668 [S0921818108001045](https://linkinghub.elsevier.com/retrieve/pii/S0921818108001045) doi:
10.1016/j.gloplacha.2008.09.001
- 2669 Sun, J., Zhang, Z., Cao, M., Windley, B. F., Tian, S., Sha, J., ... Oimahmadov, I.
2670 (2020, May). Timing of seawater retreat from proto-Paratethys, sedimentary proven-
2671 nance, and tectonic rotations in the late Eocene-early Oligocene in the Tajik Basin,
2672 Central Asia. *Palaeogeography, Palaeoclimatology, Palaeoecology*, *545*, 109657. Re-
2673 trieved 2020-11-02, from [http://www.sciencedirect.com/science/article/pii/](http://www.sciencedirect.com/science/article/pii/S0031018220301024)
2674 [S0031018220301024](http://www.sciencedirect.com/science/article/pii/S0031018220301024) doi: 10.1016/j.palaeo.2020.109657
- 2675 Sun, Q.-g., Collinson, M. E., Li, C.-S., Wang, Y.-f., & Beerling, D. J. (2002). Quantitative
2676 reconstruction of palaeoclimate from the Middle Miocene Shanwang flora, eastern

- 2677 China. *Palaeogeography, Palaeoclimatology, Palaeoecology*, 15. doi: 10.1016/S0031
2678 -0182(01)00433-3
- 2679 Sun, X., & Wang, P. (2005, July). How old is the Asian monsoon system?—Palaeobotanical
2680 records from China. *Palaeogeography, Palaeoclimatology, Palaeoecology*, 222(3-4),
2681 181–222. Retrieved 2017-10-09, from [http://linkinghub.elsevier.com/retrieve/
2682 pii/S0031018205001203](http://linkinghub.elsevier.com/retrieve/pii/S0031018205001203) doi: 10.1016/j.palaeo.2005.03.005
- 2683 Sun, Y., Liu, J., Liang, Y., Ji, J., Liu, W., Aitchison, J. C., ... Liu, Z. (2020, September).
2684 Cenozoic moisture fluctuations on the northeastern Tibetan Plateau and association
2685 with global climatic conditions. *Journal of Asian Earth Sciences*, 200, 104490. Re-
2686 trieved 2022-05-12, from [https://www.sciencedirect.com/science/article/pii/
2687 S1367912020302832](https://www.sciencedirect.com/science/article/pii/S1367912020302832) doi: 10.1016/j.jseaes.2020.104490
- 2688 Tada, R., Zheng, H., & Clift, P. D. (2016, December). Evolution and variability of the Asian
2689 monsoon and its potential linkage with uplift of the Himalaya and Tibetan Plateau.
2690 *Progress in Earth and Planetary Science*, 3(1). Retrieved 2017-10-09, from [http://
2691 www.progearthplanetsci.com/content/3/1/4](http://www.progearthplanetsci.com/content/3/1/4) doi: 10.1186/s40645-016-0080-y
- 2692 Tan, N., Zhang, Z. S., Guo, Z. T., Guo, C. C., Zhang, Z. J., He, Z. L., & Ramstein, G. (2022).
2693 Recognizing the Role of Tropical Seaways in Modulating the Pacific Circulation.
2694 *Geophysical Research Letters*, 49(19), e2022GL099674. Retrieved 2022-10-04, from
2695 <http://onlinelibrary.wiley.com/doi/abs/10.1029/2022GL099674> (_eprint:
2696 <https://agupubs.onlinelibrary.wiley.com/doi/pdf/10.1029/2022GL099674>) doi: 10
2697 .1029/2022GL099674
- 2698 Tang, H., Li, S.-F., Su, T., Spicer, R. A., Zhang, S.-T., Li, S.-H., ... Zhou, Z.-K. (2020,
2699 December). Early Oligocene vegetation and climate of southwestern China inferred
2700 from palynology. *Palaeogeography, Palaeoclimatology, Palaeoecology*, 560, 109988. Re-
2701 trieved 2022-03-11, from [https://www.sciencedirect.com/science/article/pii/
2702 S0031018220304338](https://www.sciencedirect.com/science/article/pii/S0031018220304338) doi: 10.1016/j.palaeo.2020.109988
- 2703 Tang, H., Micheels, A., Eronen, J. T., Ahrens, B., & Fortelius, M. (2013, March). Asyn-
2704 chronous responses of East Asian and Indian summer monsoons to mountain uplift
2705 shown by regional climate modelling experiments. *Climate Dynamics*, 40(5), 1531–
2706 1549. Retrieved 2021-03-10, from <https://doi.org/10.1007/s00382-012-1603-x>
2707 doi: 10.1007/s00382-012-1603-x
- 2708 Tang, Z.-H., & Ding, Z.-L. (2013, December). A palynological insight into the Miocene arid-
2709 ification in the Eurasian interior. *Palaeoworld*, 22(3-4), 77–85. Retrieved 2022-06-23,
2710 from <https://linkinghub.elsevier.com/retrieve/pii/S1871174X13000073> doi:
2711 10.1016/j.palwor.2013.05.001
- 2712 Tardif, D., Fluteau, F., Donnadiou, Y., Le Hir, G., Ladant, J.-B., Sepulchre, P., ... Dupont-
2713 Nivet, G. (2020, May). The origin of Asian monsoons: a modelling perspective.
2714 *Climate of the Past*, 16(3), 847–865. Retrieved 2020-05-08, from [https://www.clim-
2715 -past.net/16/847/2020/](https://www.clim-past.net/16/847/2020/) doi: 10.5194/cp-16-847-2020
- 2716 Tardif, D., Toumoulin, A., Fluteau, F., Donnadiou, Y., Le Hir, G., Barbolini, N., ...
2717 Dupont-Nivet, G. (2021, October). Orbital variations as a major driver of climate
2718 and biome distribution during the greenhouse to icehouse transition. *Science Ad-
2719 vances*, 7(43), eabh2819. Retrieved 2021-10-25, from [https://www.science.org/
2720 doi/10.1126/sciadv.abh2819](https://www.science.org/doi/10.1126/sciadv.abh2819) doi: 10.1126/sciadv.abh2819
- 2721 Tauxe, L., & Feakins, S. J. (2020). A Reassessment of the Chronostratig-
2722 raphy of Late Miocene C3–C4 Transitions. *Paleoceanography and Paleo-
2723 climatology*, 35(7), e2020PA003857. Retrieved 2022-06-07, from [http://
2724 onlinelibrary.wiley.com/doi/abs/10.1029/2020PA003857](http://onlinelibrary.wiley.com/doi/abs/10.1029/2020PA003857) (_eprint:
2725 <https://agupubs.onlinelibrary.wiley.com/doi/pdf/10.1029/2020PA003857>) doi:
2726 10.1029/2020PA003857
- 2727 Thomson, J. R., Holden, P. B., Anand, P., Edwards, N. R., Porchier, C. A., & Harris,
2728 N. B. W. (2021, June). Tectonic and climatic drivers of Asian monsoon evolu-
2729 tion. *Nature Communications*, 12(1), 4022. Retrieved 2021-10-05, from [http://www
2730 .nature.com/articles/s41467-021-24244-z](http://www.nature.com/articles/s41467-021-24244-z) (Bandiera_abtest: a Cc_license_type:
2731 cc_by Cg_type: Nature Research Journals Number: 1 Primary_atype: Research Pub-

- 2732 lisher: Nature Publishing Group Subject_term: Climate change;Palaeoclimate Sub-
2733 ject_term_id: climate-change;palaeoclimate) doi: 10.1038/s41467-021-24244-z
- 2734 Torsvik, T. H., Müller, R. D., Van der Voo, R., Steinberger, B., & Gaina,
2735 C. (2008). Global plate motion frames: Toward a unified model.
2736 *Reviews of Geophysics*, 46(3). Retrieved 2022-10-24, from [http://](http://onlinelibrary.wiley.com/doi/abs/10.1029/2007RG000227)
2737 onlinelibrary.wiley.com/doi/abs/10.1029/2007RG000227 (eprint:
2738 <https://agupubs.onlinelibrary.wiley.com/doi/pdf/10.1029/2007RG000227>) doi:
2739 10.1029/2007RG000227
- 2740 Toumoulin, A., Donnadiou, Y., Ladant, J., Batenburg, S. J., Poblete, F., & Dupont-Nivet,
2741 G. (2020, August). Quantifying the Effect of the Drake Passage Opening on the
2742 Eocene Ocean. *Paleoceanography and Paleoclimatology*, 35(8). Retrieved 2020-08-13,
2743 from <https://onlinelibrary.wiley.com/doi/abs/10.1029/2020PA003889> doi: 10
2744 .1029/2020PA003889
- 2745 Toumoulin, A., Tardif, D., Donnadiou, Y., Licht, A., Ladant, J.-B., Kunzmann, L., &
2746 Dupont-Nivet, G. (2022, February). Evolution of continental temperature season-
2747 ality from the Eocene greenhouse to the Oligocene icehouse –a model–data compar-
2748 ison. *Climate of the Past*, 18(2), 341–362. Retrieved 2022-02-28, from [https://](https://cp.copernicus.org/articles/18/341/2022/)
2749 cp.copernicus.org/articles/18/341/2022/ (Publisher: Copernicus GmbH) doi:
2750 10.5194/cp-18-341-2022
- 2751 Tripathi, S., Tiwari, M., Lee, J., & Khim, B.-K. (2017, February). First evidence of
2752 denitrification vis-à-vis monsoon in the Arabian Sea since Late Miocene. *Scien-*
2753 *tific Reports*, 7(1), 43056. Retrieved 2022-06-02, from [http://www.nature.com/](http://www.nature.com/articles/srep43056)
2754 [articles/srep43056](http://www.nature.com/articles/srep43056) (Number: 1 Publisher: Nature Publishing Group) doi:
2755 10.1038/srep43056
- 2756 Valcke, S., Budich, R., Carter, M., Guilyardi, E., Lautenschlager, M., Redler, R., &
2757 Steenman-Clark, L. (2006). The PRISM software framework and the OASIS cou-
2758 pler. *Annual BMRC Modelling Workshop 'The Australian Community Climate and*
2759 *Earth System Simulator (ACCESS)-challenges and opportunities'*, 10.
- 2760 van Hinsbergen, D. J. J., Lippert, P. C., Dupont-Nivet, G., McQuarrie, N., Doubrovine,
2761 P. V., Spakman, W., & Torsvik, T. H. (2012, May). Greater India Basin hypothesis
2762 and a two-stage Cenozoic collision between India and Asia. *Proceedings of the National*
2763 *Academy of Sciences*, 109(20), 7659–7664. Retrieved from [http://www.pnas.org/](http://www.pnas.org/content/109/20/7659.abstract)
2764 [content/109/20/7659.abstract](http://www.pnas.org/content/109/20/7659.abstract) doi: 10.1073/pnas.1117262109
- 2765 van Hinsbergen, D. J. J., Lippert, P. C., Li, S., Huang, W., Advokaat, E. L., & Spakman,
2766 W. (2019, June). Reconstructing Greater India: Paleogeographic, kinematic, and
2767 geodynamic perspectives. *Tectonophysics*, 760, 69–94. Retrieved 2020-10-15, from
2768 <https://linkinghub.elsevier.com/retrieve/pii/S0040195118301331> doi: 10
2769 .1016/j.tecto.2018.04.006
- 2770 Vassallo, R., Jolivet, M., Ritz, J. F., Braucher, R., Larroque, C., Sue, C., ... Javkhlanbold,
2771 D. (2007, July). Uplift age and rates of the Gurvan Bogd system (Gobi-Altay) by ap-
2772 atite fission track analysis. *Earth and Planetary Science Letters*, 259(3), 333–346. Re-
2773 trieved 2021-04-20, from [https://www.sciencedirect.com/science/article/pii/](https://www.sciencedirect.com/science/article/pii/S0012821X07002853)
2774 [S0012821X07002853](https://www.sciencedirect.com/science/article/pii/S0012821X07002853) doi: 10.1016/j.epsl.2007.04.047
- 2775 Vicente de Gouveia, S., Besse, J., Frizon de Lamotte, D., Greff-Lefftz, M., Lescanne, M.,
2776 Gueydan, F., & Leparmentier, F. (2018, April). Evidence of hotspot paths below
2777 Arabia and the Horn of Africa and consequences on the Red Sea opening. *Earth*
2778 *and Planetary Science Letters*, 487, 210–220. Retrieved 2021-10-13, from [https://](https://www.sciencedirect.com/science/article/pii/S0012821X18300487)
2779 www.sciencedirect.com/science/article/pii/S0012821X18300487 doi: 10.1016/
2780 j.epsl.2018.01.030
- 2781 Vornlocher, J., Lukens, W., Schubert, B., & Quan, C. (2021, April). Late Oligocene
2782 Precipitation Seasonality in East Asia Based on $\delta^{13}C$ Profiles in Fossil Wood. *Paleo-*
2783 *ceanography and Paleoclimatology*, 36. doi: 10.1029/2021PA004229
- 2784 Vögeli, N., Najman, Y., van der Beek, P., Huyghe, P., Wynn, P. M., Govin, G., ... Sachse,
2785 D. (2017, August). Lateral variations in vegetation in the Himalaya since the Miocene
2786 and implications for climate evolution. *Earth and Planetary Science Letters*, 471, 1–

- 2787 9. Retrieved 2022-05-02, from <https://www.sciencedirect.com/science/article/pii/S0012821X17302315> doi: 10.1016/j.epsl.2017.04.037
- 2788
- 2789 Wan, S., Li, A., Cliff, P. D., & Stuu, J.-B. W. (2007, October). Development of the East
2790 Asian monsoon: Mineralogical and sedimentologic records in the northern South China
2791 Sea since 20 Ma. *Palaeogeography, Palaeoclimatology, Palaeoecology*, *254*(3-4), 561–
2792 582. Retrieved 2022-05-03, from <https://linkinghub.elsevier.com/retrieve/pii/S0031018207003963> doi: 10.1016/j.palaeo.2007.07.009
- 2793
- 2794 Wang, B., & Ding, Q. (2008, March). Global monsoon: Dominant mode of annual
2795 variation in the tropics. *Dynamics of Atmospheres and Oceans*, *44*(3-4), 165–
2796 183. Retrieved 2019-05-16, from <https://linkinghub.elsevier.com/retrieve/pii/S0377026508000055> doi: 10.1016/j.dynatmoce.2007.05.002
- 2797
- 2798 Wang, B., Shi, G., Xu, C., Spicer, R. A., Perrichot, V., Schmidt, A. R., ... Engel, M. S.
2799 (2021). The mid-Miocene Zhangpu biota reveals an outstandingly rich rainforest
2800 biome in East Asia. *Science Advances*, *7*(18), eabg0625. Retrieved 2022-05-03,
2801 from <https://www.science.org/doi/full/10.1126/sciadv.abg0625> (Publisher:
2802 American Association for the Advancement of Science) doi: 10.1126/sciadv.abg0625
- 2803
- 2804 Wang, C., Dai, J., Zhao, X., Li, Y., Graham, S. A., He, D., ... Meng, J. (2014, May).
2805 Outward-growth of the Tibetan Plateau during the Cenozoic: A review. *Tectono-*
2806 *physics*, *621*, 1–43. Retrieved 2017-10-09, from <http://linkinghub.elsevier.com/retrieve/pii/S0040195114000729> doi: 10.1016/j.tecto.2014.01.036
- 2807
- 2808 Wang, D., Lu, S., Han, S., Sun, X., & Quan, C. (2013, January). Eocene prevalence of
2809 monsoon-like climate over eastern China reflected by hydrological dynamics. *Journal of*
2810 *Asian Earth Sciences*, *62*, 776–787. Retrieved 2022-05-04, from <https://linkinghub.elsevier.com/retrieve/pii/S1367912012005184> doi: 10.1016/j.jseaes.2012.11
2811 .032
- 2812
- 2813 Wang, H., Lu, H., Zhao, L., Zhang, H., Lei, F., & Wang, Y. (2019, November).
2814 Asian monsoon rainfall variation during the Pliocene forced by global tempera-
2815 ture change. *Nature Communications*, *10*(1), 5272. Retrieved 2022-06-09, from
2816 <https://www.nature.com/articles/s41467-019-13338-4> (Number: 1 Publisher:
2817 Nature Publishing Group) doi: 10.1038/s41467-019-13338-4
- 2818
- 2819 Wang, L., & Chen, W. (2014, March). An Intensity Index for the East Asian
2820 Winter Monsoon. *Journal of Climate*, *27*(6), 2361–2374. Retrieved 2021-10-
2821 13, from <https://journals.ametsoc.org/view/journals/clim/27/6/jcli-d-13-00086.1.xml> (Publisher: American Meteorological Society Section: Journal of
2822 Climate) doi: 10.1175/JCLI-D-13-00086.1
- 2823
- 2824 Wang, L., Kunzmann, L., Su, T., Xing, Y.-W., Zhang, S.-T., Wang, Y.-Q., & Zhou, Z.-
2825 K. (2019, May). The disappearance of *Metasequoia* (Cupressaceae) after the middle
2826 Miocene in Yunnan, Southwest China: Evidences for evolutionary stasis and inten-
2827 sification of the Asian monsoon. *Review of Palaeobotany and Palynology*, *264*, 64–
2828 74. Retrieved 2023-04-14, from <https://linkinghub.elsevier.com/retrieve/pii/S0034666718301246> doi: 10.1016/j.revpalbo.2018.12.007
- 2829
- 2830 Wang, P., Clemens, S., Beaufort, L., Braconnot, P., Ganssen, G., Jian, Z., ... Sarn-
2831 thein, M. (2005, March). Evolution and variability of the Asian monsoon system:
2832 state of the art and outstanding issues. *Quaternary Science Reviews*, *24*(5-6), 595–
2833 629. Retrieved 2020-10-11, from <https://linkinghub.elsevier.com/retrieve/pii/S0277379104002975> doi: 10.1016/j.quascirev.2004.10.002
- 2834
- 2835 Wang, Q., Li, Y., Ferguson, D. K., Mo, W.-B., & Yang, N. (2021, July). An equable
2836 subtropical climate throughout China in the Miocene based on palaeofloral evi-
2837 dence. *Earth-Science Reviews*, *218*, 103649. Retrieved 2022-05-03, from <https://www.sciencedirect.com/science/article/pii/S0012825221001501> doi: 10.1016/j.earscirev.2021.103649
- 2838
- 2839 Wang, X., Carrapa, B., Sun, Y., Dettman, D. L., Chapman, J. B., Caves Rügenstein,
2840 J. K., ... Chen, F. (2020, July). The role of the westerlies and orography in
2841 Asian hydroclimate since the late Oligocene. *Geology*, *48*(7), 728–732. Retrieved
2020-10-11, from <https://pubs.geoscienceworld.org/gsa/geology/article/48/>

- 2842 7/728/584578/The-role-of-the-westerlies-and-orography-in-Asian doi: 10
 2843 .1130/G47400.1
- 2844 Wang, X., Qiu, Z., Li, Q., Wang, B., Qiu, Z., Downs, W. R., ... Meng, Q. (2007, October).
 2845 Vertebrate paleontology, biostratigraphy, geochronology, and paleoenvironment
 2846 of Qaidam Basin in northern Tibetan Plateau. *Palaeogeography, Palaeoclimatology,*
 2847 *Palaeoecology*, 254(3-4), 363–385. Retrieved 2023-01-03, from [https://linkinghub](https://linkinghub.elsevier.com/retrieve/pii/S0031018207003057)
 2848 [.elsevier.com/retrieve/pii/S0031018207003057](https://linkinghub.elsevier.com/retrieve/pii/S0031018207003057) doi: 10.1016/j.palaeo.2007.06
 2849 .007
- 2850 Wang, Y., & Deng, T. (2005, July). A 25 m.y. isotopic record of paleodiet and environmental
 2851 change from fossil mammals and paleosols from the NE margin of the Tibetan Plateau.
 2852 *Earth and Planetary Science Letters*, 236(1-2), 322–338. Retrieved 2022-06-16, from
 2853 <https://linkinghub.elsevier.com/retrieve/pii/S0012821X0500316X> doi: 10
 2854 .1016/j.epsl.2005.05.006
- 2855 Wasiljeff, J., Salminen, J. M., Stenman, J., Zhang, Z., & Kaakinen, A. (2022, April).
 2856 Oligocene moisture variations as evidenced by an aeolian dust sequence in Inner Mon-
 2857 golia, China. *Scientific Reports*, 12. doi: 10.1038/s41598-022-09362-y
- 2858 Webb, A. A. G., Guo, H., Clift, P. D., Husson, L., Müller, T., Costantino, D., ... Wang,
 2859 Q. (2017, April). The Himalaya in 3D: Slab dynamics controlled mountain building
 2860 and monsoon intensification. *Lithosphere*, 9(4), 637–651. Retrieved 2022-06-07, from
 2861 <https://doi.org/10.1130/L636.1> doi: 10.1130/L636.1
- 2862 Webster, P. J., Magaña, V. O., Palmer, T. N., Shukla, J., Tomas, R. A., Yanai, M., &
 2863 Yasunari, T. (1998, June). Monsoons: Processes, predictability, and the prospects
 2864 for prediction. *Journal of Geophysical Research: Oceans*, 103(C7), 14451–14510. Re-
 2865 trieved 2020-06-19, from <http://doi.wiley.com/10.1029/97JC02719> doi: 10.1029/
 2866 97JC02719
- 2867 Webster, P. J., & Yang, S. (1992, July). Monsoon and Enso: Selectively Interactive Systems.
 2868 *Quarterly Journal of the Royal Meteorological Society*, 118(507), 877–926. Retrieved
 2869 2019-07-05, from <http://doi.wiley.com/10.1002/qj.49711850705> doi: 10.1002/
 2870 qj.49711850705
- 2871 Wei, G., Li, X.-H., Liu, Y., Shao, L., & Liang, X. (2006). Geochemical
 2872 record of chemical weathering and monsoon climate change since the early
 2873 Miocene in the South China Sea. *Paleoceanography*, 21(4). Retrieved 2022-
 2874 05-03, from <https://onlinelibrary.wiley.com/doi/abs/10.1029/2006PA001300>
 2875 (_eprint: <https://onlinelibrary.wiley.com/doi/pdf/10.1029/2006PA001300>) doi: 10
 2876 .1029/2006PA001300
- 2877 Wei, H.-H., & Bordoni, S. (2016, August). On the Role of the African Topography in
 2878 the South Asian Monsoon. *Journal of the Atmospheric Sciences*, 73(8), 3197–3212.
 2879 Retrieved 2019-11-15, from [http://journals.ametsoc.org/doi/10.1175/JAS-D-15-](http://journals.ametsoc.org/doi/10.1175/JAS-D-15-0182.1)
 2880 [-0182.1](http://journals.ametsoc.org/doi/10.1175/JAS-D-15-0182.1) doi: 10.1175/JAS-D-15-0182.1
- 2881 Wei, J., Wang, Y., Wang, G., Wei, Z., Wei, H., Zhang, T., ... Li, L. (2022, April).
 2882 Biomarker Records From Eocene Lacustrine Sequence in the Eastern Tibet Plateau
 2883 and Its Implication for Organic Matter Sources. *Frontiers in Earth Science*, 10,
 2884 849041. doi: 10.3389/feart.2022.849041
- 2885 Westerhold, T., Marwan, N., Drury, A. J., Liebrand, D., Agnini, C., Anagnostou, E.,
 2886 ... Zachos, J. C. (2020, September). An astronomically dated record of Earth's
 2887 climate and its predictability over the last 66 million years. *Science*, 369(6509),
 2888 1383–1387. Retrieved 2020-09-12, from [https://www.sciencemag.org/lookup/doi/](https://www.sciencemag.org/lookup/doi/10.1126/science.aba6853)
 2889 [10.1126/science.aba6853](https://www.sciencemag.org/lookup/doi/10.1126/science.aba6853) doi: 10.1126/science.aba6853
- 2890 Westerweel, J., Licht, A., Cogné, N., Roperch, P., Dupont-Nivet, G., Thi, M. K., ...
 2891 Aung, D. W. (2020). Burma Terrane Collision and Northward Indentation in
 2892 the Eastern Himalayas Recorded in the Eocene-Miocene Chindwin Basin (Myan-
 2893 mar). *Tectonics*, 39(10), e2020TC006413. Retrieved 2021-03-29, from [http://](http://agupubs.onlinelibrary.wiley.com/doi/abs/10.1029/2020TC006413)
 2894 agupubs.onlinelibrary.wiley.com/doi/abs/10.1029/2020TC006413 (_eprint:
 2895 <https://onlinelibrary.wiley.com/doi/pdf/10.1029/2020TC006413>) doi: [https://doi](https://doi.org/10.1029/2020TC006413)
 2896 [.org/10.1029/2020TC006413](https://doi.org/10.1029/2020TC006413)

- 2897 Westerweel, J., Roperch, P., Licht, A., Dupont-Nivet, G., Win, Z., Poblete, F., ... Aung,
2898 D. W. (2019, October). Burma Terrane part of the Trans-Tethyan arc during collision
2899 with India according to palaeomagnetic data. *Nature Geoscience*, *12*(10), 863–868.
2900 Retrieved 2019-10-17, from <http://www.nature.com/articles/s41561-019-0443-2>
2901 doi: 10.1038/s41561-019-0443-2
- 2902 White, R. H., Battisti, D. S., & Roe, G. H. (2017). Mongolian Mountains Matter Most:
2903 Impacts of the Latitude and Height of Asian Orography on Pacific Wintertime Atmo-
2904 spheric Circulation. *JOURNAL OF CLIMATE*, *30*, 18.
- 2905 Wichura, H., Jacobs, L. L., Lin, A., Polcyn, M. J., Manthi, F. K., Winkler, D. A., ...
2906 Clemens, M. (2015, March). A 17-My-old whale constrains onset of uplift and
2907 climate change in east Africa. *Proceedings of the National Academy of Sciences*,
2908 *112*(13), 3910–3915. Retrieved 2021-04-07, from [http://www.pnas.org/content/](http://www.pnas.org/content/112/13/3910)
2909 [112/13/3910](http://www.pnas.org/content/112/13/3910) (Publisher: National Academy of Sciences Section: Physical Sciences)
2910 doi: 10.1073/pnas.1421502112
- 2911 Wolfe, J. (1993). A method of obtaining climatic parameters from leaf assemblages. *US*
2912 *Government Printing Office*.(2040-2041).
- 2913 Wu, F., Fang, X., Yang, Y., Dupont-Nivet, G., Nie, J., Fluteau, F., ... Han, W. (2022,
2914 October). Reorganization of Asian climate in relation to Tibetan Plateau uplift. *Nature*
2915 *Reviews Earth & Environment*, *3*(10), 684–700. Retrieved 2022-10-24, from [http://](http://www.nature.com/articles/s43017-022-00331-7)
2916 www.nature.com/articles/s43017-022-00331-7 (Number: 10 Publisher: Nature
2917 Publishing Group) doi: 10.1038/s43017-022-00331-7
- 2918 Wu, G., Liu, Y., He, B., Bao, Q., Duan, A., & Jin, F.-F. (2012, May). Thermal Controls
2919 on the Asian Summer Monsoon. *Scientific Reports*, *2*(1), 404. Retrieved 2023-03-31,
2920 from <https://www.nature.com/articles/srep00404> doi: 10.1038/srep00404
- 2921 Wu, M., Zhuang, G., Hou, M., & Liu, Z. (2021, July). Expanded lacustrine sedimentation
2922 in the Qaidam Basin on the northern Tibetan Plateau: Manifestation of climatic
2923 wetting during the Oligocene icehouse. *Earth and Planetary Science Letters*, *565*,
2924 116935. Retrieved 2022-05-04, from [https://linkinghub.elsevier.com/retrieve/](https://linkinghub.elsevier.com/retrieve/pii/S0012821X21001941)
2925 [pii/S0012821X21001941](https://linkinghub.elsevier.com/retrieve/pii/S0012821X21001941) doi: 10.1016/j.epsl.2021.116935
- 2926 Xia, K., Su, T., Liu, Y.-S. C., Xing, Y.-W., Jacques, F. M., & Zhou, Z.-K. (2009,
2927 May). Quantitative climate reconstructions of the late Miocene Xiaolongtan megaflora
2928 from Yunnan, southwest China. *Palaeogeography, Palaeoclimatology, Palaeoecology*,
2929 *276*(1-4), 80–86. Retrieved 2022-03-22, from [https://linkinghub.elsevier.com/](https://linkinghub.elsevier.com/retrieve/pii/S0031018209000819)
2930 [retrieve/pii/S0031018209000819](https://linkinghub.elsevier.com/retrieve/pii/S0031018209000819) doi: 10.1016/j.palaeo.2009.02.024
- 2931 Xiao, G. Q., Abels, H. A., Yao, Z. Q., Dupont-Nivet, G., & Hilgen, F. J. (2010, July). Asian
2932 aridification linked to the first step of the Eocene-Oligocene climate Transition (EOT)
2933 in obliquity-dominated terrestrial records (Xining Basin, China). *Climate of the Past*,
2934 *6*(4), 501–513. Retrieved 2017-10-09, from <http://www.clim-past.net/6/501/2010/>
2935 doi: 10.5194/cp-6-501-2010
- 2936 Xie, S.-P., Xu, H., Saji, N. H., Wang, Y., & Liu, W. T. (2006, July). Role of Narrow
2937 Mountains in Large-Scale Organization of Asian Monsoon Convection*. *Journal of*
2938 *Climate*, *19*(14), 3420–3429. Retrieved 2022-07-08, from [http://journals.ametsoc](http://journals.ametsoc.org/doi/10.1175/JCLI3777.1)
2939 [.org/doi/10.1175/JCLI3777.1](http://journals.ametsoc.org/doi/10.1175/JCLI3777.1) doi: 10.1175/JCLI3777.1
- 2940 Xie, Y., Wu, F., Fang, X., Song, J., & Niu, Z. (2022, August). Late Eocene onset of the East
2941 Asian Monsoon in the Qingjiang Basin of Central Jiangxi Province (Southeast China)
2942 revealed by a major vegetation transition from desert to forest. *Palaeogeography,*
2943 *Palaeoclimatology, Palaeoecology*, *602*, 111179. doi: 10.1016/j.palaeo.2022.111179
- 2944 Xing, Y., Utescher, T., Jacques, F. M., Su, T., Liu, Y. C., Huang, Y., & Zhou, Z.
2945 (2012, November). Paleoclimatic estimation reveals a weak winter monsoon in south-
2946 western China during the late Miocene: Evidence from plant macrofossils. *Palaeo-*
2947 *geography, Palaeoclimatology, Palaeoecology*, *358-360*, 19–26. Retrieved 2022-05-04,
2948 from <https://linkinghub.elsevier.com/retrieve/pii/S0031018212004129> doi:
2949 10.1016/j.palaeo.2012.07.011
- 2950 Xiong, Z., Ding, L., Spicer, R. A., Farnsworth, A., Wang, X., Valdes, P. J., ... Yue, Y. (2020,
2951 August). The early Eocene rise of the Gonjo Basin, SE Tibet: From low desert to

- 2952 high forest. *Earth and Planetary Science Letters*, 543, 116312. Retrieved 2020-10-12,
 2953 from <https://linkinghub.elsevier.com/retrieve/pii/S0012821X20302569> doi:
 2954 10.1016/j.epsl.2020.116312
- 2955 Xiong, Z., Liu, X., Ding, L., Farnsworth, A., Spicer, R. A., Xu, Q., ... Yue, Y. (2022).
 2956 The rise and demise of the Paleogene Central Tibetan Valley. *Science Advances*,
 2957 8(6), eabj0944. Retrieved 2022-02-10, from <http://www.science.org/doi/10.1126/sciadv.abj0944> (Publisher: American Association for the Advancement of Science)
 2958 doi: 10.1126/sciadv.abj0944
- 2959
- 2960 Xu, Q., Ding, L., Spicer, R. A., Liu, X., Li, S., & Wang, H. (2018, February). Stable iso-
 2961 topes reveal southward growth of the Himalayan-Tibetan Plateau since the Paleocene.
 2962 *Gondwana Research*, 54, 50–61. Retrieved 2020-10-20, from [https://linkinghub](https://linkinghub.elsevier.com/retrieve/pii/S1342937X17303295)
 2963 [.elsevier.com/retrieve/pii/S1342937X17303295](https://linkinghub.elsevier.com/retrieve/pii/S1342937X17303295) doi: 10.1016/j.gr.2017.10.005
- 2964 Xu, Q., Ding, L., Zhang, L., Cai, F., Lai, Q., Yang, D., & Liu-Zeng, J. (2013, January).
 2965 Paleogene high elevations in the Qiangtang Terrane, central Tibetan Plateau. *Earth*
 2966 *and Planetary Science Letters*, 362, 31–42. Retrieved 2020-10-17, from [http://www](http://www.sciencedirect.com/science/article/pii/S0012821X1200684X)
 2967 [.sciencedirect.com/science/article/pii/S0012821X1200684X](http://www.sciencedirect.com/science/article/pii/S0012821X1200684X) doi: 10.1016/j
 2968 [.epsl.2012.11.058](http://www.sciencedirect.com/science/article/pii/S0012821X1200684X)
- 2969 Yang, C., Dang, H., Zhou, X., Zhang, H., Wang, X., Wang, Y., ... Jian, Z. (2021, April).
 2970 Upper ocean hydrographic changes in response to the evolution of the East Asian
 2971 monsoon in the northern South China Sea during the middle to late Miocene. *Global*
 2972 *and Planetary Change*, 201, 103478. doi: 10.1016/j.gloplacha.2021.103478
- 2973 Yang, W., Zuo, R., Wang, X., Song, Y., Jiang, Z., Luo, Q., ... Zhang, Z. (2019, Jan-
 2974 uary). Sensitivity of lacustrine stromatolites to Cenozoic tectonic and climatic forcing
 2975 in the southern Junggar Basin, NW China: New insights from mineralogical, stable
 2976 and clumped isotope compositions. *Palaeogeography, Palaeoclimatology, Palaeoecol-*
 2977 *ogy*, 514, 109–123. Retrieved 2022-06-17, from [https://linkinghub.elsevier.com/](https://linkinghub.elsevier.com/retrieve/pii/S0031018218303985)
 2978 [retrieve/pii/S0031018218303985](https://linkinghub.elsevier.com/retrieve/pii/S0031018218303985) doi: 10.1016/j.palaeo.2018.10.011
- 2979 Yang, X., Groeneveld, J., Jian, Z., Steinke, S., & Giosan, L. (2020). Middle
 2980 Miocene Intensification of South Asian Monsoonal Rainfall. *Paleoceanography and*
 2981 *Paleoclimatology*, 35(12), e2020PA003853. Retrieved 2021-03-17, from [http://](http://agupubs.onlinelibrary.wiley.com/doi/abs/10.1029/2020PA003853)
 2982 agupubs.onlinelibrary.wiley.com/doi/abs/10.1029/2020PA003853 (eprint:
 2983 <https://onlinelibrary.wiley.com/doi/pdf/10.1029/2020PA003853>) doi: [https://doi](https://doi.org/10.1029/2020PA003853)
 2984 [.org/10.1029/2020PA003853](https://doi.org/10.1029/2020PA003853)
- 2985 Yao, Y.-F., Bruch, A. A., Mosbrugger, V., & Li, C.-S. (2011, May). Quantitative re-
 2986 construction of Miocene climate patterns and evolution in Southern China based
 2987 on plant fossils. *Palaeogeography, Palaeoclimatology, Palaeoecology*, 304(3-4), 291–
 2988 307. Retrieved 2022-05-06, from [https://linkinghub.elsevier.com/retrieve/](https://linkinghub.elsevier.com/retrieve/pii/S003101821000221X)
 2989 [pii/S003101821000221X](https://linkinghub.elsevier.com/retrieve/pii/S003101821000221X) doi: 10.1016/j.palaeo.2010.04.012
- 2990 Yarmolyuk, V. V., Kudryashova, E. A., Kozlovsky, A. M., & Lebedev, V. A. (2008, October).
 2991 Late Cenozoic volcanism of Khangai (Central Mongolia): Evidence for recent orogeny
 2992 in Central Asia. *Doklady Earth Sciences*, 422(1), 1032–1036. Retrieved 2021-03-
 2993 29, from <http://link.springer.com/10.1134/S1028334X08070064> doi: 10.1134/
 2994 [S1028334X08070064](http://link.springer.com/10.1134/S1028334X08070064)
- 2995 Yu, E., Zhang, R., Jiang, D., Ramstein, G., Zhang, Z., & Sun, J. (2018, October). High-
 2996 resolution simulation of Asian monsoon response to regional uplift of the Tibetan
 2997 Plateau with regional climate model nested with global climate model. *Global and*
 2998 *Planetary Change*, 169, 34–47. Retrieved 2021-09-24, from [https://linkinghub](https://linkinghub.elsevier.com/retrieve/pii/S0921818118300407)
 2999 [.elsevier.com/retrieve/pii/S0921818118300407](https://linkinghub.elsevier.com/retrieve/pii/S0921818118300407) doi: 10.1016/j.gloplacha.2018
 3000 [.07.002](https://linkinghub.elsevier.com/retrieve/pii/S0921818118300407)
- 3001 Yuan, Q., Barbolini, N., Ashworth, L., Rydin, C., Gao, D.-L., Shan, F.-S., ... Vajda, V.
 3002 (2021, July). Palaeoenvironmental changes in Eocene Tibetan lake systems traced by
 3003 geochemistry, sedimentology and palynofacies. *Journal of Asian Earth Sciences*, 214,
 3004 104778. Retrieved 2022-05-04, from [https://linkinghub.elsevier.com/retrieve/](https://linkinghub.elsevier.com/retrieve/pii/S1367912021001164)
 3005 [pii/S1367912021001164](https://linkinghub.elsevier.com/retrieve/pii/S1367912021001164) doi: 10.1016/j.jseaes.2021.104778
- 3006 Yuan, Q., Barbolini, N., Rydin, C., Gao, D.-L., Wei, H.-C., Fan, Q.-S., ... Vajda, V. (2020,

- 3007 November). Aridification signatures from fossil pollen indicate a drying climate in
 3008 east-central Tibet during the late Eocene. *Climate of the Past*, 16(6), 2255–2273.
 3009 Retrieved 2022-05-04, from <https://cp.copernicus.org/articles/16/2255/2020/>
 3010 doi: 10.5194/cp-16-2255-2020
- 3011 Yuan, W., Carter, A., Dong, J., Bao, Z., An, Y., & Guo, Z. (2006, January). Meso-
 3012 zoic–Tertiary exhumation history of the Altai Mountains, northern Xinjiang, China:
 3013 New constraints from apatite fission track data. *Tectonophysics*, 412(3), 183–193. Re-
 3014 trieved 2021-03-26, from [https://www.sciencedirect.com/science/article/pii/](https://www.sciencedirect.com/science/article/pii/S004019510500449X)
 3015 [S004019510500449X](https://www.sciencedirect.com/science/article/pii/S004019510500449X) doi: 10.1016/j.tecto.2005.09.007
- 3016 Zhang, R., Jiang, D., Liu, X., & Tian, Z. (2012, December). Modeling the climate effects of
 3017 different subregional uplifts within the Himalaya-Tibetan Plateau on Asian summer
 3018 monsoon evolution. *Chinese Science Bulletin*, 57(35), 4617–4626. Retrieved 2017-10-
 3019 09, from <http://link.springer.com/10.1007/s11434-012-5284-y> doi: 10.1007/
 3020 [s11434-012-5284-y](http://link.springer.com/10.1007/s11434-012-5284-y)
- 3021 Zhang, R., Jiang, D., Ramstein, G., Zhang, Z., Lippert, P. C., & Yu, E. (2018, February).
 3022 Changes in Tibetan Plateau latitude as an important factor for understanding East
 3023 Asian climate since the Eocene: A modeling study. *Earth and Planetary Science*
 3024 *Letters*, 484, 295–308. Retrieved 2018-01-16, from [http://linkinghub.elsevier](http://linkinghub.elsevier.com/retrieve/pii/S0012821X1730746X)
 3025 [.com/retrieve/pii/S0012821X1730746X](http://linkinghub.elsevier.com/retrieve/pii/S0012821X1730746X) doi: 10.1016/j.epsl.2017.12.034
- 3026 Zhang, R., Jiang, D., & Zhang, Z. (2017, December). Effects of the uplifts of the main and
 3027 marginal Tibetan Plateau on the Asian climate under modern and ~30 Ma boundary
 3028 conditions. *Palaeogeography, Palaeoclimatology, Palaeoecology*. Retrieved 2018-01-16,
 3029 from <http://linkinghub.elsevier.com/retrieve/pii/S0031018217308866> doi:
 3030 [10.1016/j.palaeo.2017.12.022](http://linkinghub.elsevier.com/retrieve/pii/S0031018217308866)
- 3031 Zhang, R., Jiang, D., Zhang, Z., Cheng, Z., & Zhang, Q. (2017). Compari-
 3032 son of the climate effects of surface uplifts from the northern Tibetan Plateau,
 3033 the Tianshan, and the Mongolian Plateau on the East Asian climate. *Journal of*
 3034 *Geophysical Research: Atmospheres*, 122(15), 7949–7970. Retrieved 2022-
 3035 12-19, from <https://onlinelibrary.wiley.com/doi/abs/10.1002/2017JD026470>
 3036 (_eprint: <https://onlinelibrary.wiley.com/doi/pdf/10.1002/2017JD026470>) doi: 10
 3037 [.1002/2017JD026470](https://onlinelibrary.wiley.com/doi/pdf/10.1002/2017JD026470)
- 3038 Zhang, R., Jiang, D., Zhang, Z., & Zhang, C. (2021). Effects of Ti-
 3039 betan Plateau Growth, Paratethys Sea Retreat and Global Cooling on
 3040 the East Asian Climate by the Early Miocene. *Geochemistry, Geo-*
 3041 *physics, Geosystems*, 22(6), e2021GC009655. Retrieved 2021-09-24, from
 3042 <http://onlinelibrary.wiley.com/doi/abs/10.1029/2021GC009655> (_eprint:
 3043 <https://agupubs.onlinelibrary.wiley.com/doi/pdf/10.1029/2021GC009655>) doi: 10
 3044 [.1029/2021GC009655](https://agupubs.onlinelibrary.wiley.com/doi/pdf/10.1029/2021GC009655)
- 3045 Zhang, Z., Flatøy, F., Wang, H., Bethke, I., Bentsen, M., & Guo, Z. (2012, January). Early
 3046 Eocene Asian climate dominated by desert and steppe with limited monsoons. *Journal*
 3047 *of Asian Earth Sciences*, 44, 24–35. Retrieved 2017-10-09, from [http://linkinghub](http://linkinghub.elsevier.com/retrieve/pii/S1367912011002148)
 3048 [.elsevier.com/retrieve/pii/S1367912011002148](http://linkinghub.elsevier.com/retrieve/pii/S1367912011002148) doi: 10.1016/j.jseaes.2011.05
 3049 [.013](http://linkinghub.elsevier.com/retrieve/pii/S1367912011002148)
- 3050 Zhang, Z., Ramstein, G., Schuster, M., Li, C., Contoux, C., & Yan, Q. (2014, Septem-
 3051 ber). Aridification of the Sahara desert caused by Tethys Sea shrinkage during the
 3052 Late Miocene. *Nature*, 513(7518), 401–404. Retrieved 2019-09-06, from [http://](http://www.nature.com/articles/nature13705)
 3053 www.nature.com/articles/nature13705 doi: 10.1038/nature13705
- 3054 Zhang, Z., & Sun, J. (2011, January). Palynological evidence for Neogene environ-
 3055 mental change in the foreland basin of the southern Tianshan range, northwest-
 3056 ern China. *Global and Planetary Change*, 75(1-2), 56–66. Retrieved 2022-05-04,
 3057 from <https://linkinghub.elsevier.com/retrieve/pii/S0921818110002304> doi:
 3058 [10.1016/j.gloplacha.2010.10.006](https://linkinghub.elsevier.com/retrieve/pii/S0921818110002304)
- 3059 Zhang, Z., Wang, H., Guo, Z., & Jiang, D. (2007, March). What triggers the transi-
 3060 tion of palaeoenvironmental patterns in China, the Tibetan Plateau uplift or the
 3061 Paratethys Sea retreat? *Palaeogeography, Palaeoclimatology, Palaeoecology*, 245(3-4),

- 317–331. Retrieved 2017-10-09, from <http://linkinghub.elsevier.com/retrieve/pii/S0031018206004469> doi: 10.1016/j.palaeo.2006.08.003
- 3062
3063
3064 Zhang, Z., Xiao, W., Majidifard, M. R., Zhu, R., Wan, B., Ao, S., ... Esmaili, R. (2017,
3065 June). Detrital zircon provenance analysis in the Zagros Orogen, SW Iran: impli-
3066 cations for the amalgamation history of the Neo-Tethys. *International Journal of*
3067 *Earth Sciences*, 106(4), 1223–1238. Retrieved 2022-03-04, from [https://doi.org/](https://doi.org/10.1007/s00531-016-1314-3)
3068 [10.1007/s00531-016-1314-3](https://doi.org/10.1007/s00531-016-1314-3) doi: 10.1007/s00531-016-1314-3
- 3069 Zhang, Z., Zhang, Z., He, Z., Tan, N., Guo, Z., Zhu, J., ... de Boer, A. M. (2022). Impact
3070 of Mountains in Southern China on the Eocene Climates of East Asia. *Journal of Geo-*
3071 *physical Research: Atmospheres*, 127(17), e2022JD036510. Retrieved 2022-12-05, from
3072 <http://onlinelibrary.wiley.com/doi/abs/10.1029/2022JD036510> (eprint:
3073 <https://agupubs.onlinelibrary.wiley.com/doi/pdf/10.1029/2022JD036510>) doi: 10
3074 .1029/2022JD036510
- 3075 Zhao, H., Qiang, X., Xu, X., & Sun, Y. (2020, April). Iron oxide characteris-
3076 tics of the Chinese loess-red clay sequences and their implications for the evo-
3077 lution of the East Asian summer monsoon since the Late Oligocene. *Palaeo-*
3078 *geography, Palaeoclimatology, Palaeoecology*, 543, 109604. Retrieved 2022-06-09,
3079 from <https://linkinghub.elsevier.com/retrieve/pii/S0031018219308995> doi:
3080 10.1016/j.palaeo.2020.109604
- 3081 Zhao, L., Lu, H., Wang, H., Meadows, M., Ma, C., Tang, L., ... Zhang, H. (2020, Octo-
3082 ber). Vegetation dynamics in response to evolution of the Asian Monsoon in a warm
3083 world: Pollen evidence from the Weihe Basin, central China. *Global and Planetary*
3084 *Change*, 193, 103269. Retrieved 2022-06-09, from [https://linkinghub.elsevier](https://linkinghub.elsevier.com/retrieve/pii/S0921818120301600)
3085 [.com/retrieve/pii/S0921818120301600](https://linkinghub.elsevier.com/retrieve/pii/S0921818120301600) doi: 10.1016/j.gloplacha.2020.103269
- 3086 Zheng, H., Wei, X., Tada, R., Clift, P. D., Wang, B., Jourdan, F., ... He, M. (2015,
3087 June). Late Oligocene–early Miocene birth of the Taklimakan Desert. *Proceedings*
3088 *of the National Academy of Sciences*, 112(25), 7662–7667. Retrieved 2022-02-11,
3089 from <http://www.pnas.org/lookup/doi/10.1073/pnas.1424487112> doi: 10.1073/
3090 pnas.1424487112
- 3091 Zheng, H., Yang, Q., Cao, S., Clift, P. D., He, M., Kano, A., ... Jourdan, F. (2022,
3092 December). From desert to monsoon: irreversible climatic transition at ~ 36 Ma
3093 in southeastern Tibetan Plateau. *Progress in Earth and Planetary Science*, 9(1),
3094 12. Retrieved 2022-05-02, from [https://progearthplanetsci.springeropen.com/](https://progearthplanetsci.springeropen.com/articles/10.1186/s40645-022-00470-x)
3095 [articles/10.1186/s40645-022-00470-x](https://progearthplanetsci.springeropen.com/articles/10.1186/s40645-022-00470-x) doi: 10.1186/s40645-022-00470-x
- 3096 Zhisheng, A., Guoxiong, W., Jianping, L., Youbin, S., Yimin, L., Weijian, Z., ... Juan,
3097 F. (2015, May). Global Monsoon Dynamics and Climate Change. *Annual Review of*
3098 *Earth and Planetary Sciences*, 43(1), 29–77. Retrieved 2017-10-09, from [http://www](http://www.annualreviews.org/doi/10.1146/annurev-earth-060313-054623)
3099 [.annualreviews.org/doi/10.1146/annurev-earth-060313-054623](http://www.annualreviews.org/doi/10.1146/annurev-earth-060313-054623) doi: 10.1146/
3100 annurev-earth-060313-054623
- 3101 Zhisheng, A., Kutzbach, J. E., Prell, W. L., & Porter, S. C. (2001, May). Evolution of Asian
3102 monsoons and phased uplift of the Himalaya–Tibetan plateau since Late Miocene
3103 times. *Nature*, 411(6833), 62–66. Retrieved 2021-09-16, from [http://www.nature](http://www.nature.com/articles/35075035)
3104 [.com/articles/35075035](http://www.nature.com/articles/35075035) (Bandiera_abtest: a Cg_type: Nature Research Journals
3105 Number: 6833 Primary_atype: Research Publisher: Nature Publishing Group) doi:
3106 10.1038/35075035
- 3107 Zhou, P., Ireland, T., Murray, R. W., & Clift, P. D. (2021, June). Ma-
3108 rine sedimentary records of chemical weathering evolution in the western
3109 Himalaya since 17 Ma. *Geosphere*, 17(3), 824–853. Retrieved 2022-
3110 09-13, from [https://pubs.geoscienceworld.org/gsa/geosphere/article/17/3/](https://pubs.geoscienceworld.org/gsa/geosphere/article/17/3/824/595660/Marine-sedimentary-records-of-chemical-weathering)
3111 [824/595660/Marine-sedimentary-records-of-chemical-weathering](https://pubs.geoscienceworld.org/gsa/geosphere/article/17/3/824/595660/Marine-sedimentary-records-of-chemical-weathering) doi: 10
3112 .1130/GES02211.1
- 3113 Zhuang, G., Pagani, M., & Zhang, Y. G. (2017, July). Monsoonal upwelling in the western
3114 Arabian Sea since the middle Miocene. *Geology*, 45(7), 655–658. Retrieved 2022-05-02,
3115 from <https://doi.org/10.1130/G39013.1> doi: 10.1130/G39013.1
- 3116 Ziegler, C. L., Murray, R. W., Hovan, S. A., & Rea, D. K. (2007, February). Re-

3117 solving eolian, volcanogenic, and authigenic components in pelagic sediment from
3118 the Pacific Ocean. *Earth and Planetary Science Letters*, 254(3), 416–432. Re-
3119 trieved 2022-03-25, from [https://www.sciencedirect.com/science/article/pii/](https://www.sciencedirect.com/science/article/pii/S0012821X06008661)
3120 [S0012821X06008661](https://www.sciencedirect.com/science/article/pii/S0012821X06008661) doi: 10.1016/j.epsl.2006.11.049
3121 Zoura, D., Hill, D., Dolan, A., Hunter, S., Tang, Z., & Haywood, A. (2019, August). Atmo-
3122 spheric carbon dioxide, ice sheet and topographic constraints on palaeo moisture avail-
3123 ability in Asia. *Earth and Planetary Science Letters*, 519, 12–27. Retrieved 2019-09-12,
3124 from <https://linkinghub.elsevier.com/retrieve/pii/S0012821X19302390> doi:
3125 10.1016/j.epsl.2019.04.035

3126 8 Supplementary

	Reference
1	(Averyanova et al., 2021)
2	(Hellwig et al., 2018)
3	(Macaulay et al., 2016)
4	(Caves Rugenstein et al., 2017)
5	(Carrapa et al., 2015)
6	(J. Sun et al., 2022)
7	(J. Sun et al., 2010)
8	(J. Sun & Windley, 2015)
9	(Baldermann et al., 2021)
10	(Caves Rugenstein et al., 2014)
11	(Kent-Corson et al., 2009)
12	(Zheng et al., 2015)
13	(Meijer et al., 2021)
14	(Licht et al., 2014)
15	(Wasiljeff et al., 2022)
16	(Hoorn et al., 2012)
17	(X. Ma & Jiang, 2015)
18	(Guo et al., 2002)
19	(Guo et al., 2008)
20	(Q. Yuan et al., 2020)
21	(Ao et al., 2016)
22	(Ao et al., 2021)
23	(Shen et al., 2017)
24	(S. Li et al., 2018)
25	(C. Huang & Hinnov, 2019)
26	(Ling et al., 2021)
27	(Spicer et al., 2017)
28	(Herman et al., 2017)
29	(Vornlocher et al., 2021)
30	(J. Ren et al., 2021)
31	(Q. Wang et al., 2021)
32	(Fang et al., 2021)
33	(Zheng et al., 2022)
34	(Sorrel et al., 2017)
35	(Jacques, Guo, et al., 2011)
36	(Xia et al., 2009)
37	(Xing et al., 2012)
38	(Wan et al., 2007)
39	(Jia et al., 2003)
40	(Clift et al., 2008)
41	(Clift, 2020)
42	(Z. Ding et al., 2021)
43	(Srivastava et al., 2012)
44	(Bhatia, Khan, et al., 2021)
45	(Shukla et al., 2014)
46	(Khan et al., 2014)
47	(Vögeli et al., 2017)
48	(Bhatia et al., 2022)
49	(Bhatia, Srivastava, et al., 2021)
50	(Srivastava et al., 2018)
51	(Sanyal et al., 2004)
52	(S. Ali et al., 2021)
53	(Betzler et al., 2016)
54	(Betzler et al., 2018)
55	(Beasley et al., 2021)
56	(Zhuang et al., 2017)

Table 3. List of references used in Figure 2 for paleoclimate indicators compilation

	Reference (suite)
57	(Page et al., 2019)
58	(Q. Yuan et al., 2021)
59	(Meng et al., 2018)
60	(Miao et al., 2013)
61	(Z. Zhang & Sun, 2011)
62	(J. Sun & Zhang, 2008)
63	(Q.-g. Sun et al., 2002)
64	(J. Sun et al., 2020)
65	(T. Su, Spicer, et al., 2019)
66	(M. Wu et al., 2021)
67	(Song et al., 2020)
68	(Miao, Wu, et al., 2016)
69	(D. Rea et al., 1985)
70	(Pettke et al., 2002)
71	(Ziegler et al., 2007)
72	(B. Li et al., 2016)
73	(Garziona et al., 2005)
74	(Qiang et al., 2011)
75	(Bougeois et al., 2018)
76	(W. Yang et al., 2019)
77	(J. Lee et al., 2020)
78	(Bolton et al., 2022)
79	(Hui et al., 2021)
80	(Miao, Song, et al., 2016)
81	(H. Zhao et al., 2020)
82	(C. Yang et al., 2021)
83	(L. Zhao et al., 2020)
84	(Heermance et al., 2018)
85	(J. Liu et al., 2016)
86	(Jiang & Ding, 2008)
87	(Peng et al., 2016)
88	(Suarez et al., 2011)
89	(Barbolini et al., 2020)
90	(Y. Ma et al., 2005)
91	(H. Wang et al., 2019)
92	(Jiang et al., 2017)
93	(W. Liu et al., 2014)
94	(Kaakinen et al., 2006)
95	(Y. Wang & Deng, 2005)
96	(F. Li et al., 2008)
97	(Z. Liu et al., 2014)
98	(Miao et al., 2011)
99	(Charreau et al., 2012)
100	(Holbourn et al., 2018)
101	(G. Wei et al., 2006)
102	(Y. Huang et al., 2007)
103	(Gupta et al., 2015)
104	(X. Yang et al., 2020)
105	(Bialik et al., 2020)
106	(H. Tang et al., 2020)
107	(H. Huang et al., 2021)
108	(Hoorn et al., 2000)
109	(Polissar et al., 2021)
110	(Y. Xie et al., 2022)

Table 4. (suite) List of references used in Figure 2 for paleoclimate indicators compilation

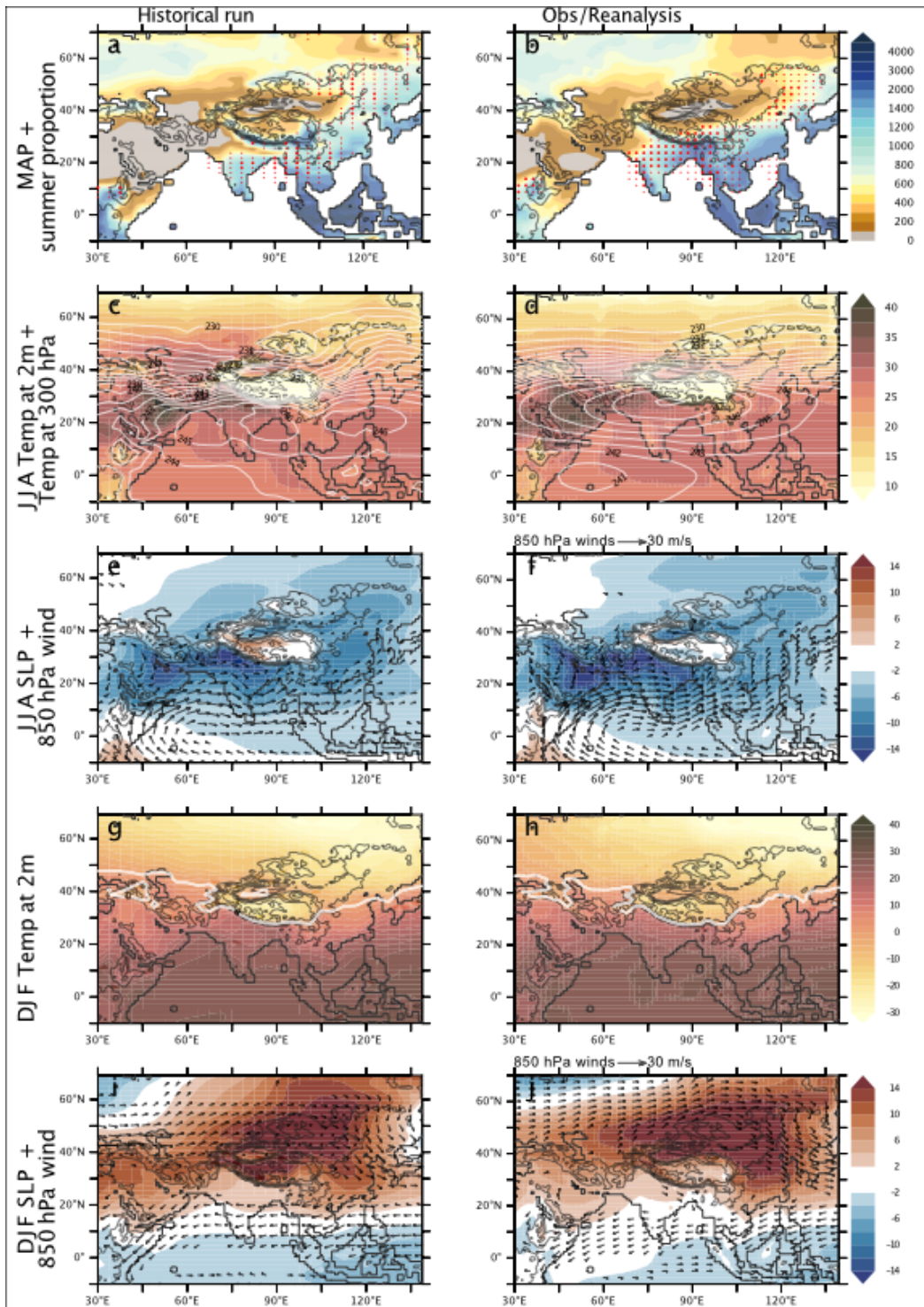


Figure 14. Comparison of monsoon diagnostics obtained in our control historical simulation (**Left column**) with modern observations and reanalysis (**Right column**). (**a, b**) Mean Annual Precipitations (shading, mm/yr), and regions where the Monsoon Precipitation Index is over 0.5 (thin red dots) and 0.75 (thick red dots); (**c, d**) JJA mean 2 m temperature (shading, Celsius) and 300 hPa atmospheric temperature (white contour, Kelvin); (**e, f**) JJA normalized Sea Level Pressure anomalies (shading, hPa) and 850 hPa winds (vectors over 4 m/s); (**g, h**) DJF mean 2 m temperature (shading, Celsius); (**i, j**) DJF normalized Sea Level Pressure anomalies (shading, hPa) and 850 hPa winds (vectors over 4 m/s). In all captions, topography in gray contour, each 1000 m. On the right column, precipitation are from GPCP, pressure and 300hPa temperature from ERAINT, 850hPa winds and surface temperature from ERA40.

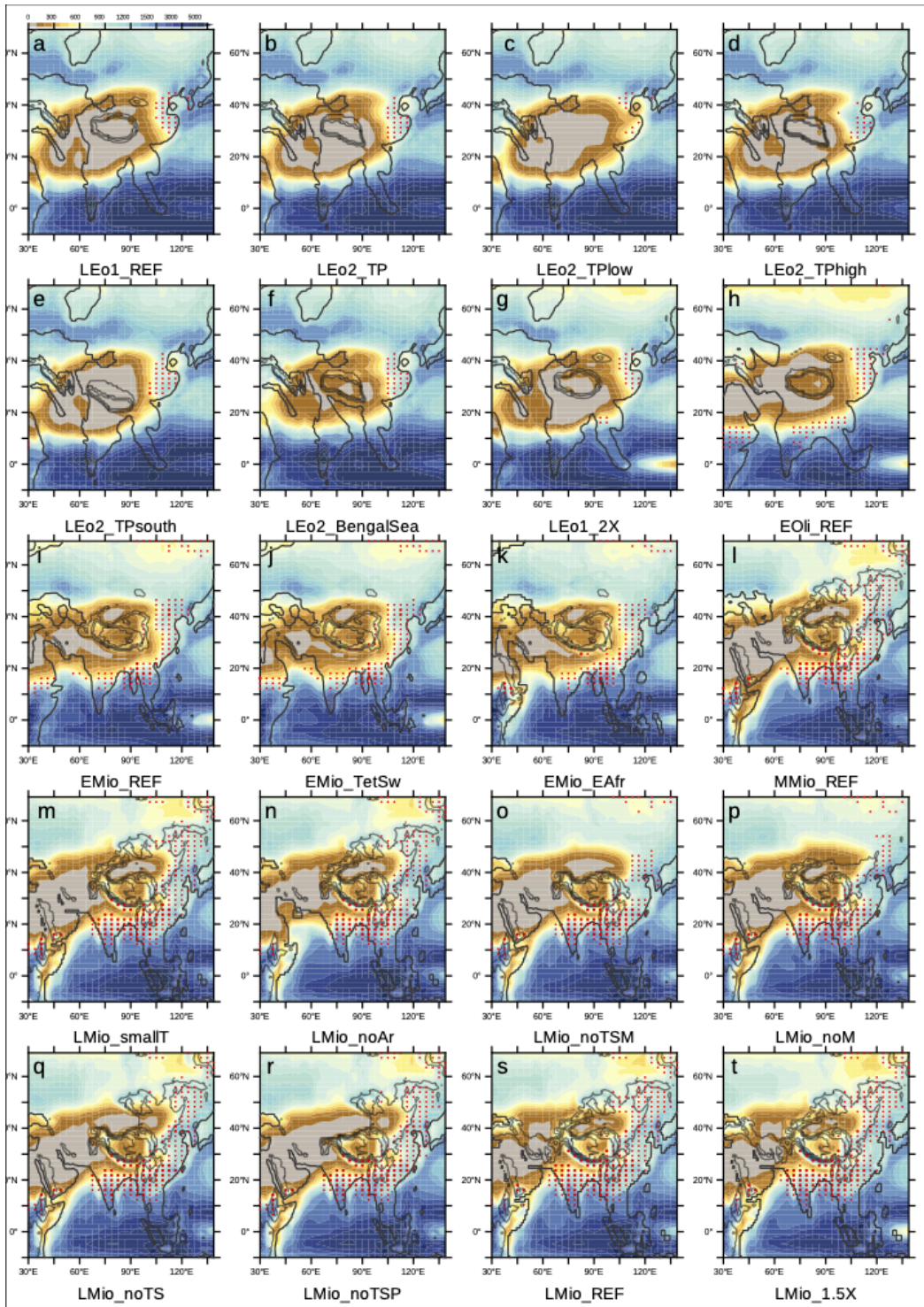


Figure 15. Mean Annual Precipitation (shading, mm/yr), overlain with regions where the Monsoon Precipitation Index (B. Wang & Ding, 2008) is over 0.5 (thin red dots) and 0.75 (thick red dots), for all reference and sensitivity experiments.

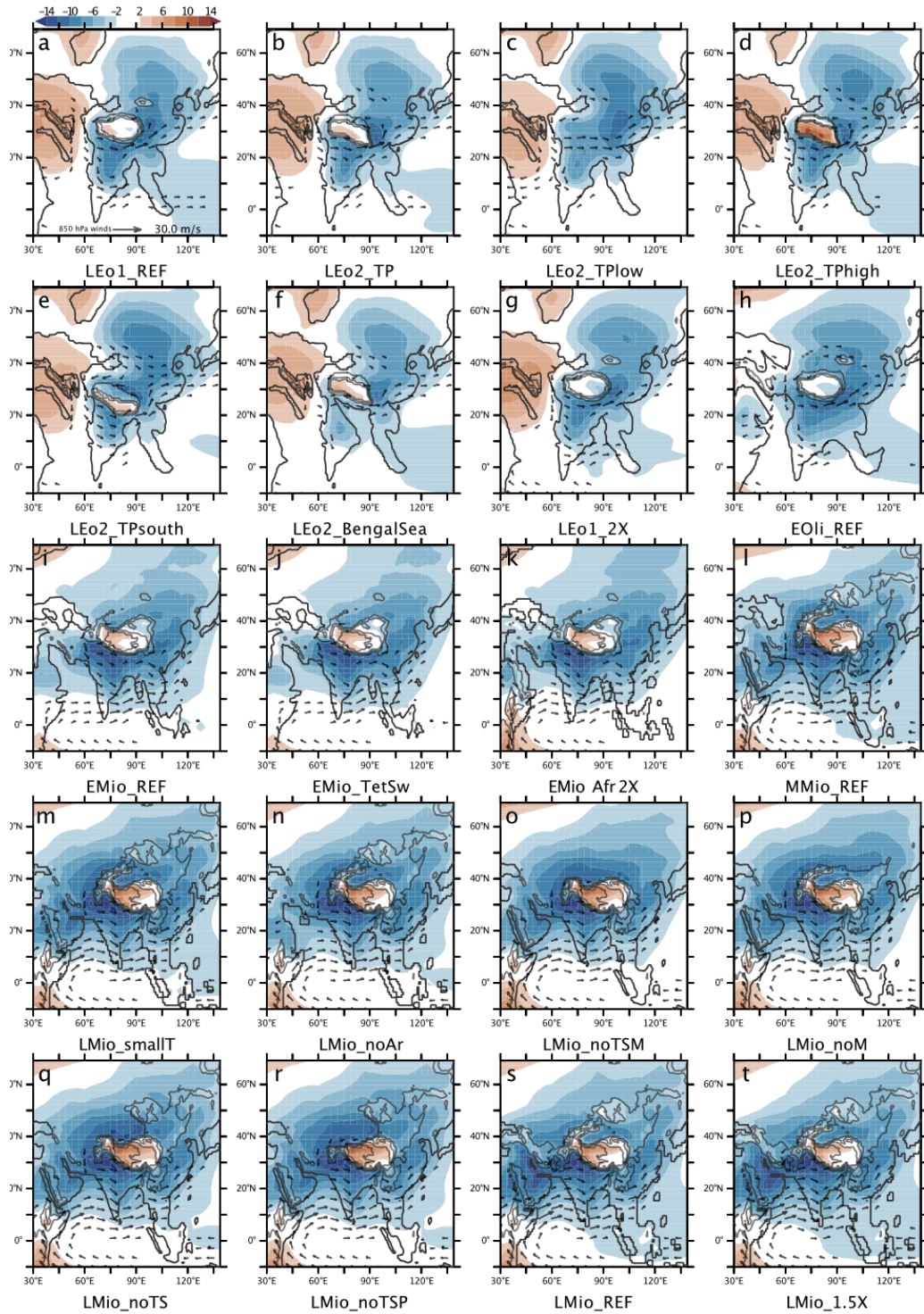


Figure 16. June-August (JJA) normalized Sea Level Pressure anomalies (shading, hPa) and 850 hPa winds over 4 m/s (vectors), for all reference and sensitivity experiments.

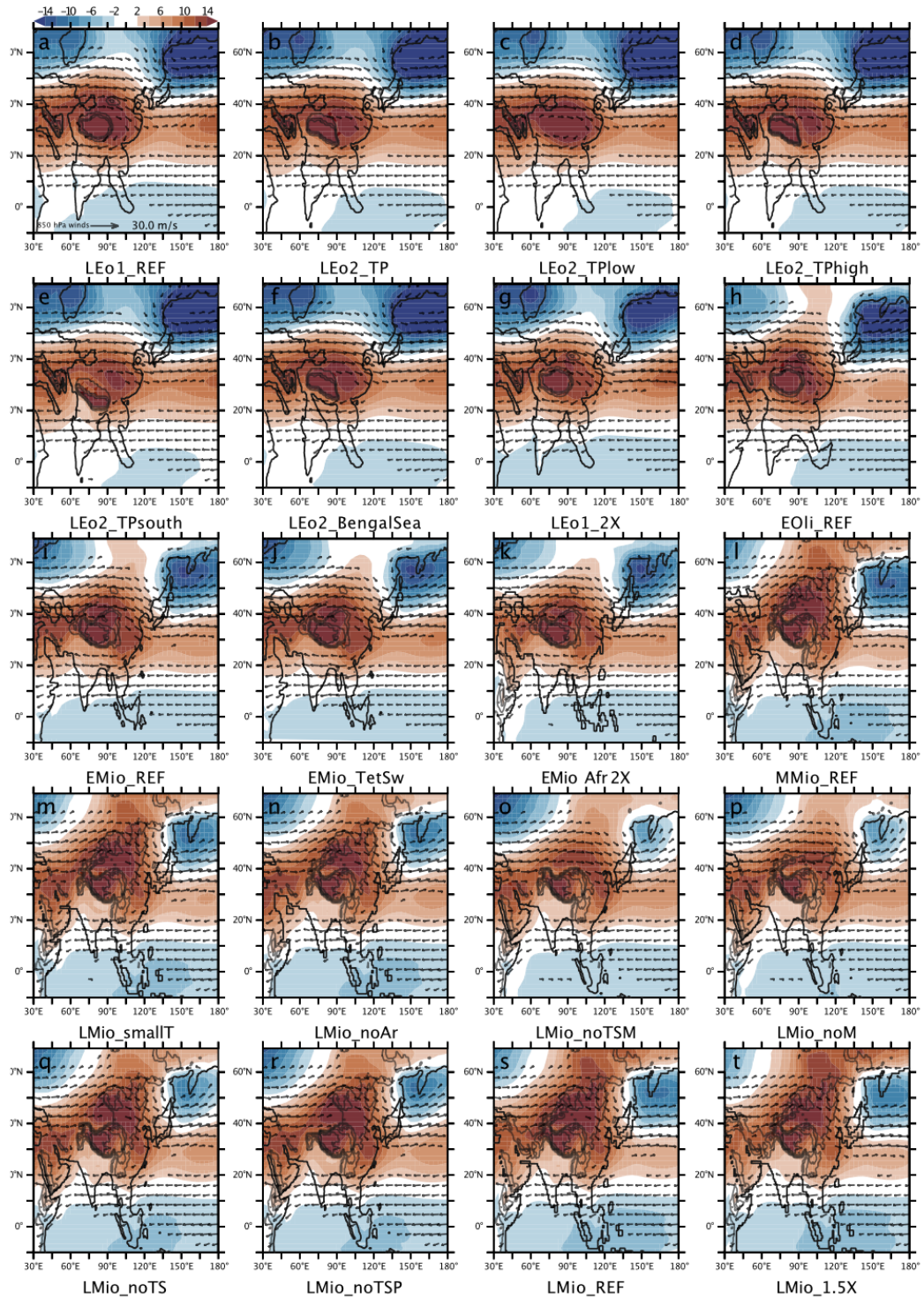


Figure 17. December-February (DJF) normalized Sea Level Pressure anomalies (shading, hPa) and 850 hPa winds over 4 m/s (vectors), for all reference and sensitivity experiments.

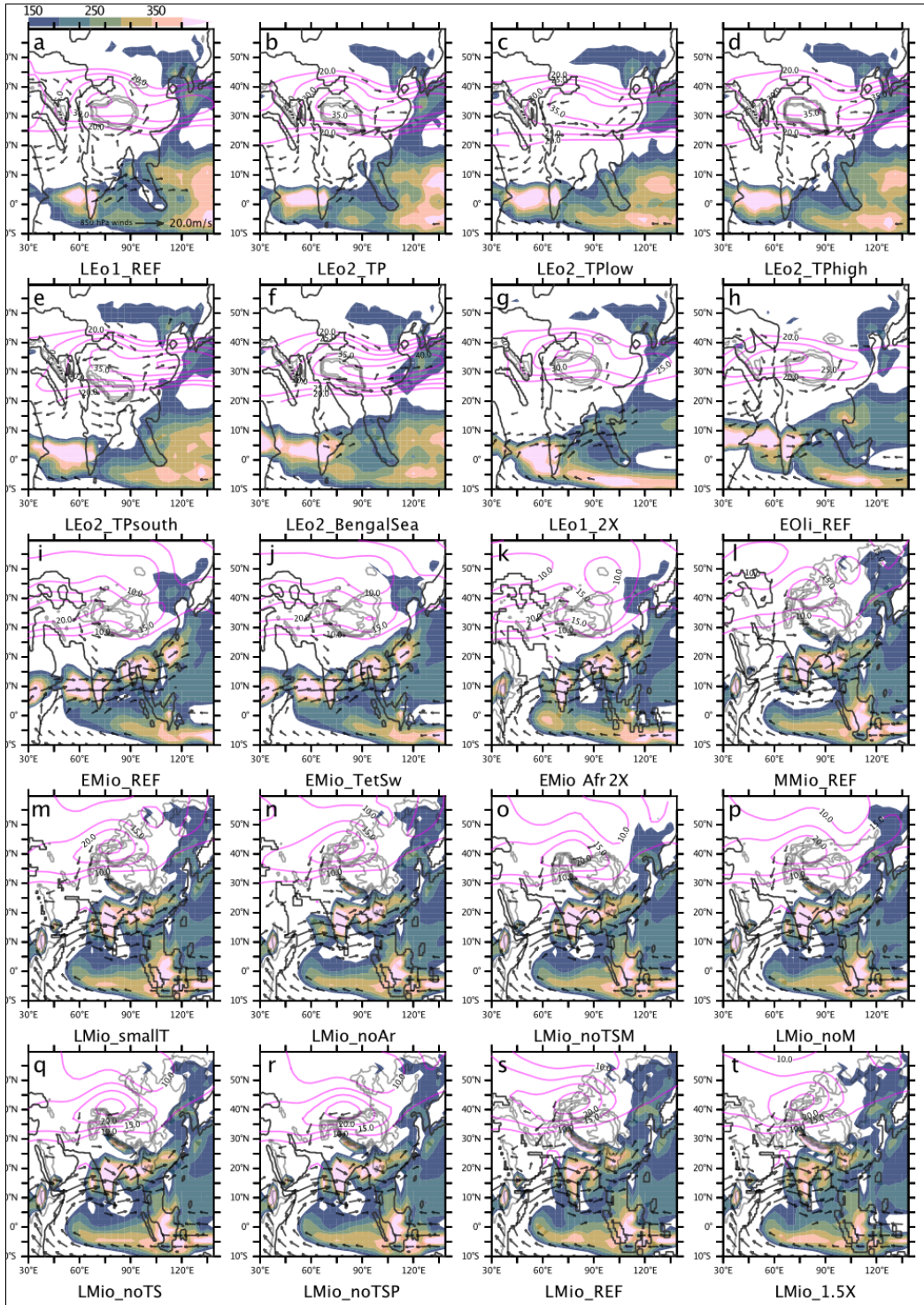


Figure 18. Jet Stream velocity and localization over Asia in August (purple outline), for all sensitivity experiments and precipitation for the month of August (shading, mm/month).